USGS
science for a changing world

V_{S30} at Three Strong-Motion Recording Stations in Napa and Solano Counties, California—Lovall Valley Road, Broadway Street and Sereno Drive in Vallejo, and Vallejo Fire Station—Calculations Determined From S-wave Refraction Tomography and Multichannel Analysis of Surface Waves (Rayleigh and Love)

Open-File Report 2018–1162

U.S. Department of the Interior
U.S. Geological Survey

Cover. Photograph showing USGS personnel preparing to generate shear-wave energy for the seismic survey near Vallejo Fire Station in Vallejo, California (U.S. Geological Survey photograph by Rufus Catchings, 2014).

V_{S30} at Three Strong-Motion Recording Stations in Napa and Solano Counties, California—Lovall Valley Road, Broadway Street and Sereno Drive in Vallejo, and Vallejo Fire Station—Calculations Determined From S-wave Refraction Tomography and Multichannel Analysis of Surface Waves (Rayleigh and Love)

By Joanne H. Chan, Rufus D. Catchings, Mark R. Goldman, and Coyn J. Criley

Open-File Report 2018–1162

U.S. Department of the Interior
U.S. Geological Survey

U.S. Department of the Interior
RYAN K. ZINKE, Secretary

U.S. Geological Survey
James F. Reilly II, Director

U.S. Geological Survey, Reston, Virginia: 2018

For more information on the USGS—the Federal source for science about the Earth, its natural and living resources, natural hazards, and the environment—visit https://www.usgs.gov/ or call 1–888–ASK–USGS (1–888–275–8747).

For an overview of USGS information products, including maps, imagery, and publications, visit https://store.usgs.gov/.

Any use of trade, firm, or product names is for descriptive purposes only and does not imply endorsement by the U.S. Government.

Although this information product, for the most part, is in the public domain, it also may contain copyrighted materials as noted in the text. Permission to reproduce copyrighted items must be secured from the copyright owner.

Suggested citation:
Chan, J.H., Catchings, R.D., Goldman, M.R., and Criley, C.J., 2018, V_{S30} at three strong-motion recording stations in Napa and Solano Counties, California—Lovall Valley Road, Broadway Street and Sereno Drive in Vallejo, and Vallejo Fire Station—Calculations determined from S-wave refraction tomography and multichannel analysis of surface waves (Rayleigh and Love): U.S. Geological Survey Open-File Report 2018–1162, 62 p., https://doi.org/10.3133/ofr20181162.

ISSN 2331-1258 (online)

Acknowledgments

We thank Steve Bohlen, the City of Vallejo, and Kaiser Permanente in Vallejo for field site access. We thank U.S. Geological Survey (USGS) scientist Joe Svitek and volunteers Coye Slayday-Criley-Brooks, Daniel Brooks, Jeremy Cordova, Rob Huggins, and Adrian McEvilly for assistance in the field. We also thank Jemile Erdem (USGS) and Luther Strayer (California State University, East Bay) for critical reviews.

Contents

Figures

Tables

Conversion Factors

International System of Units to U.S. customary units

Multiply	By	To obtain
	Length	
centimeter (cm)	0.3937	inch (in.)
meter (m)	3.281	foot (ft)
kilometer (km)	0.6214	mile (mi)
	Flow rate	
meter per second (m/s)	3.281	foot per second (ft/s)
	Mass	
meter (m)	3.281	foot (ft)
kilogram (kg)	2.205	pound avoirdupois (lb)

Abbreviations

1D	one dimensional
2D	two dimensional
AWD	accelerated weight drop
CGS	California Geological Survey
CMPCC	common mid-point cross-correlation
FZTW	Fault-zone trapped waves
g	acceleration due to gravity at the Earth's surface
Hz	hertz
KRE	Kreuzer Lane
Ma	million years ago or mega-annum
MASW	multichannel analysis of surface waves
MAS_LW	MASW for Love waves
MAS_RW	MASW for Rayleigh waves
M_w	moment magnitude
NCSN	Northern California Seismic Network
NSMP	National Strong Motion Project
PGA	peak ground accelerations
PGV	peak ground velocity
USGS	U.S. Geological Survey
V_P	P-wave or compression-wave velocity
V_S	S-wave or shear-wave velocity
V_{S18}	time-averaged shear-wave velocity in the upper 18 meters of the subsurface
V_{S30}	time-averaged shear-wave velocity in the upper 30 meters of the subsurface
WNFZ	West Napa Fault Zone

V_{S30} at Three Strong-Motion Recording Stations in Napa and Solano Counties, California—Lovall Valley Road, Broadway Street and Sereno Drive in Vallejo, and Vallejo Fire Station—Calculations Determined From S-wave Refraction Tomography and Multichannel Analysis of Surface Waves (Rayleigh and Love)

By Joanne H. Chan, Rufus D. Catchings, Mark R. Goldman, and Coyn J. Criley

Abstract

The August 24, 2014, moment magnitude (M_w) 6.0 South Napa earthquake caused an estimated $400 million in structural damage to the City of Napa, California. In 2015, we acquired high-resolution P- and S-wave seismic data near three strong-motion recording stations in Napa and Solano Counties where high peak ground accelerations (PGAs) were recorded during the South Napa earthquake. In this report, we present results from three sites—Lovall Valley Loop Road in Napa County (Northern California Seismic Network station, NCSN N019B) and Broadway Street and Sereno Drive (California Geological Survey station, CGS 68294) and Vallejo Fire Station (National Strong Motion Project station, NSMP 1759) in the City of Vallejo, California. To characterize the recording sites in terms of shallow-depth, shear-wave velocities (V_S), we used both surface waves (Rayleigh and Love) and body waves (S-wave) to evaluate the time-averaged V_S in the upper 30 meters of the subsurface (V_{S30}). We used two-dimensional (2D) multichannel analysis of surface waves (MASW) to evaluate V_S from surface waves, and a refraction tomography inversion algorithm, developed by Hole in 1992, to evaluate V_S from the body waves. As determined by the tomography and MASW analysis for Love waves, we found V_{S30} near the strong-motion recording stations at Lovall Valley Loop Road, Broadway Street and Sereno Drive, and the Vallejo Fire Station to be from 711 meters per second (m/s) to 767 m/s, 455 to 673 m/s, and 490 to 583 m/s, respectively. We found that V_{S30} determined from Love waves were higher than those determined from Rayleigh waves at the Lovall Valley Loop Road recording site (221 m/s higher) and at the Vallejo Fire Station site (62 and 48 m/s higher); however, V_{S30} from Love waves was lower than those from Rayleigh waves at the Broadway Street and Sereno Drive site (78 m/s lower). We also found that V_{S30} varied depending on the number of shot points used in our MASW analysis for both Love and Rayleigh waves . Furthermore, V_{S30} values determined from S-wave refraction tomography are generally closer to those determined from MASW using Love waves than those determined using Rayleigh waves.

Introduction

In May 2015, we acquired high-resolution seismic profiles near three strong-motion recording stations in Napa and Solano Counties, California (fig. 1; stations 4 to 6). These three strong-motion stations recorded horizontal peak ground accelerations (PGAs) ranging from 0.329 *g* (the acceleration due to gravity at the Earth's surface) to 0.469 *g* (table 1), among the highest recorded in the Napa and Vallejo areas during the August 24, 2014, moment magnitude (M_w) 6.0 South Napa earthquake. Our goal was to evaluate the seismic velocities of the underlying geologic materials at the strong-motion sites using P- and S-wave refraction tomography and analysis of surface waves and to evaluate time-averaged shear-wave velocities (V_S) in the upper 30 meters (m) of the subsurface (V_{S30}) at the sites using methods similar to those used by Catchings and others (2018). In this report, we present results from the three sites—Lovall Valley Loop Road in Napa County (NCSN N019B), Broadway Street and Sereno Drive in Vallejo (CGS 68294), and Vallejo Fire Station on Marin Street and Overland Alley (NSMP 1759).

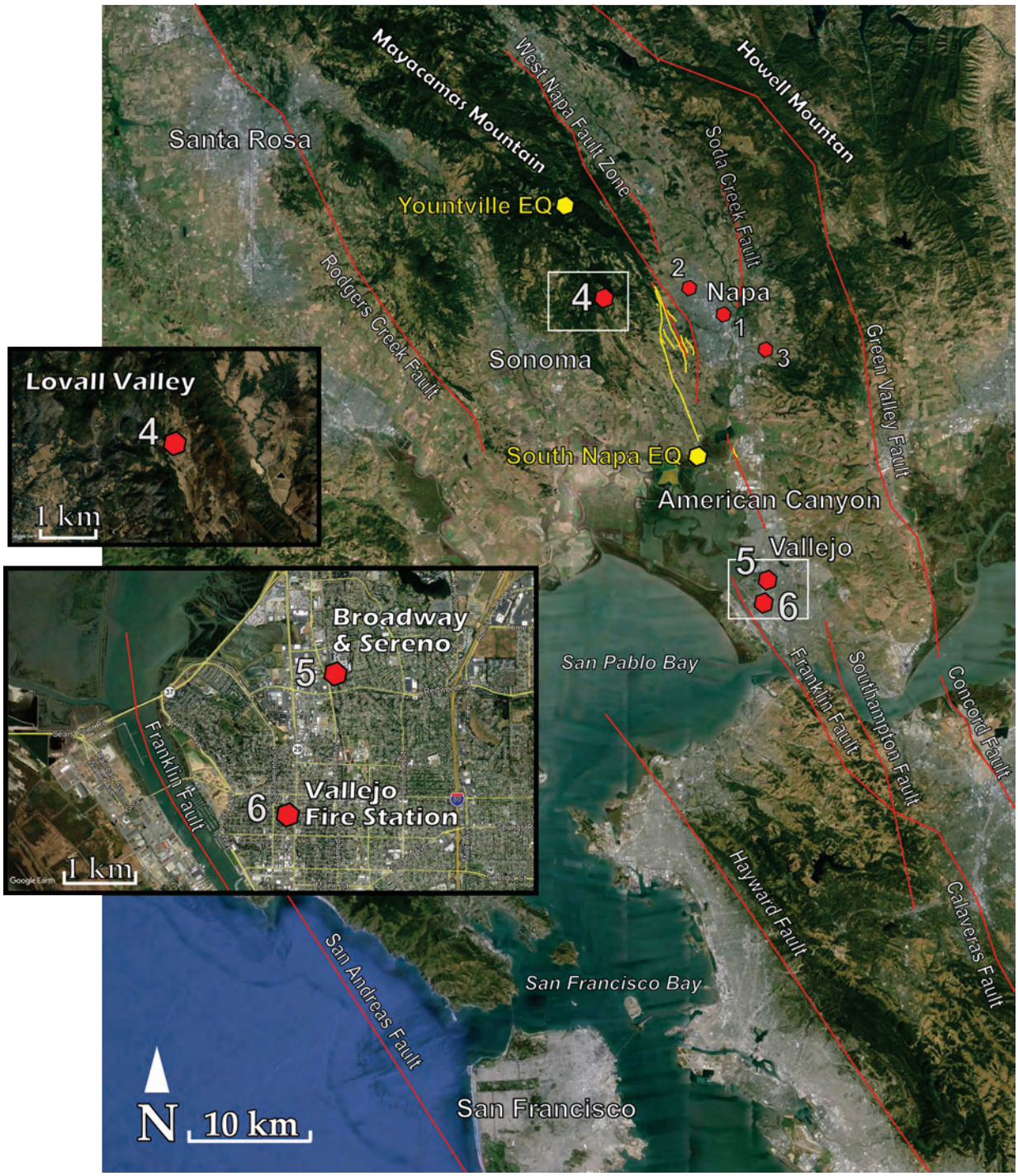

Figure 1. Google Earth satellite image of the San Francisco Bay region, California, showing major faults (red lines), mapped surface ruptures (yellow lines), and the locations (red dots) of our seismic surveys. Yellow dots are the approximate epicenters of the 2000 moment magnitude (M_w) 4.9 Yountville and the 2014 M_w 6.0 South Napa earthquakes. The two white boxes show the areas for three seismic surveys in Napa and Solano Counties detailed in this report; insets show closer views of these areas. Red dot 4 is Lovall Valley Loop Road (N15-4), red dot 5 is Broadway Street and Sereno Drive (N15-5), and red dot 6 is Vallejo Fire Station (N15-6.1 and N15-6.2). Numbers 1 to 3 are locations of additional seismic surveys described in Chan and others (2018). EQ, earthquake; km, kilometers.

Table 1. Peak ground acceleration (PGA), peak ground velocity (PGV), epicentral distance, and location of three strong-motion stations in Napa and Solano Counties, California, that recorded high PGA values during the 2014 moment-magnitude-6.0 South Napa, California, earthquake (Center for Engineering Strong Motion Center, 2017).
[CGS, California Geological Survey; NCSN, Northern California Seismic Network; NSMP, National strong Motion Project; NA, not applicable]

Station name	Station number	Network	PGA, in centimeters per second	PGV, in centimeters per second	Epicentral distance, in kilometers	Latitude (north)/ longitude (west)
Lovall Valley Loop Road, Napa	N019B	NCSN	0.469	16.74	11.9	38.301/122.402
Broadway Street and Sereno Dive, Vallejo	68294	CGS	0.469	16.74	12	38.125/122.249
Vallejo Fire Station	1759	NSMP	0.329	21.1	13.4	38.108/122.256

Napa Valley is located approximately 50 kilometers (km) northeast of San Francisco, California, and is primarily known for its wine industry, which contributes an estimated $13 billion to the local economy and as much as $50 billion to the American economy (Stonebridge Research Group, 2012). Napa County is home to more than 136,000 residents, with more than 76,000 of them living in the City of Napa (U.S. Census, 2010). Geographically, Napa Valley is a structural and topographic depression situated between the Howell Mountains to the east and the Mayacamas Mountains to the west, and between the towns of Calistoga in the north and American Canyon in the south (fig. 1). Within the valley, the surface geology consists dominantly of Quaternary unconsolidated alluvium and is underlain and bordered by late Miocene to Pliocene volcanic rocks and Late Jurassic to Cretaceous Great Valley Sequence, Franciscan Complex rocks, and sediments (Kunkel and Upson, 1960; Howell and Swinchatt, 2000; Wagner and others, 2011). Known faults in the Napa Valley are the West Napa Fault Zone (WNFZ) that trends along the western side of the valley, the northeast-trending Soda Creek Fault, and an unnamed fault to the northeast that trends along the terraces west of and along the foothills of the Howell Mountains (fig. 1). The West Napa Fault is known to be Holocene active (Wagner and others, 2011); it was first mapped by Weaver (1949), and, subsequently, by others starting in the 1970s (Fox and others, 1973; Helley and Herd, 1977; Graymer and others, 2006). The 2000 M_w 4.9 Yountville earthquake occurred along the WNFZ, and previous studies by Langenheim and others (2006, 2010) suggest the fault has accommodated 5 to 40 km of lateral displacement during the late Neogene and Quaternary. The 2014 South Napa earthquake similarly occurred along the WNFZ, approximately 20 km southeast of the Yountville epicenter (fig. 1); both earthquakes caused significant damage in Napa, with more than $400 million in damage to private and commercial properties in 2014. The severity of structural damage caused by the 2014 earthquake resulted from a combination of building age, underlying geology, and basin depth (Boatwright and others, 2015).

Tectonic and Geological Setting

Napa Valley's basin topography began in the late Neogene when the Mendocino triple junction, the northward migration of the transition from subduction to transform motion between the Pacific and North American Plates, passed through the present latitude of Napa. Further basin evolution followed transpressional tectonic forces resulting from three main factors: a vector change in plate motion that

began approximately 8 million years ago (mega-annum or Ma) (Atwater and Stock, 2010), Sonoma Volcanic activity between 8 and 2.5 Ma (Wagner and others, 2011), and compressional deformation that extended into the Quaternary (Graymer and others, 2007). Gravity and magnetic studies by Langenheim and others (2010) suggest the WNFZ dips steeply to the southwest and is primarily a right-lateral, strike-slip fault. The westward dip-slip motion along the WNFZ appears to have resulted in the formation of the deepest part of the Napa Valley near downtown Napa (Langenheim and others, 2010; Catchings and others, 2016). The WNFZ may extend northward to the Maacama Fault, and southward, the WNFZ connects to the Franklin Fault south of Vallejo, likely extending to the Calaveras Fault; this suggests that the WNFZ and its connecting faults may be approximately 110 km long (Catchings and others, 2016). The Soda Creek Fault is mapped along the southeastern margin of the Napa Valley (fig. 1) and accommodates both horizontal and vertical motion, resulting in more than 200 m of vertical displacement (Weaver, 1949), and it may extend northward to within 2 km of the Maacama Fault near Calistoga, ~40 km northwest of downtown Napa (Langenheim and others, 2010).

Late Cenozoic volcanic rocks north of San Pablo Bay are part of a belt of volcanic fields that are younger towards the northwest (Fox and others, 1985a, 1985b). The volcanics are often fault-bounded and displaced dextrally by the fault system on the east side of San Francisco Bay (Graymer and others, 2002). The Sonoma Volcanics include rhyolite, dacite, andesite, basalt, volcanic breccia, glass, and volcanic sand and gravel that were derived from various eruptive sources in the area north of San Francisco Bay (Graymer and others, 2007; Wagner and others, 2011). Pliocene Sonoma Volcanic tuffs are commonly andesitic in composition and are found in the towns of Napa, Sonoma, and Glen Ellen (Wagner and others, 2011). These tuffs are interpreted as originating from the Napa Valley eruptive center (Sweetkind and others, 2005). The oldest of the tuffs from the Napa Valley eruptive center is the Pinole Tuff (5.4–5.2 Ma), followed by the tuff of Mark West Springs (5–4.8 Ma), Lawlor Tuff (4.84 Ma), Huichica Tuff (4.71 Ma), and lastly, Napa-Healdsburg Tuff (<4.7 Ma) (Wagner and others, 2011). The strong-motion site at Lovall Valley Loop Road is underlain by Pliocene to Miocene aged volcanic rocks (Tpmv) that have been eroded and since covered by Pleistocene alluvium (Qpa) from the southwest (fig. 2*A*).

Mesozoic rocks and sediments of the Franciscan and Great Valley complexes underlie the Sonoma Volcanics in the Napa Valley. The Franciscan Complex originated from Jurassic to Cretaceous oceanic crust and contains graywacke, argillite, basalt, serpentinite, chert, limestone, sandstone, and other high-grade metamorphic rocks (Graymer and others, 2007). The Great Valley Complex consists of Jurassic Coast Range Ophiolite and Jurassic to Cretaceous Great Valley Sequence. The Coast Range Ophiolite outcrops near Lake Berryessa and consists of serpentinite, gabbro, diabase, and basalt, whereas the Great Valley Sequence contains sandstone, shale, and conglomerate (Graymer and others, 2007). Cretaceous aged Great Valley sedimentary rocks (Ks) are seen to the east of the strong-motion instrument at Lovall Valley Loop Road (fig. 2*A*) and to the east of Broadway Street and Sereno Drive in Vallejo (fig. 2*B*), whereas the strong-motion instrument at Vallejo Fire Station is on top of the same unit (fig. 2*B*).

Quaternary surficial deposits cover much of the Napa Valley. These Quaternary deposits are primarily artificial fill, Holocene stream channel deposits, late Pleistocene to Holocene terrace deposits, late Pleistocene to Holocene alluvial fan deposits, early Pleistocene to Holocene alluvium, and bay mud (Knudsen and others, 2000; Graymer and others, 2007). Langenheim and others (2006, 2010) suggest the sedimentary basin beneath the Napa Valley is as deep as 2 km on the basis of gravity data, but recently acquired seismic-refraction data show the basin to be less than 1 km deep (Catchings and others, 2016). Quaternary sediments and alluviums appear in low-lying areas and along creeks near the

strong-motion instrument at Lovall Valley Loop Road (fig. 2*A*) and adjacent to the Napa River in Vallejo (fig. 2*B*).

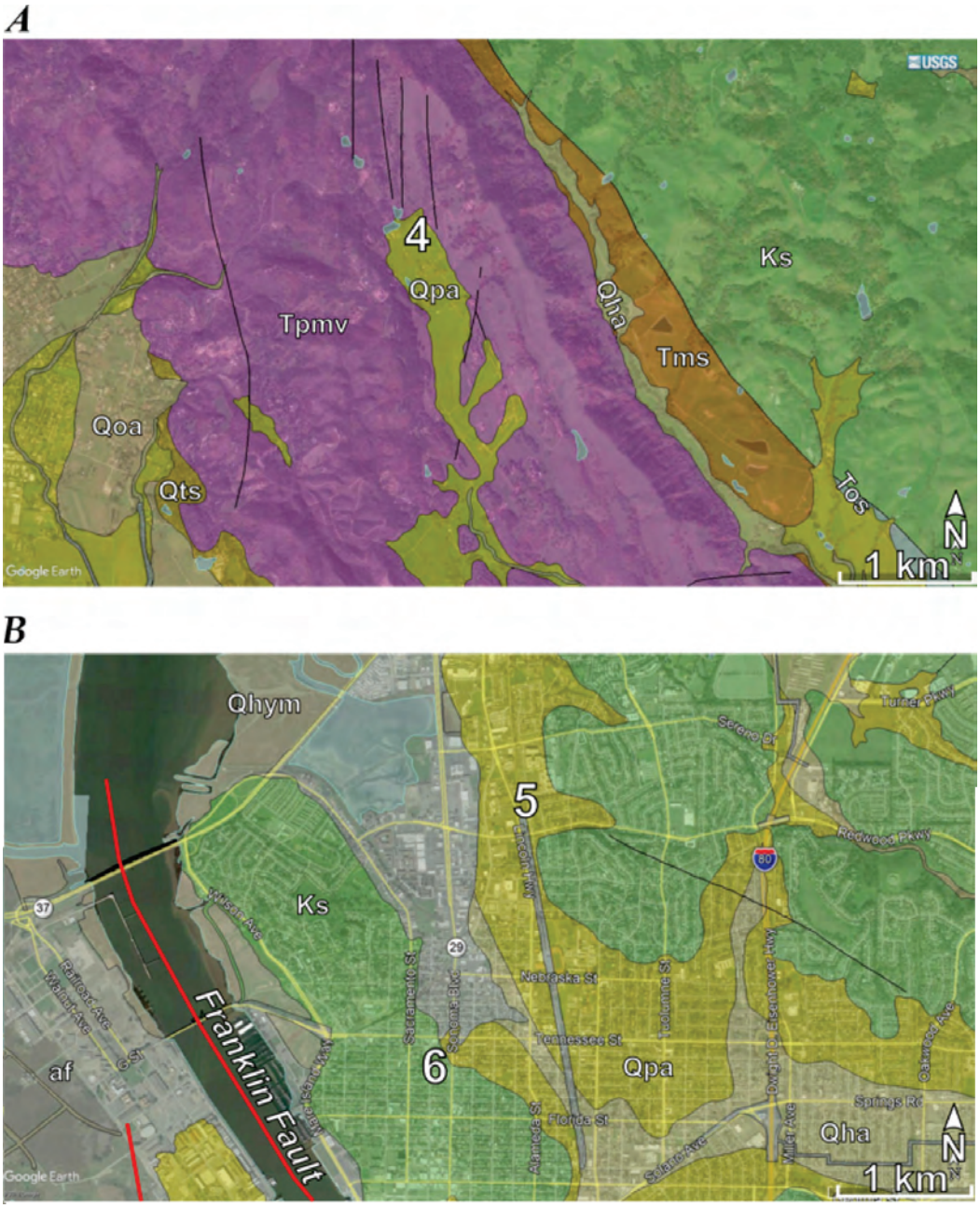

Figure 2. Google Earth images of parts of Napa and Solano Counties, California, overlain with geologic maps. *A*, Map (modified from Graymer and others, 2007) of our study area at Lovall Valley Loop Road (4) in Napa County. Cretaceous Great Valley sedimentary rocks (Ks), Sonoma Volcanics (Tpmv), Miocene sedimentary rocks (Tms), early Pleistocene sediments (Qts), a sliver of Oligocene sedimentary rocks (Tos) in the southwest, and Quaternary surficial deposits (Qoa, Qha, Qpa). Black lines denote unnamed Quaternary-active faults. *B*, Map (modified from Graymer and others, 2007) of our study area in Vallejo in Solano County, at Broadway Street and Sereno Drive (5) and at Vallejo Fire Station (6) in Vallejo, California. Cretaceous Great Valley sedimentary rocks (Ks) and Quaternary surficial deposits (Qha, Qhym, Qpa, af). Black line denotes unnamed Quaternary-active fault (possible Southampton Fault). See figure 1 for locations of maps. km, kilometer.

August 24, 2014, M_W 6.0 South Napa Earthquake

The epicenter of the South Napa earthquake was located near American Canyon, approximately 13 km southeast of the strong-motion instrument on Lovall Loop Road in Napa and 10 to 11 km northwest of the two strong-motion stations in Vallejo (fig. 1). The earthquake caused an estimated $400 million in damage to private and commercial properties in the City of Napa (County of Napa, 2014), and more than $5 million in damages to the City of Vallejo (Fimrite, 2014). The distribution of red- and yellow-tagged structures in the City of Napa suggests damage highly correlated with buildings that predate 1950; however, damage patterns do not apparently correlate with the underlying geology in Napa (Boatwright and others, 2015). More than 450 structures were red- or yellow-tagged in Vallejo after the earthquake, with notable damage occurring on Mare Island and in downtown Vallejo (City of Vallejo, 2014). Postearthquake field mapping identified ~12.5 km of surface rupture distributed along subparallel strands of the WNFZ (Brocher and others, 2015; Delong and others, 2015). Overall, more than 30 km of surface deformation was observed from a combination of field observations and geodesy (Delong and others, 2015). Measurements based on alignment arrays and offset features identified as much as 50 centimeters (cm) of coseismic slip in the northern section of the rupture and as much as 50 cm of postseismic slip in the southern section approximately one year after the event (Morelan and others, 2015; Lienkaemper and others, 2016). The amount of coseismic and postseismic slip was unusually large for strike-slip earthquakes in California with similar hypocentral depths and magnitudes (Brocher and others, 2015). Earthquake relocation suggests the mainshock and many of the aftershocks occurred near the intersection of two fault planes, one which dips southwest (mainshock) and another northeast (Brocher and others, 2015). Fault-zone trapped waves (FZTWs; also known as guided waves) suggest a low-velocity waveguide along the WNFZ that is at least 400 m in width and 5 to 6 km in depth (Catchings and others, 2016; Li and others, 2016). Furthermore, guided-wave studies suggest the greatest reduction in velocity occurs within approximately 200 m of the WNFZ at much shallower depths. The overall length of the WNFZ is not well understood; however, postearthquake studies using guided waves (Catchings and others, 2016; Li and others, 2016) and strong-motion data (Baltay and Boatwright, 2015) suggest connectivity between the WNFZ and Franklin Fault, which has been mapped southward to the Calaveras Fault. Furthermore, gravity (Langenheim and others, 2010) and guided-wave (Catchings and others, 2016) studies suggest the WNFZ may extend northward to the Maacama Fault. Therefore, the combined length of the WNFZ and the Franklin Fault may be nearly 110 km in length (Catchings and others, 2016).

Seismic Survey

Data Acquisition

In May 2015, we acquired high-resolution P- and S-wave seismic data along linear profiles near strong-motion recording stations in Napa (fig. 1) that recorded high PGAs during the 2014 South Napa earthquake. As dictated by location and accessibility, we generated P-wave data using one of three active sources—a 226-kilogram (kg) accelerated weight drop (AWD), a 3.5-kg sledgehammer/steel-plate combination, and 400-grain Betsy-Seisgun™ blasts in ~0.4-m-deep boreholes. S-wave sources were generated by horizontally striking an aluminum block with a 3.5-kg sledgehammer. Along each profile, we deployed collocated (1-m offset) P-wave sources and 40-hertz (Hz), vertical-component geophones every 3 meters to record P-wave data. We then replaced the vertical-component geophones with 4.5-Hz, horizontal-component geophones and collocated S-wave sources (1-m offset) with the geophones to record S-wave data. To record the data (Goldman and others, 2018), we used as many as

two 60-channel, Geometrics StrataView RX-60™ seismographs that were connected to the geophones via refraction cables.

Profile N15-4—Lovall Valley Loop Road (NCSN N019B)

Profile N15-4 was oriented northwest to southeast on a private property on Lovall Valley Loop Road in Napa County (fig. 3). The strong-motion recording station (NCSN N019B) was housed inside a residential building, approximately 20 m from the seismic profile. We deployed 67 P- and S-wave geophones along profile N15-4, with 3-m spacing between each geophone. To generate P-waves, we primarily used the Betsy-Seisgun™; however, we used the 226-kg AWD where a "seisgun" might damage buried irrigation pipes. To generate S-waves, we used a 3.5-kg sledgehammer/aluminum block combination. The elevation of the geophones along our array varied by approximately 2.4 m over the 198-m length of the seismic profile (Goldman and others, 2018).

Figure 3. Google Earth satellite image of seismic profile N15-4 on private property on Lovall Valley Loop Road in Napa County, California. Red line represents the seismic profile from northwest to southeast. Yellow star represents the approximate location (meter 115 on seismic profile) of the strong-motion station housed inside the private residence. NW, northwest; SE, southeast; m, meters.

Profile N15-5—Broadway Street and Sereno Drive in Vallejo (CGS 68294)

Profile N15-5 was oriented southeast to northwest on Alameda Street and extended to the Kaiser Permanente hospital parking lot (fig. 4). The strong-motion station (CGS 68294) was located

approximately 30 m west of the seismic profile. We deployed 60 P- and S-wave geophones along profile N15-5, with 3-m spacing between each geophone. To generate P-waves, we used the 226-kg AWD where there was sufficient room to operate the AWD, and we switched to the 3.5-kg sledgehammer/steel-plate combination source where there was not. To generate S-waves, we used the sledgehammer/aluminum block combination. The geophone elevation varied by approximately 6.4 m over the 177-m length of the linear array (Goldman and others, 2018).

Figure 4. Google Earth satellite image of seismic profile N15-5 at Kaiser Permanente and Alameda Street in Vallejo, California, near the Broadway Street and Sereno Drive strong-motion station. Red line represents the seismic profile from northwest to southeast. Yellow star represents the approximate location (meter 109 on seismic profile) of the strong-motion station at the Kaiser Permanente parking lot. NW, northwest; SE, southeast; m, meters.

Profile N15-6.1 and N15-6.2—Vallejo Fire Station (NSMP 1759)

Profile N15-6.1 was oriented south to north on Marin Street, and profile N15-6.2 was oriented west to east on Overland Alley (fig. 5). The strong-motion station (NSMP 1759) was housed inside Vallejo Fire Station, approximately 20 m from the seismic profiles. We deployed 30 P- and S-wave geophones along profile N15-6.1 and 29 P- and S-wave geophones along profile N15-6.2, with 3-m spacing between each geophone along both profiles. As with profile N15-5, we used the 226-kg AWD as our P-wave source, collocated with each geophone. We used the 3.5-kg sledgehammer/aluminum block combination as our S-wave source. The geophone elevation varied by approximately 3.5 m over

the 87-m length of profile N15-6.1 and 3.3 m over the 84-m length of profile N15-6.2 (Goldman and others, 2018).

Figure 5. Google Earth satellite image of seismic profiles N15-6.1 and N15-6.2 adjacent to Vallejo Fire Station in Vallejo, California. Red lines represent the seismic profile from north to south on Marin Street and from west to east on Overland Alley. Yellow star represents the approximate location (meter 64 and 17 on seismic profiles) of the strong-motion station housed inside the fire station. N, north; S, south; W, west; E, east; m, meters.

Seismic-Imaging Methods

We used the shoot-through seismic-acquisition method, which allowed us to develop two-dimensional P-wave refraction tomography models, S-wave refraction tomography models, and multi-channel analysis of surface waves (MASW; Rayleigh-wave, $MASRW$; Love-wave, $MASLW$) models from the recorded data.

Refraction-Tomography Modeling

We used the refraction tomography method to model subsurface P- and S-wave velocities. We first processed the seismic data (Goldman and others, 2018) with ProMax™, a commercial seismic-processing software package. First-arrivals from P- and S-wave shot gathers were evaluated and inverted to develop seismic-velocity models using the algorithm of Hole (1992). The algorithm uses finite differences (solving the eikonal equation) to compute first-arrival travel times from the source to the receiver in a starting velocity model. It then uses back-projection of the data misfits to update the model. This process is repeated in iterative steps until a satisfactory misfit among observed and calculated first-arrivals is obtained. We developed P- and S-wave starting models based on one-dimensional (1D) velocities derived from the shot gathers and parameterized our initial 2D models into

3-m by 3-m vertical and horizontal grids based on geophone and shot spacing. In modeling, we used 20 to 30 iterations to develop the final velocity models.

Profile N15-4 consisted of 4,422 traces (66 shots and 67 geophones) for the P-wave dataset and 4,489 traces (67 shots and 67 geophones) for the S-wave dataset. Our P- and S-wave datasets for profiles N15-5, N15-61, and N15-62 consisted of 3,480 traces (58 shots and 60 geophones), 870 traces (29 shots and 30 geophones), and 841 traces (29 shots and 29 geophones), respectively. Generally, the large number of first arrivals used for each profile allows for a well-determined velocity model.

Multichannel Analysis of Surface Waves (MAS_RW) and Love Waves (MAS_LW)

Our data acquisition method allows us to use Rayleigh and Love waves to develop 2D S-wave velocity models from P- and S-wave data, respectively, using the MASW method. We used both vertical- and horizontal- component geophones along each profile, which allows for the ability to analyze both Rayleigh and Love waves for V_S. The MASW method takes advantage of the dispersive nature of surface waves to infer shear-wave velocities in the shallow subsurface (Park and others, 1999; Xia and others, 2000). Surface waves are often used in geotechnical site investigations and other shallow subsurface studies (Pujol, 2003; Ivanov and others, 2003, 2013; Miller and others, 1999; Park, 2000, 2013; Odum and others, 2013; Yong and others, 2013). We use the Common Mid-Point Cross-Correlation (CMPCC) method, developed by Hayashi (2003) and Hayashi and Suzuki (2004), to construct phase velocity (dispersion) curves. We used surface-wave modeling software (SeisImagerSW™ by Geometrics) to iteratively invert the dispersion curves using a non-linear, least-squares approach. Depth is calculated based on one-third of the wavelength, which is determined from dividing the phase velocity by frequency (Hayashi and others, 2016; Geometrics, Inc., 2016). The inversion results of 1D models are combined to construct two-dimensional S-wave velocity models. We varied the number of shots used for the CMPCC method (all shots versus end shots), and we generated additional 2D S-wave velocity models for comparison.

To prepare the data for modeling, P- and S-wave datasets were first converted from SEGY to SEG2 format. We used SeisImagerSW™ to construct CMPCC gathers that were then used to calculate phase velocities. To ensure fundamental modes were correctly picked by SeisImagerSW™, we examined and manually adjusted the picks before inversion of the dispersion curves. The starting models (table 2) assume 30-m depth and 10-layers with thickness increasing with depth (Hayashi and others, 2016; Geometrics, Inc., 2016); inverted results may show models at less than or greater than 30-m depth.

In general, depth of penetration for a seismic-refraction survey is approximately 1/3 to 1/5 of the length of the geophone spread (Reynolds, 2011), and we found that depth of penetration for MAS_RW models were approximately half of that for MAS_LW models at the three sites due to higher frequency (40 Hz) geophones used for P-wave data acquisition (Ivanov, 2008).

Table 2. Parameters for inversion of initial models in multichannel analysis of surface waves for both Rayleigh and Love waves for seismic profiles in Napa and Solano Counties, California.

Seismic profile	Depth, in meters	Number of layers	Layer thickness		Inversion
			Gradient	Bottom layer multiplier	
N15-4	40	15	0.5	3	20
N15-5	40	15	0.5	3	20
N15-6.1	30	10	0.5	3	20
N15-6.2	30	10	0.5	3	20

V_{S30} Calculations

V_{S30} is the time-averaged V_S to a depth of 30 m (International Code Council, Inc., 2009); it is a parameter used to account for site amplification in ground-motion models and to characterize site conditions in ground-motion prediction equations (GMPEs). V_{S30} is also a parameter used for establishing building codes for seismic safety (Building Seismic Safety Council, 2003). Previous study by Boore and others (2011) shows close correlation between V_{S20} and V_{S30} in California. As a result, near the ends of our models, where velocities were not determined to 30 m depth, we calculated V_{S20}. V_{SZ} given Z is less than 30 m depth is calculated (International Code Council, Inc., 2009) using interpolated shear-wave velocities.

Results

We present velocity results by site to evaluate S-wave velocity structures and V_{S30} from the three methods—S-wave refraction tomography, MAS_LW, and MAS_RW. Appendix 1 shows dispersion curves for Rayleigh (left column) and Love (right column) waves at locations nearest to the strong-motion station at each seismic profile. We varied the number of shots used in the $MAS_{R,L}W$ analysis (CMPCC constructed using all shots in the profile, CMPCC constructed using two end shots, and a single shot gather nearest to the strong-motion station), which affected the distinctness of the fundamental modes from higher modes in the dispersion curves. Appendix 2 shows dispersion curve picks for Rayleigh (red triangles) and Love (blue circles) waves along the entire length of the profiles using various number of shots for $MAS_{R,L}W$ analysis. Dispersion curve picks show variability across the full length of the profiles and differences between Rayleigh and Love waves. Table 3 and figures in appendix 3 show V_{S30} values and 1D velocity-depth profiles nearest to the strong-motion recording stations. Velocities are not well-constrained when few dispersion data are available, and V_{S30} values are determined from interpolated velocities.

Table 3. Time-averaged shear-wave velocity to a depth of 30 meters (V_{S30}) nearest to the strong-motion recording station at each of the three sites in Napa County and in Vallejo in Solano County, California.

[See appendix 3 for one-dimensional velocity-depth profiles that correspond to the V_{S30} shown in this table. *represents time averaged V_{SZ} given Z less than 30 meters depth (International Code Council, Inc., 2009). NCSN, Northern California Seismic Network; CGS, California Geological Survey; NSMP, National Strong Motion Project; RMSE, root-mean-square error; 1D, one dimensional; 2D, two dimensional; MAS_LW, multichannel analysis of surface waves for Love waves; MAS_RW, multichannel analysis of surface waves for Rayleigh waves; NA, not applicable; m/s, meters per second]

	N15-4 NCSN N019B		N15-5 CGS 68294		N15-6.1 NSMP 1759		N15-6.2 NSMP 1759	
	V_{S30} (m/s)	RMSE (m/s)	V_{S30} (m/s)	RMSE (m/s)	V_{S30} (m/s)	RMSE (m/s)	V_{S30} (m/s)	RMSE (m/s)
S-wave refraction tomography	767	NA	673	NA	542*/583	NA	493*/561	NA
All shot gathers								
2D MAS_LW	711	6.4	455	44.4	567*	53.2	490	17.2
2D MAS_RW	490	5.7	533	16.0	505*	15.5	442*	25.4
End shots								
2D MAS_LW	705	11.6	567	42.6	510	42.0	478	47.5
2D MAS_RW	525*	12.0	696*	17.6	557*	8.7	467	21.1
Single shot gather								
1D MAS_LW	669	15.4	620	8.8	552	7.2	435	8.1
1D MAS_RW	485	7.3	678	4.1	534	7.5	372	4.0

Profile N15-4—Lovall Valley Loop Road (NCSN N019B)

P-wave Tomography (V_P) Model

Along the seismic profile near Lovall Valley Loop Road, P-wave velocities (compressional wave velocity, V_P) range from 750 m/s in the near surface to about 2,000 m/s at 32 m depth (fig. 6). Velocity contours from the surface to 15 m depth exhibit a broad peak, whereby the apex is located between distance meters 50 and 100 of the profile. The 1,500 m/s contour, which has been shown to coincide with the top of groundwater in other studies (Catchings and others, 2001, 2006, 2013, 2017a, b) is located at approximately 17 m depth.

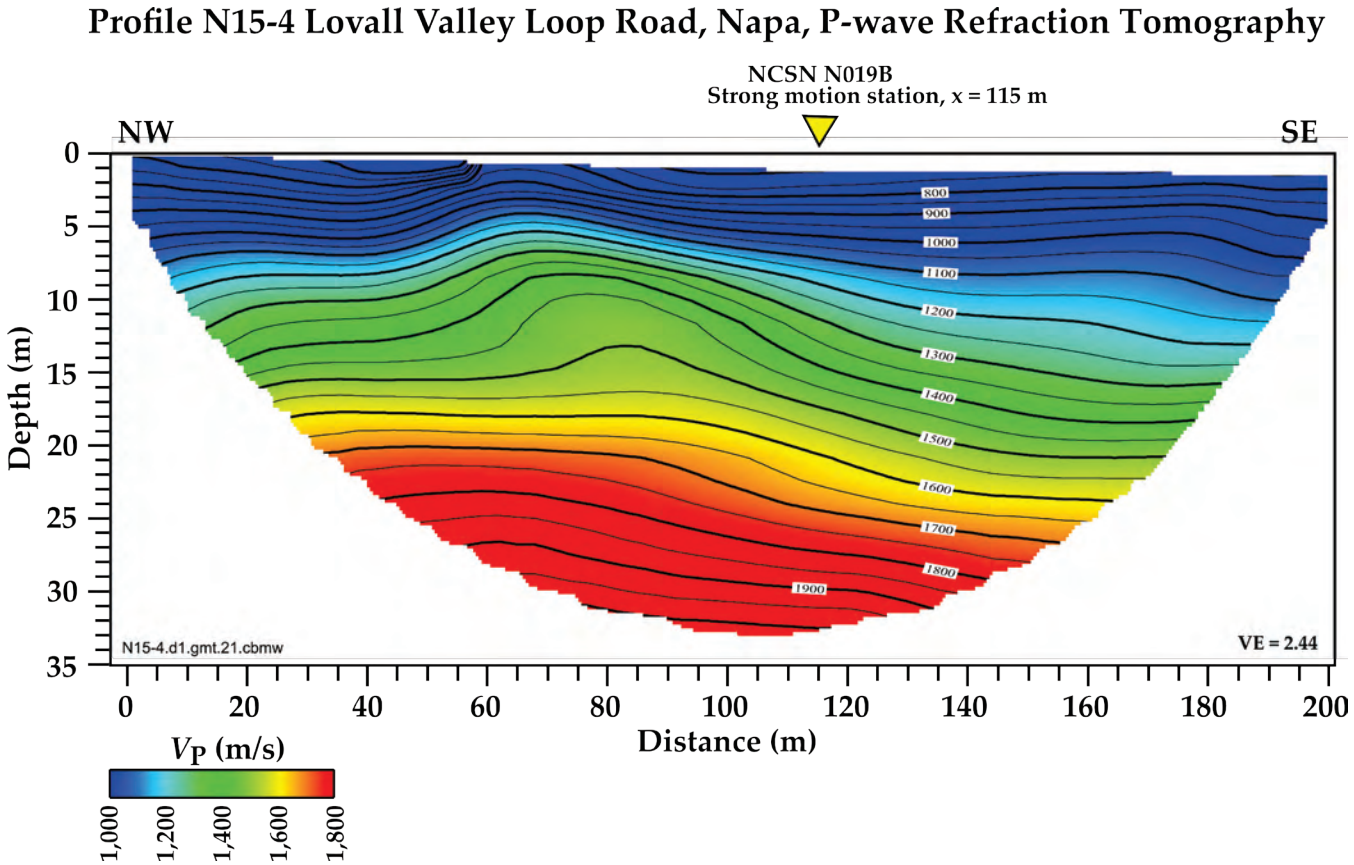

Figure 6. Illustration showing P-wave refraction tomography model for profile N15-4 on Lovall Valley Loop Road private property in Napa County, California. P-wave velocities range from about 750 meters per second (m/s) in the near surface to 2,000 m/s at 32 m depth. Velocity contours show undulating structures in the upper 20 m of the model. Strong-motion recording station is nearest to distance meter 115 of our seismic profile. NCSN, Northern California Seismic Network; NW, northwest; SE, southeast; VE, vertical exaggeration; V_P, P-wave velocity.

S-wave Tomography (V_S) Model

S-wave velocities (V_S) determined from tomography range from 400 m/s in the near surface to about 1,200 m/s at 55 m depth (fig. 7). Variation in V_S in the upper 40 m of the seismic profile suggests probable lithological variations. Velocity contours from the surface to 40 m depth also exhibit a broad peak, whereby the apex is located between distance meters 30 and 120 of the profile. From S-wave tomography, we calculated V_{S30} to be 767 m/s at the strong-motion station near distance meter 115.

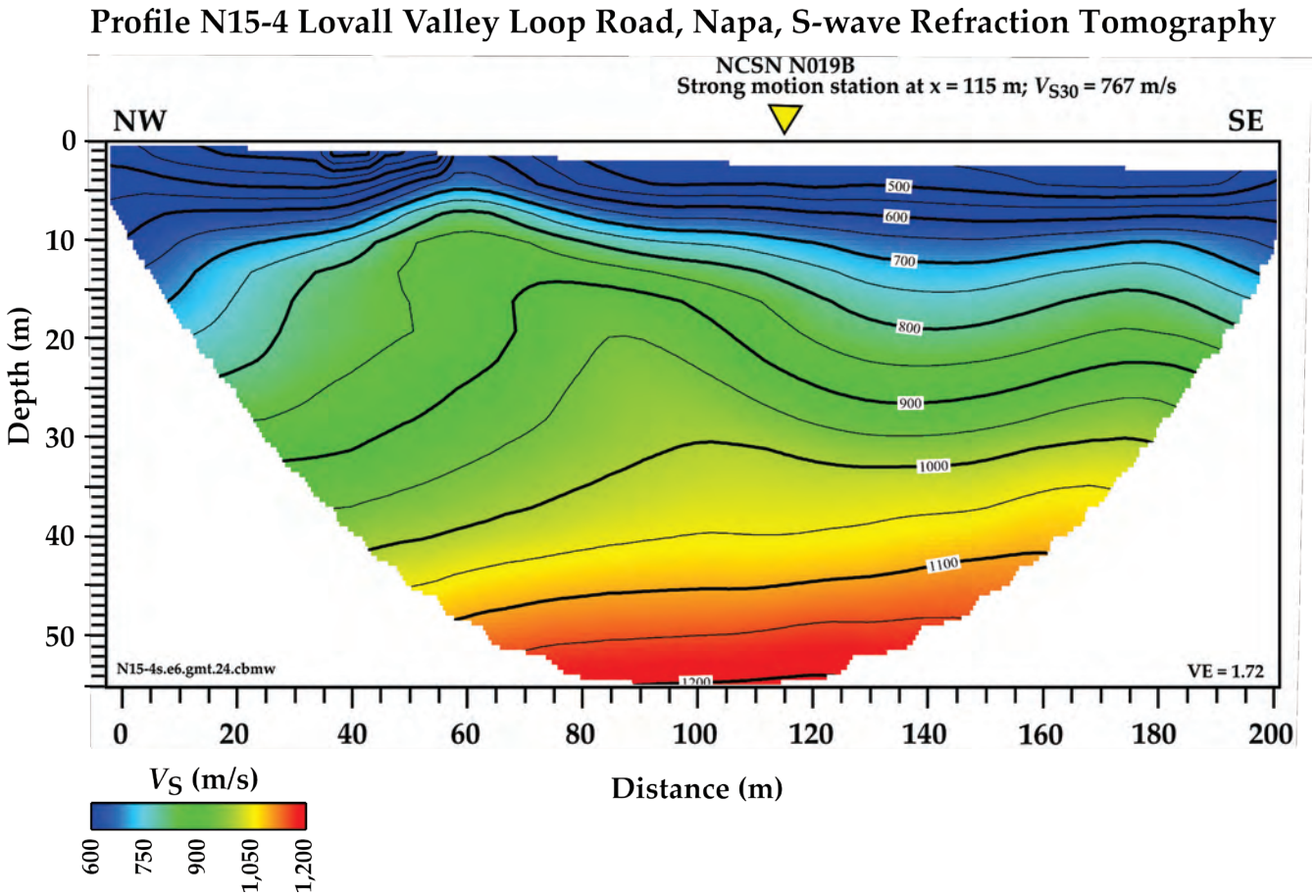

Figure 7. Illustration showing S-wave refraction tomography model for profile N15-4 on Lovall Valley Loop Road private property in Napa, California. S-wave velocities range from 400 meters per second (m/s) in the near surface to about 1,200 m/s at 55 meters (m) depth. Strong-motion recording station is nearest to distance meter 115 of our seismic profile, where we calculated V_{S30} to be 767 m/s based on refraction tomography. NCSN, Northern California Seismic Network; NW, northwest; SE, southeast; VE, vertical exaggeration; V_S, shear-wave velocity; V_{S30}, time-averaged shear-wave velocity in the upper 30 meters of the subsurface.

MASLW 2D S-wave Velocity Model

The Love wave dispersion curves (appendix 1, right column), which represent the location (meter 115) on our seismic profile nearest to the strong-motion recording station, show adjusted picks (red circles) for the fundamental mode at phase velocities between 600 and 900 m/s and at frequencies between 4 and 26 Hz. Love wave dispersion curve picks across the entire length of the profile (appendix 2, blue circles) vary between the number of shots used during CMPCC construction (all shots along the profile versus two end shots) and at each single shot gather along the profile. Table 3 and figures in appendix 3 show V_{S30} and 1D velocity-depth models near the strong-motion station; these results come from using varying MASLW methods: 2D MASLW (all shots; V_{S30}=711 m/s), 2D MASLW (end shots; V_{S30}=705 m/s), and at a shot gather located at distance meter 115 (V_{S30}=669 m/s), the closest location to the strong-motion recorder.

Along the seismic profile near Lovall Valley Loop Road, 2D MASLW-determined V_S ranges from 400 m/s in the near surface to about 925 m/s at approximately 50 m depth (fig. 8). A broad peak does not appear in the 2D MASLW model; instead, the velocity contours show a low-velocity region at depths between approximately 15 and 35 m between distance meters 60 and 180.

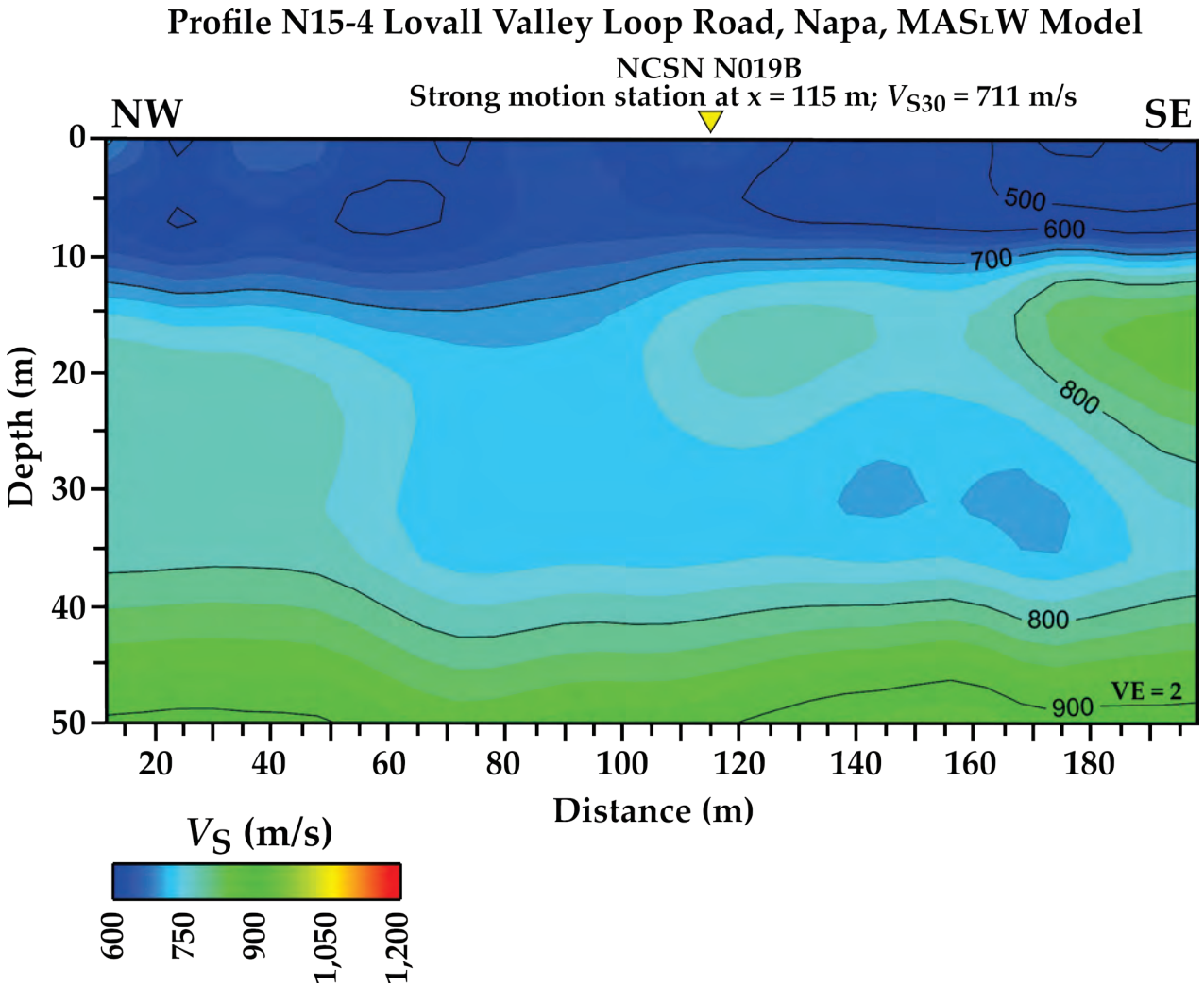

Figure 8. Illustration showing two-dimensional MASLW (multichannel analysis of surface waves for Love waves) shear-wave velocity model for profile N15-4 on Lovall Valley Loop Road private property in Napa County, California. S-wave velocities range from 400 meters per second (m/s) in the near surface to about 925 m/s at approximately 50 meters (m) depth. Strong-motion recording station is nearest to distance meter 115 of our seismic profile, where we calculated time-averaged shear-wave velocity in the upper 30 meters of the subsurface (V_{S30}) to be 711 m/s based on MASLW. NCSN, Northern California Seismic Network; NW, northwest; SE, southeast; VE, vertical exaggeration; V_S, shear-wave velocity.

MASRW 2D S-wave Velocity Model

The Rayleigh-wave dispersion curves (appendix 1, left column), which represent the location (meter 115) on our seismic profile nearest to the strong-motion recording station, show adjusted picks (red circles) for the fundamental mode at phase velocities between 400 and 600 m/s and at frequencies between 8 and 24 Hz. The fundamental modes are distinct from higher modes in the dispersion curves. Rayleigh wave dispersion curve picks across the entire length of the profile (appendix 2, red triangles) vary between the number of shots used during CMPCC construction (all shots along the profile versus two end shots) and at each single shot gather along the profile. Table 3 and figures in appendix 3 show V_{S30} and 1D velocity-depth results near the strong-motion station; the results come from using varying MASRW methods: 2D MASRW (all shots; V_{S30}=490 m/s), 2D MASRW (end shots; V_{S30}=525 m/s), and

at a shot gather located at distance meter 115 (V_{S30}=485 m/s), the closest location to the strong-motion recorder.

Along the seismic profile near Lovall Valley Loop Road, 2D MASRW-determined V_S ranges from 250 m/s in the near surface to about 700 m/s at 30 m depth (fig.9). The model suggests little horizontal variation in V_S along the seismic profile and does not show the broad peak seen in the tomography models. Generally, the velocities determined from the MASRW technique are lower than those determined from S-wave refraction tomography and from MASLW.

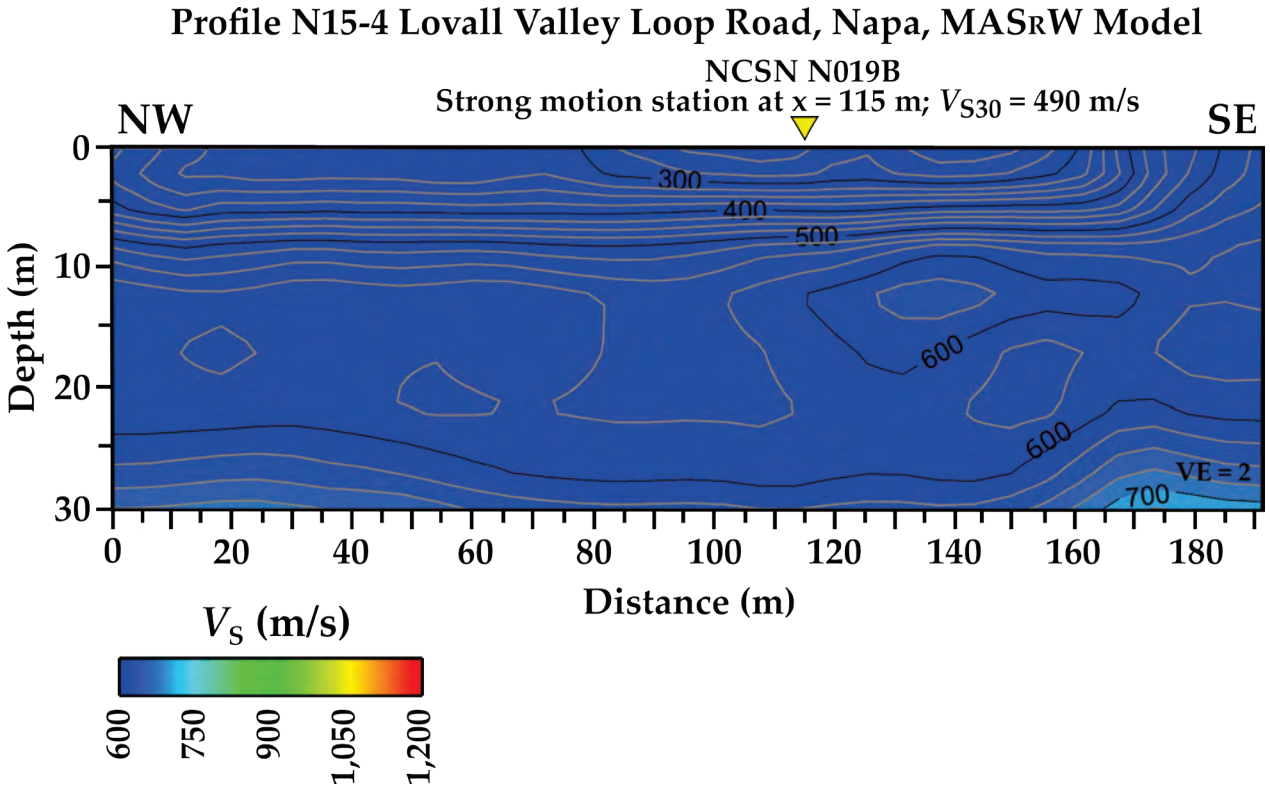

Figure 9. Illustration showing two-dimensional MASRW (multichannel analysis of surface waves for Rayleigh waves) shear-wave velocity model for profile N15-4 on Main Street in downtown Napa, California. S-wave velocities range from 250 meters per second (m/s) at the near surface to about 700 m/s at approximately 30 m depth. Strong-motion recording station is nearest to distance meter 115 of our seismic profile, where we calculated time-averaged shear-wave velocity in the upper 30 meters of the subsurface (V_{S30}) to be 490 m/s based on MASRW. NCSN, Northern California Seismic Network; NW, northwest; SE, southeast; VE, vertical exaggeration; V_S, shear-wave velocity; V_{S30}, time-averaged shear-wave velocity in the upper 30 meters of the subsurface.

Profile N15-5—Broadway Street and Sereno Drive in Vallejo (CGS 68294)

P-wave Tomography (V_P) Model

Along our seismic profile near Broadway Street and Sereno Drive in Vallejo, P-wave velocities range from 960 m/s in the near surface to about 3600 m/s at approximately 27 m depth (fig. 10). Velocity contours form a broad peak in the bottom 30 m of the model from distance meters 10 to 170 m of the profile. The model's velocity contours show a slight peak shape at the northern end of the profile from the surface to approximately 20 m depth. In general, velocity contours show a slight undulating

pattern in the upper 20 m of the profile, becoming significant below 20 m depth. The 1,500 m/s velocity contour (top of ground water) is located approximately 11 to 16 m below the surface.

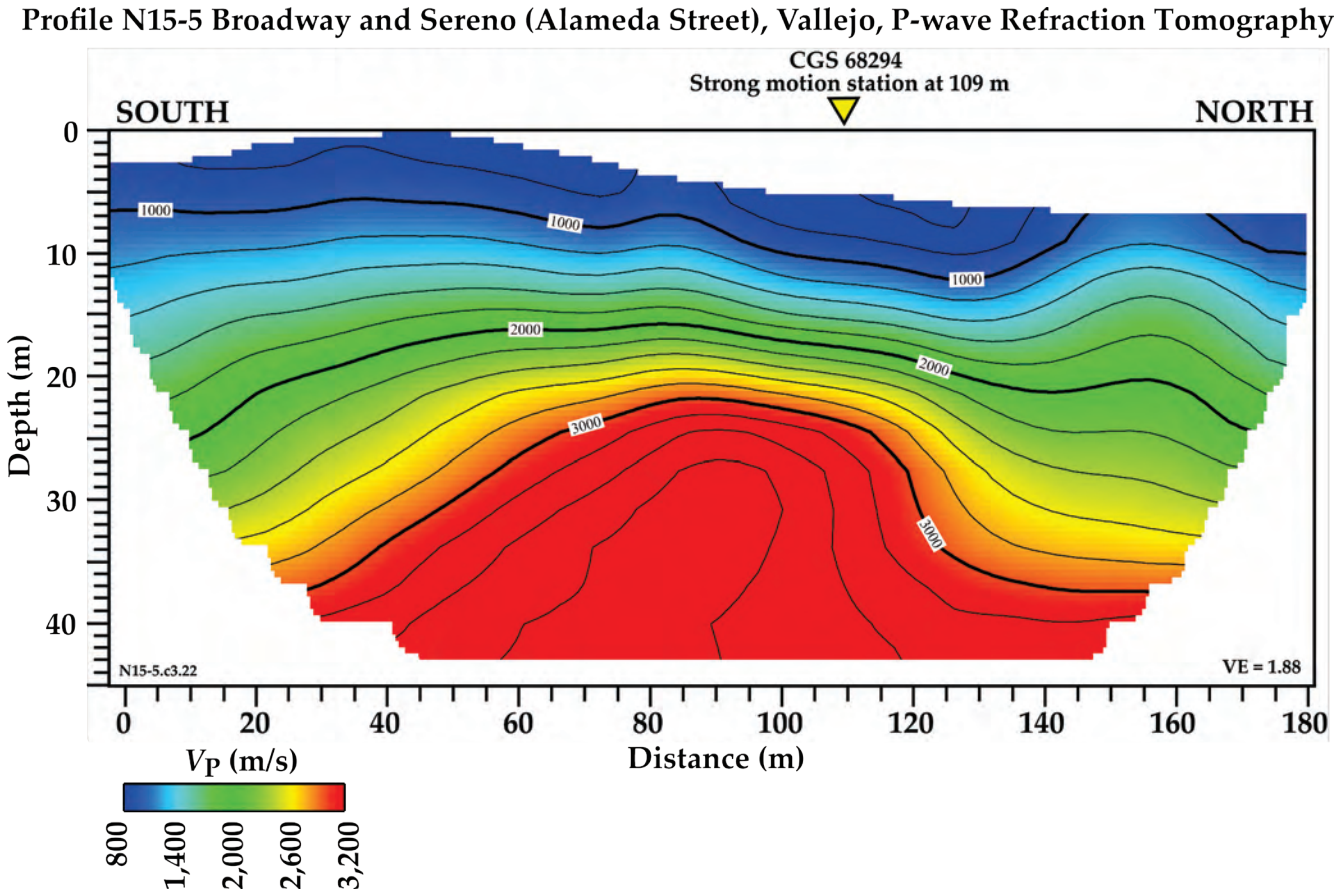

Figure 10. Illustration showing P-wave refraction tomography model for profile N15-5 on Alameda Street and Kaiser Permanente hospital parking lot in Vallejo, California, near the Broadway Street and Sereno Drive strong-motion station. P-wave velocities range from 960 meters per second (m/s) at the near surface to about 3,600 m/s at depth. Strong-motion recording station is nearest to distance meter 109 of our seismic profile. CGS, California Geological Survey; VE, vertical exaggeration; V_P, P-wave velocity; m, meters.

S-wave Tomography (V_S) Model

V_S determined from tomography ranges from 300 m/s in the near surface to more than 1,000 m/s at 40 m depth (fig. 11). Velocity contours form a broad, peak shape below approximately 13 m depth between distance meters 15 and 130. The peak shape dips to the south, similar to that seen in the P-wave refraction tomography model.

From refraction tomography, we calculated V_{S30} at the strong-motion recording station (meter 109) to be 673 m/s.

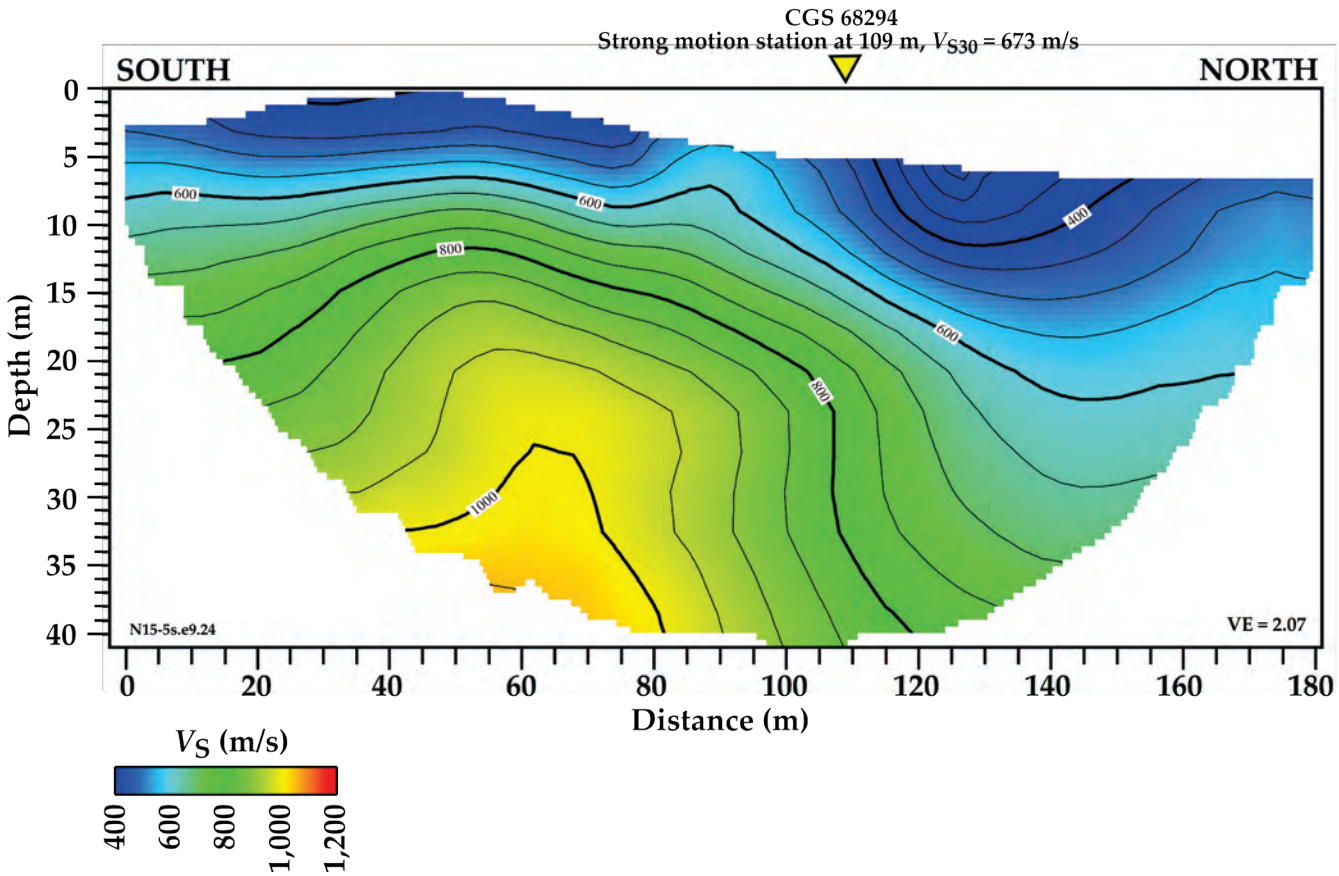

Figure 11. Illustration showing S-wave refraction tomography model for profile N15-5 on Alameda Street and Kaiser Permanente hospital parking lot in Vallejo, California, near the Broadway Street and Sereno Drive strong-motion station. S-wave velocities range from 300 meters per second (m/s) at the near surface to more than 4,000 m/s at depth. Strong-motion recording station is nearest to distance meter 109 of our seismic profile, where we calculated time-averaged shear-wave velocity in the upper 30 meters of the subsurface (V_{S30}) to be 673 m/s based on refraction tomography. CGS, California Geological Survey; VE, vertical exaggeration; V_S, shear-wave velocity; m, meters.

MASLW 2D S-wave Velocity Model

The Love wave dispersion curves (appendix 1, right column), which represent the location (meter 109) on our seismic profile nearest to the strong-motion recording station, show adjusted picks (red circles) for the fundamental mode at phase velocities between 200 and 1,300 m/s and at frequencies between 4 and 23 Hz. Love wave dispersion curve picks across the entire length of the profile (appendix 2, blue circles) vary between the number of shots used during CMPCC construction (all shots along the profile versus two end shots) and at each single shot gather along the profile. Table 3 and figures in appendix 3 show V_{S30} and 1D velocity-depth results near the strong-motion station; the results come from using varying MASLW methods: 2D MASLW (all shots; V_{S30}=455 m/s), 2D MASLW (end shots; V_{S30}=567 m/s), and at a shot gather located at distance meter 109 (V_{S30}=620 m/s), the closest location to the strong-motion recorder.

Along our seismic profile near Broadway Street and Sereno Drive, 2D MASLW-determined V_S ranges from 300 m/s in the near surface to more than 1000 m/s below 50 m depth (fig. 12). Velocity contours show a peak shape below 10 m depth between distance meters 12 and 80; the peak shape does

not dip to the south as seen in the refraction tomography models. The apex of the peak-shaped velocity structure, as best represented by the 800-m contour interval, occurs at distance meter 30, which is approximately 30 m south of the apex observed in the S-wave refraction tomography model. The lowest shear wave velocities (<400 m/s) are in the upper 10 m of the subsurface between distance meters 80 and 167. Generally, shear wave velocities decrease towards the northern end of the profile.

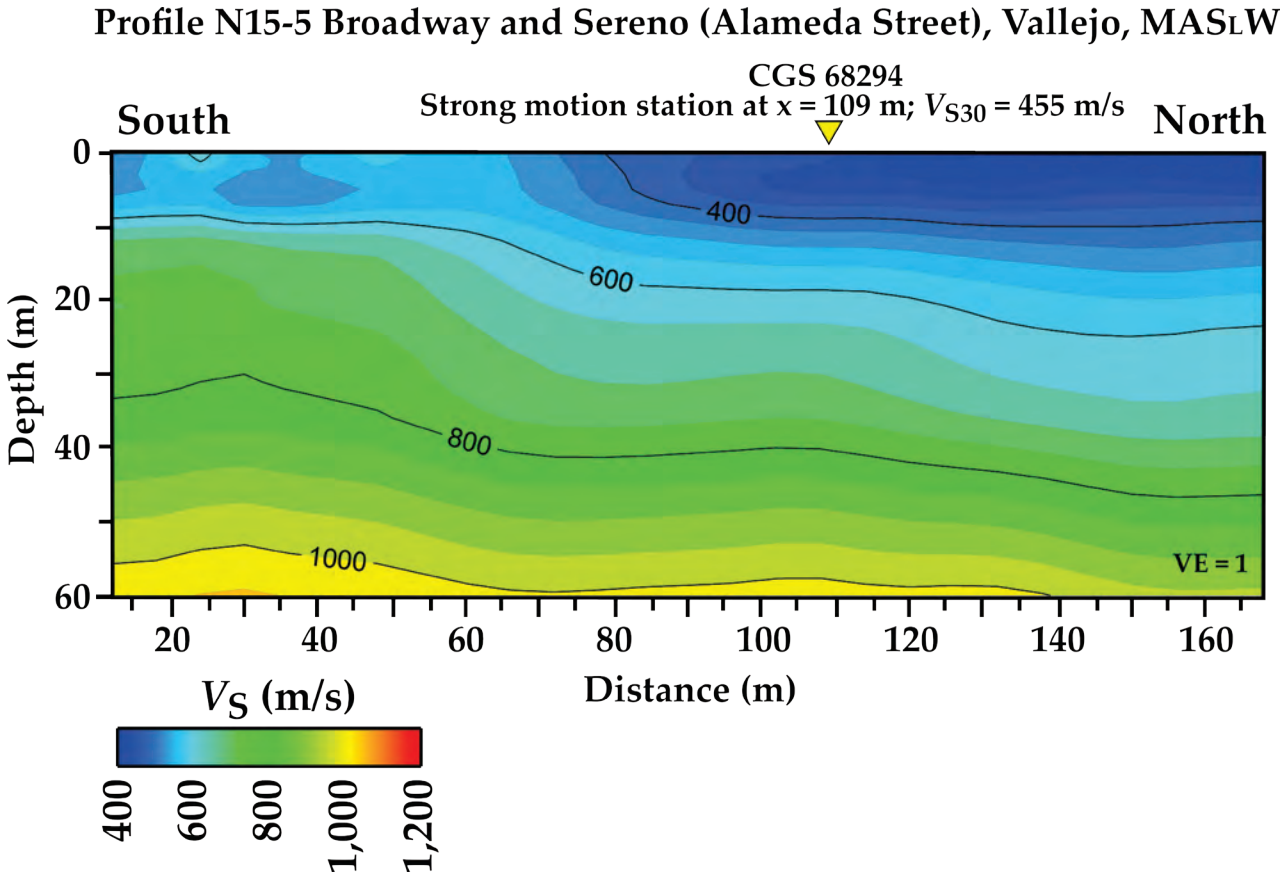

Figure 12. Illustration showing two-dimensional MASLW (multichannel analysis of surface waves for Love waves) shear-wave velocity model for profile N15-5 on Alameda Street and Kaiser Permanente hospital parking lot in Vallejo, California, near the Broadway Street and Sereno Drive strong-motion station. S-wave velocities range from 300 meters per second (m/s) at the near surface to more than 1,000 m/s below 50 meters (m) depth. Strong-motion recording station is nearest to distance meter 109 of our seismic profile, where we calculated time-averaged shear-wave velocity in the upper 30 meters of the subsurface (V_{S30}) to be 455 m/s based on MASLW. CGS, California Geological Survey; VE, vertical exaggeration; V_S, shear-wave velocity.

MASRW 2D S-wave Velocity Model

The Rayleigh wave dispersion curves (appendix 1, left column), which represent the location (meter 109) on our seismic profile nearest to the strong-motion recording station, show adjusted picks (red circles) for the fundamental mode at phase velocities between 400 and 900 m/s and at frequencies between 4 and 28 Hz. The fundamental modes are distinct from higher modes in the dispersion curves. Rayleigh wave dispersion curve picks across the entire length of the profile (appendix 2, red triangles) vary between the number of shots used during CMPCC construction (all shots along the profile versus two end shots) and at each single shot gather along the profile. The varying topography at the site may have caused the fundamental mode to slightly merge with higher modes in the dispersion curves. Table

3 and figures in appendix 3 show V_{S30} and 1D velocity-depth results near the strong-motion station; the results come from using varying MASRW methods: 2D MASRW (all shots; V_{S30}=533 m/s), 2D MASRW (end shots; V_{S30}=696 m/s), and at a shot gather located at distance meter 109 (V_{S30}=678 m/s), the closest location to the strong-motion recorder.

Along the seismic profile near Broadway Street and Sereno Drive, V_S ranges from 300 m/s in the near surface to more than 800 m/s at 30 m depth (fig. 13). Depth of resolution for the MASRW model is 30 m, which is half of the MASLW model. Velocity contours show a peak shape below 10 m depth between distance meters 40 and 100; the peak-shaped structure does not dip to the south as seen in the refraction tomography models. The apex of the peak-shaped velocity structure, as best represented by the 800-m contour interval, is at distance meter 70, which is approximately 5 m north of the apex observed in the S-wave refraction tomography model. The lowest shear wave velocities (<400 m/s) are in the upper 10 m of the subsurface between distance meters 95 and 170; the shallow-depth velocities compare reasonably well between the MASRW-determined model, the MASLW-determined model, and the S-wave refraction tomography model.

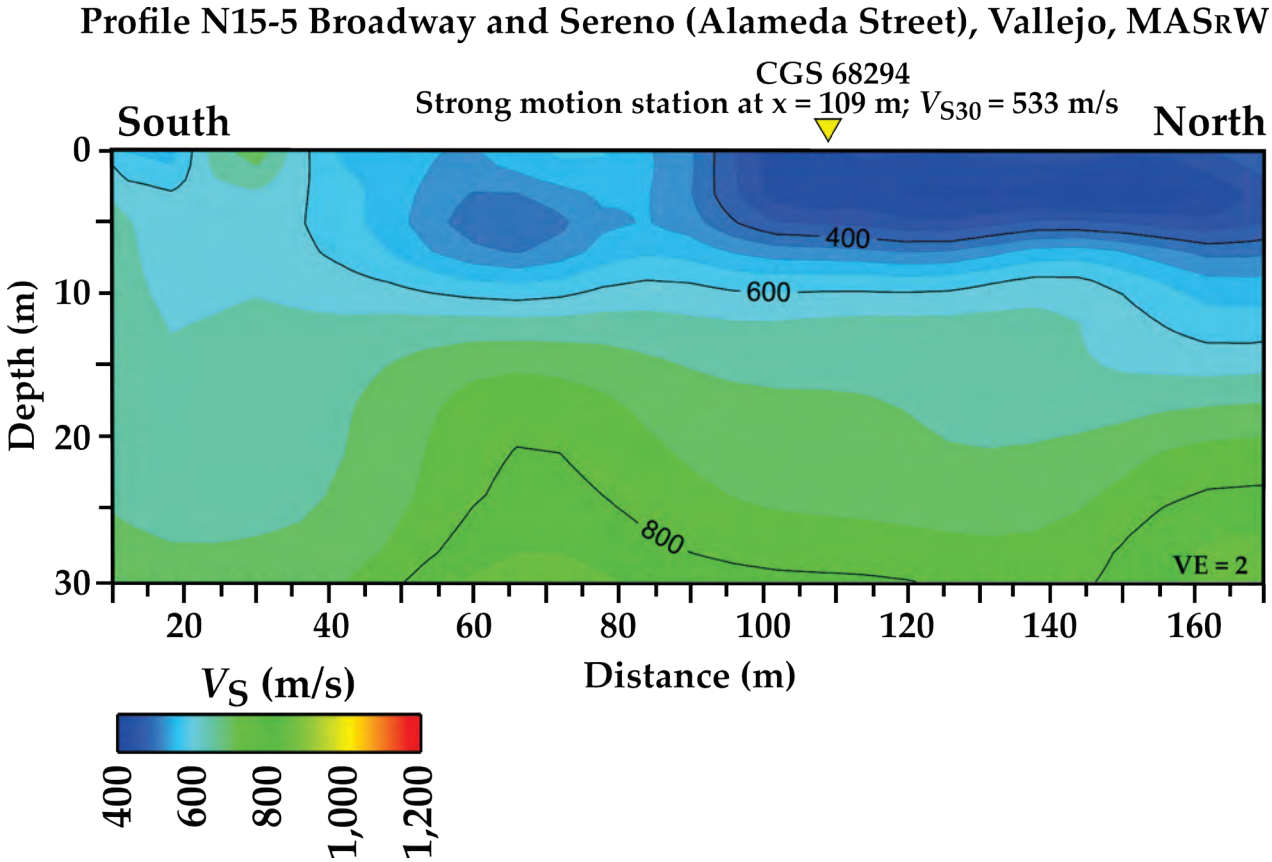

Figure 13. Illustration showing two-dimensional MASRW (multichannel analysis of surface waves for Rayleigh waves) shear-wave velocity model for profile N15-5 on Alameda Street and Kaiser Permanente hospital parking lot in Vallejo, California, near the Broadway Street and Sereno Drive strong-motion station. S-wave velocities range from 300 meters per second (m/s) at the near surface to more than 800 m/s at 30 meters (m) depth. Strong-motion recording station is nearest to distance meter 109 of our seismic profile, where we calculated time-averaged shear-wave velocity in the upper 30 meters of the subsurface (V_{S30}) to be 533 m/s based on MASRW. CGS, California Geological Survey; VE, vertical exaggeration; V_S, shear-wave velocity.

Profile N15-6.1—Vallejo Fire Station on Marin Street (NSMP 1759)

P-wave Tomography (V_P) Model

Along our seismic profile at Vallejo Fire Station on Marin Street, P-wave velocities range from 700 m/s in the near surface to 3,200 m/s at approximately 33 m depth (fig. 14). In general, velocity contours show a slight undulating pattern across the profile, with the upper 10 m and bottom 15 m of the model showing more lateral changes in P-wave velocity. The 1,500 m/s velocity contour (top of groundwater) varies between about 8 and 14 m beneath the surface.

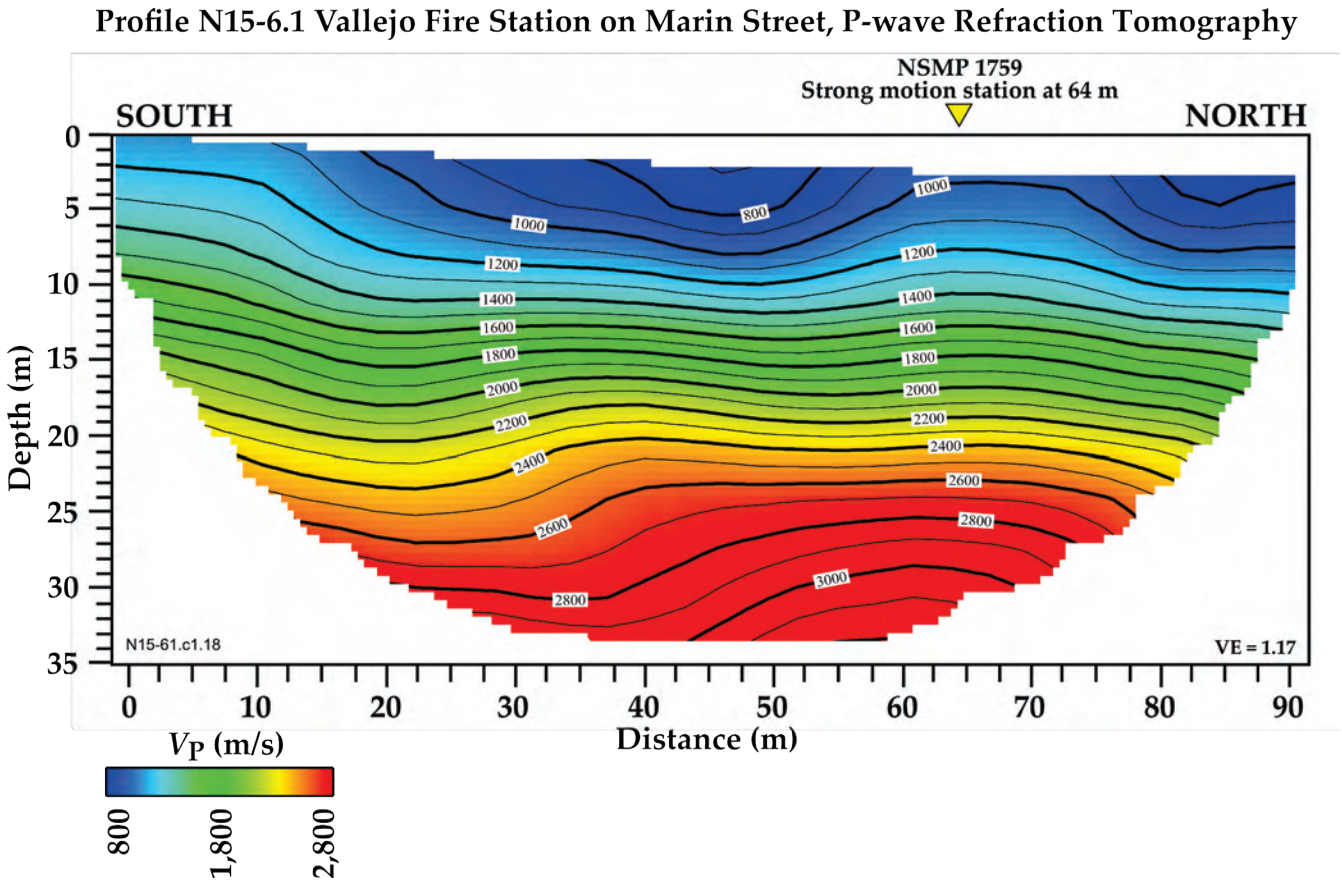

Figure 14. Illustration showing P-wave refraction tomography model for profile N15-6.1 on Marin Street adjacent to Vallejo Fire Station in Vallejo, California. P-wave velocities range from 700 meters per second (m/s) at the near surface to about 3,200 m/s at approximately 33 meters (m) depth. Strong-motion recording station is nearest to distance meter 64 m of our seismic profile. NSMP, National Strong Motion Project; VE, vertical exaggeration; V_P, P-wave velocity.

S-wave Tomography (V_S) Model

V_S determined from tomography ranges from 360 m/s in the near surface to about 700 m/s at approximately 23 m depth (fig. 15). Velocity contours show a significant undulating pattern across the profile, with the upper 13 m of the model showing the greatest lateral changes in S-wave velocities. The lowest velocities (<400 m/s) occur at three discreet locations in the upper 10 m of the profile—between distance meters 0 and 11, distance meters 38 and 57, and distance meters 77 and 85.

Ray coverage reached a maximum depth of 20 m at distance meter 64, which is the point along the seismic profile closest to the strong-motion recording station. We calculated V_{S20} to be 542 m/s; V_{S30} is calculated to be 583 m/s based on interpolated velocities below 20 m depth.

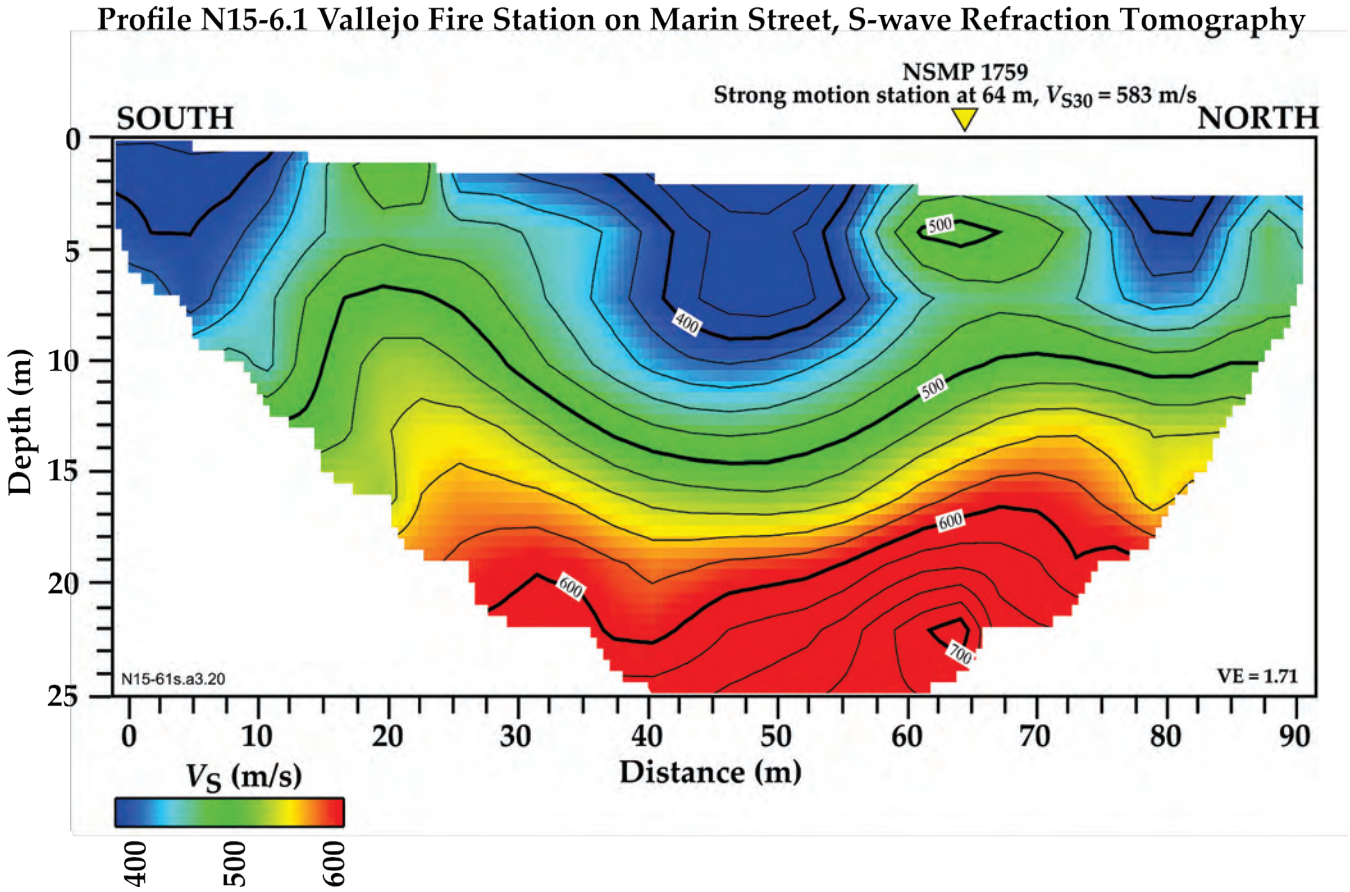

Figure 15. Illustration showing S-wave refraction tomography model for profile N15-6.1 on Marin Street adjacent to Vallejo Fire Station in Vallejo, California. S-wave velocities range from 360 meters per second (m/s) at the near surface to about 700 m/s at approximately 23 m depth. Velocity contours show strong lateral changes in S-wave velocities, particularly in the upper 13 meters (m) of the model. Strong-motion recording station is nearest to distance meter 64 of our seismic profile, where we calculated time-averaged shear-wave velocity in the upper 30 meters of the subsurface (V_{S30}) to be 583 m/s based on interpolated tomography velocities below 20 m depth. NSMP, National Strong Motion Project; VE, vertical exaggeration; V_S, shear-wave velocity.

MASLW 2D S-wave Velocity Model

The Love wave dispersion curves (appendix 1, right column), which represent the location (meter 64) on our seismic profile nearest to the strong-motion recording station, show adjusted picks (red circles) for the fundamental mode at phase velocities between 400 and 800 m/s and at frequencies between 3 and 35 Hz. Love wave dispersion curve picks across the entire length of the profile (appendix 2, blue circles) vary between the number of shots used during CMPCC construction (all shots along the profile versus two end shots) and at each single shot gather along the profile. Table 3 and figures in appendix 3 show V_{S30} and 1D velocity-depth results near the strong-motion station; the results come from using varying MASLW methods—2D MASLW (all shots; V_{S30}=567 m/s), 2D MASLW (end shots;

V_{S30}=510 m/s), and at a shot gather located at distance meter 64 (V_{S30}=552 m/s), the closest location to the strong-motion recorder.

Along the Marin Street seismic profile, 2D MASLW-determined V_S ranges from 250 m/s in the near surface to about 900 m/s at approximately 40 m depth (fig. 16). Velocity contours show an undulating pattern that represents significant lateral changes in velocities across the profile. The lowest S-wave velocities (<400 m/s) occur at three discreet locations in the upper 15 m of the profile—between distance meters 0 and 17, distance meters 26 and 42, and distance meters 52 and 63. These low velocity areas are offset to the south from those in the S-wave refraction tomography model.

V_S determined by MASLW is generally lower than determined by S-wave tomography by approximately 100 m/s at depths below 10 m, except for the northern end (distance meters 75 to 85) of the profile, where V_S determined from MASLW is higher in the upper 10 m of the profile.

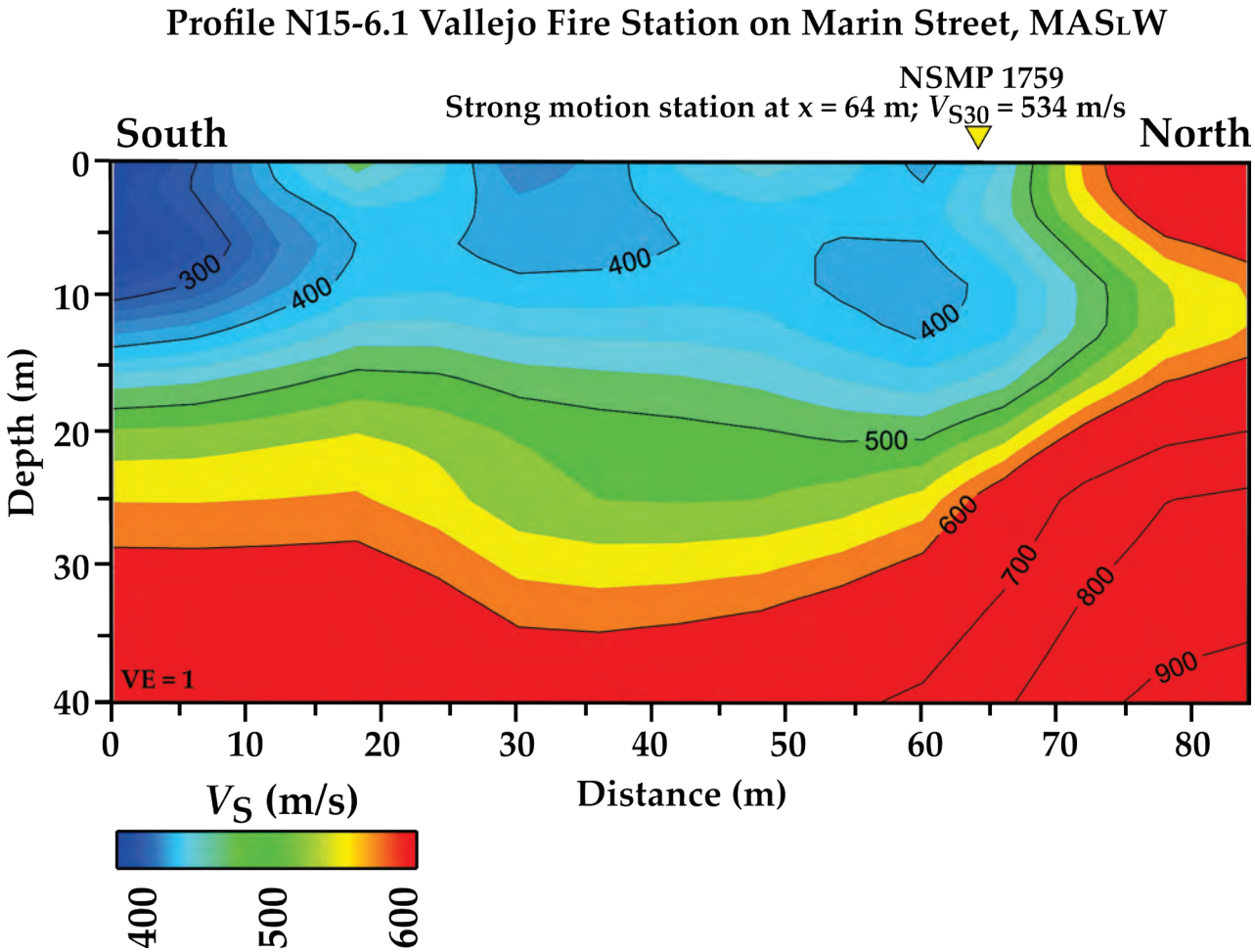

Figure 16. Illustration showing two-dimensional MASLW (multichannel analysis of surface waves for Love waves) shear-wave velocity model for profile N15-6.1 on Marin Street adjacent to Vallejo Fire Station in Vallejo, California. S-wave velocities range from 250 meters per second (m/s) at the near surface to more than 900 m/s below 35 m depth. Velocity contours show significant lateral changes in S-wave velocities in the upper 10 meters (m) of the model. Strong-motion recording station is nearest to distance meter 64 of our seismic profile, where we calculated time-averaged shear-wave velocity in the upper 30 meters of the subsurface (V_{S30}) to be 567 m/s based on MASLW. NSMP, National Strong Motion Project VE, vertical exaggeration; V_S, shear-wave velocity.

MAS_RW 2D S-wave Velocity Model

The Rayleigh wave dispersion curves (appendix 1, left column), which represent the location (meter 64) on our seismic profile nearest to the strong-motion recording station, show adjusted picks (red circles) for the fundamental mode at phase velocities between 300 and 800 m/s and at frequencies between 5 and 45 Hz. Fundamental modes are distinct from higher modes, which are observed at higher frequencies and at higher phase velocities. Rayleigh wave dispersion curve picks across the entire length of the profile (appendix 2, red triangles) vary between the number of shots used during CMPCC construction (all shots along the profile versus two end shots) and at each single shot gather along the profile. Table 3 and figures in appendix 3 show V_{S30} and 1D velocity-depth models near the strong-motion station; the results are derived using varying MAS_RW methods: 2D MAS_RW (all shots; V_{S30}=505 m/s), 2D MAS_RW (end shots; V_{S30}=557 m/s), and at a shot gather located at distance meter 64 (V_{S30}=534 m/s), the closest location to the strong-motion recorder.

Along the Marin Street seismic profile, V_S ranges from 300 m/s near the surface at the southern end of the profile to about 700 m/s at 18 m depth (fig. 17). Strong lateral variations in velocities are observed across the profile. The lowest S-wave velocities (<400 m/s) occur at three discreet locations in the upper 4 m of the profile—between distance meters 0 and 22, distance meters 42 and 57, and distance meters 63 and 90. Both MAS_RW and S-wave tomography models show a low-velocity area between distance meters 42 and 57. Generally, we observe V_S to be higher in the MAS_RW model relative to the MAS_LW model along the Vallejo Fire Station on Marin Street profile; V_S is similar (<100 m/s difference) between MAS_RW and S-wave refraction tomography models.

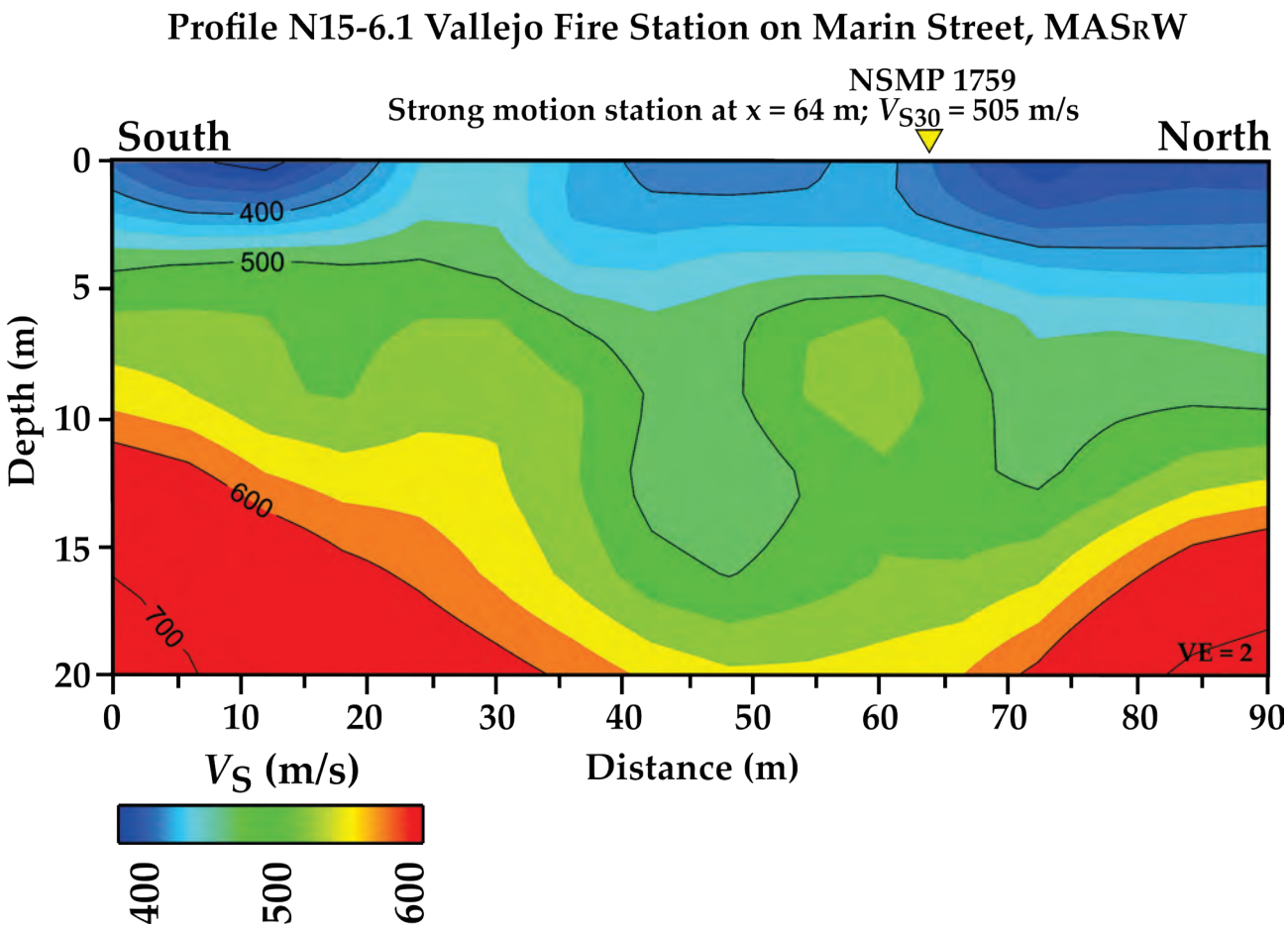

Figure 17. Illustration showing two-dimensional MASRW (multichannel analysis of surface waves for Rayleigh waves) shear-wave velocity model for profile N15-6.1 on Marin Street adjacent to Vallejo Fire Station in Vallejo, California. S-wave velocities range from 300 meters per second (m/s) at the near surface to about 700 m/s below 18 meters (m) depth. Velocity contours show strong lateral changes in S-wave velocities across the model. Strong-motion recording station is nearest to distance meter 64 of our seismic profile, where we calculated time-averaged shear-wave velocity in the upper 30 meters of the subsurface (V_{S30}) to be 505 m/s based on interpolated velocities below 20 m depth based on MASRW. NSMP, National Strong Motion Project VE, vertical exaggeration; V_S, shear-wave velocity.

Profile N15-6.2—Vallejo Fire Station on Overland Alley (NSMP 1759)

P-wave Tomography (V_P) Model

Along our seismic profile at Vallejo Fire Station on Overland Alley, P-wave velocities range from 1,500 m/s in the near surface to 3,100 m/s below 7 m depth near distance meter 65 (fig. 18). Velocity contours show a peak shape in the eastern half of the profile and significant lateral changes in P-wave velocity. The 1,500 m/s velocity contour (top of groundwater) is located just below the ground surface at both the western and eastern ends of the profile.

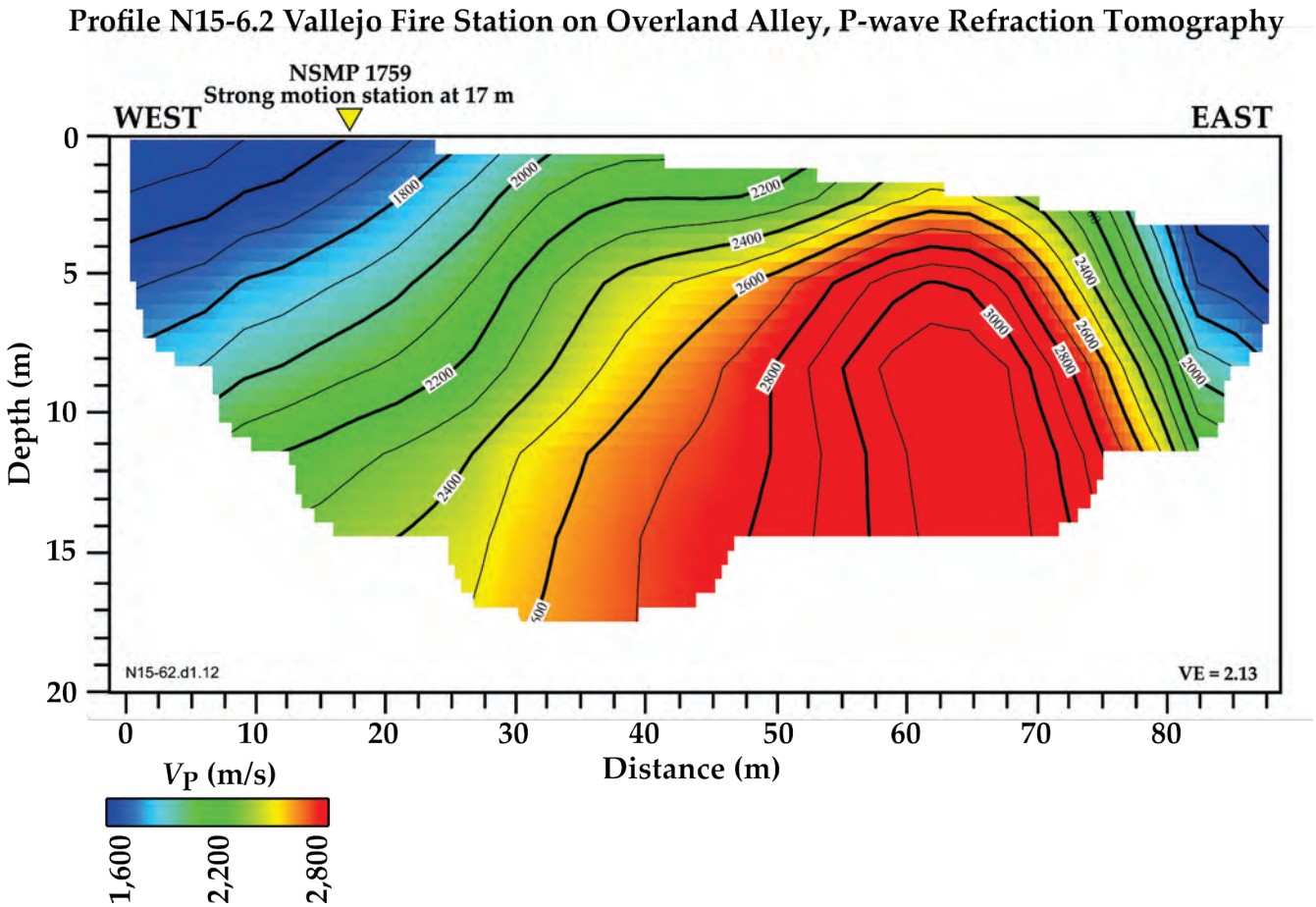

Figure 18. Illustration showing P-wave refraction tomography model for profile N15-6.2 on Overland Alley adjacent to Vallejo Fire Station in Vallejo, California. P-wave velocities range from 1,500 meters per second (m/s) at the near surface to 3,100 m/s at depth. The tomography model shows significant lateral changes in velocity, and P-wave velocities increase toward distance meter 63. Strong-motion station is nearest to distance meter 17 of our seismic profile. NSMP, National Strong Motion Project; VE, vertical exaggeration; V_P, P-wave velocity; m, meters.

S-wave Tomography (V_S) Model

V_S determined from tomography ranges from 325 m/s in the near surface to more than 650 m/s below 17 to 22 m depth (fig. 19). Velocity contours show two peak-shaped structures on both the western and eastern ends of the profile at approximately 1 to 2 m depths. S-wave velocities generally increase towards the west, which coincides with increasing elevation. Ray coverage reached a maximum depth of 18 m at distance meter 17, which is the point along the seismic profile closest to the strong-motion recording station. We calculated time-averaged shear-wave velocity in the upper 18 meters of the subsurface (V_{S18}) to be 493 m/s; V_{S30} is calculated to be 561 m/s based on interpolated velocities below 18 m depth.

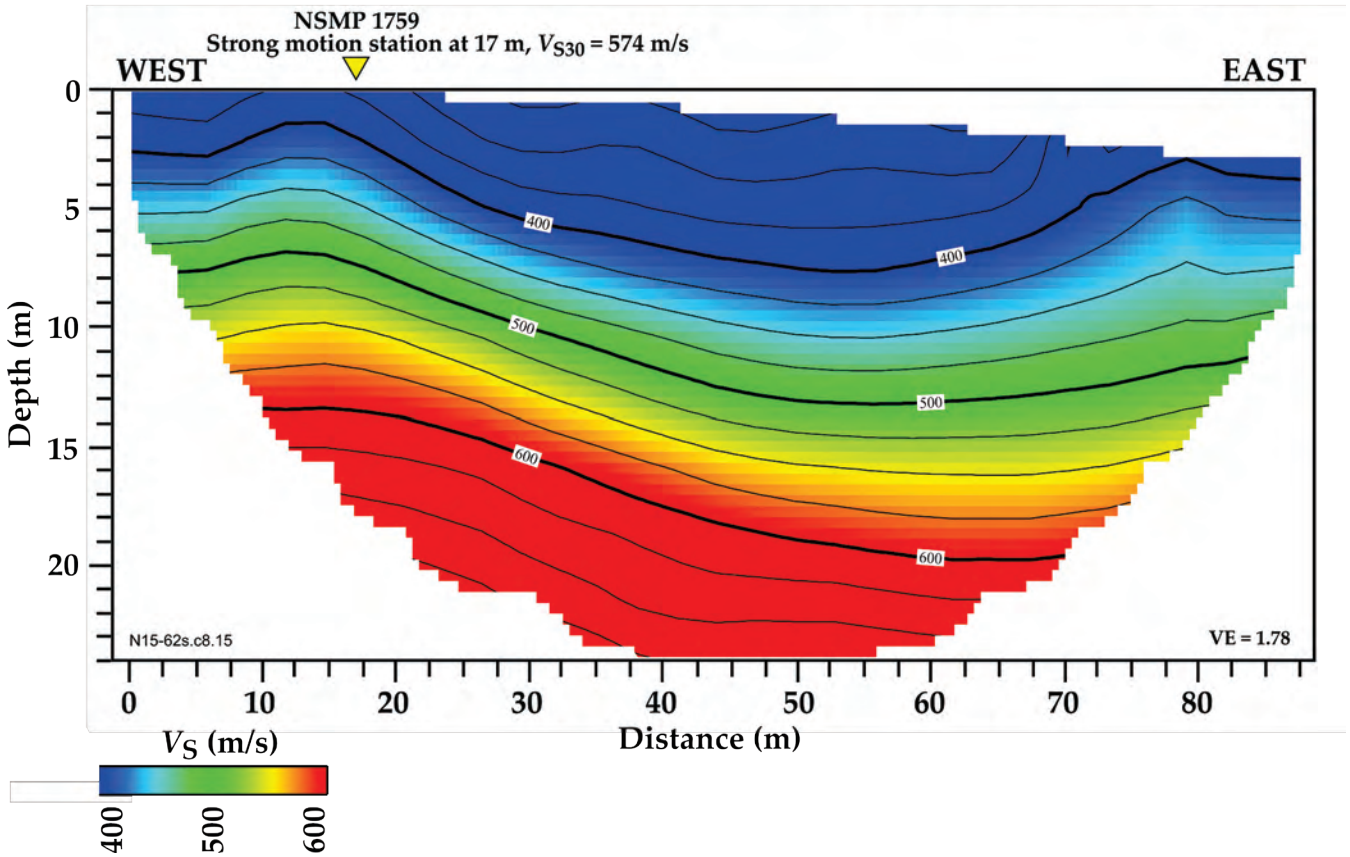

Figure 19. Illustration showing S-wave refraction tomography model for profile N15-6.2 on Overland Alley adjacent to Vallejo Fire Station in Vallejo, California. S-wave velocities range from 325 meters per second (m/s) in the near surface to more than 650 m/s at depth. Velocities generally increase to the west, which coincides with increasing elevation. Strong-motion station is nearest to distance meter 17 of our seismic profile, where we calculated time-averaged shear-wave velocity in the upper 30 meters of the subsurface (V_{S30}) to be 561 m/s based on interpolated tomography velocities below 25 meters (m). NSMP, National Strong Motion Project VE, vertical exaggeration; V_S, shear-wave velocity.

$MASW$ 2D S-wave Velocity Model

The Love wave dispersion curves (appendix 1, right column), which represent the location (meter 17) on our seismic profile nearest to the strong-motion recording station, show adjusted picks (red circles) for the fundamental mode at phase velocities between 300 and 700 m/s and at frequencies between 3 and 24 Hz. Love wave dispersion curve picks across the entire length of the profile (appendix 2, blue circles) vary between the number of shots used during CMPCC construction (all shots along the profile versus two end shots) and at each single shot gather along the profile. Table 3 and figures in appendix 3 show V_{S30} and 1D velocity-depth results near the strong-motion station; the results come from using varying $MASW$ methods—2D $MASW$ (all shots; V_{S30}=490 m/s), 2D $MASW$ (end shots; V_{S30}=478 m/s), and at a shot gather located at distance meter 17 (V_{S30}=435 m/s), the closest location to the strong-motion recorder.

Along the Overland Alley seismic profile, 2D $MASW$-determined V_S ranges from 350 m/s in the near surface to more than 600 m/s at approximately 35 m depth (fig. 20). Velocity contours do not show two peak-shaped structures at both ends of the profile in the upper 2 m as seen in the S-wave

tomography; however, velocities do increase towards both ends of the profile at the near surface. The lowest S-wave velocities (<400 m/s) occur in the upper 8 m, between distance meters 18 and 72. V_S determined by MASLW is generally lower than S-wave tomography by approximately 100 to 150 m/s at depths below 15 m.

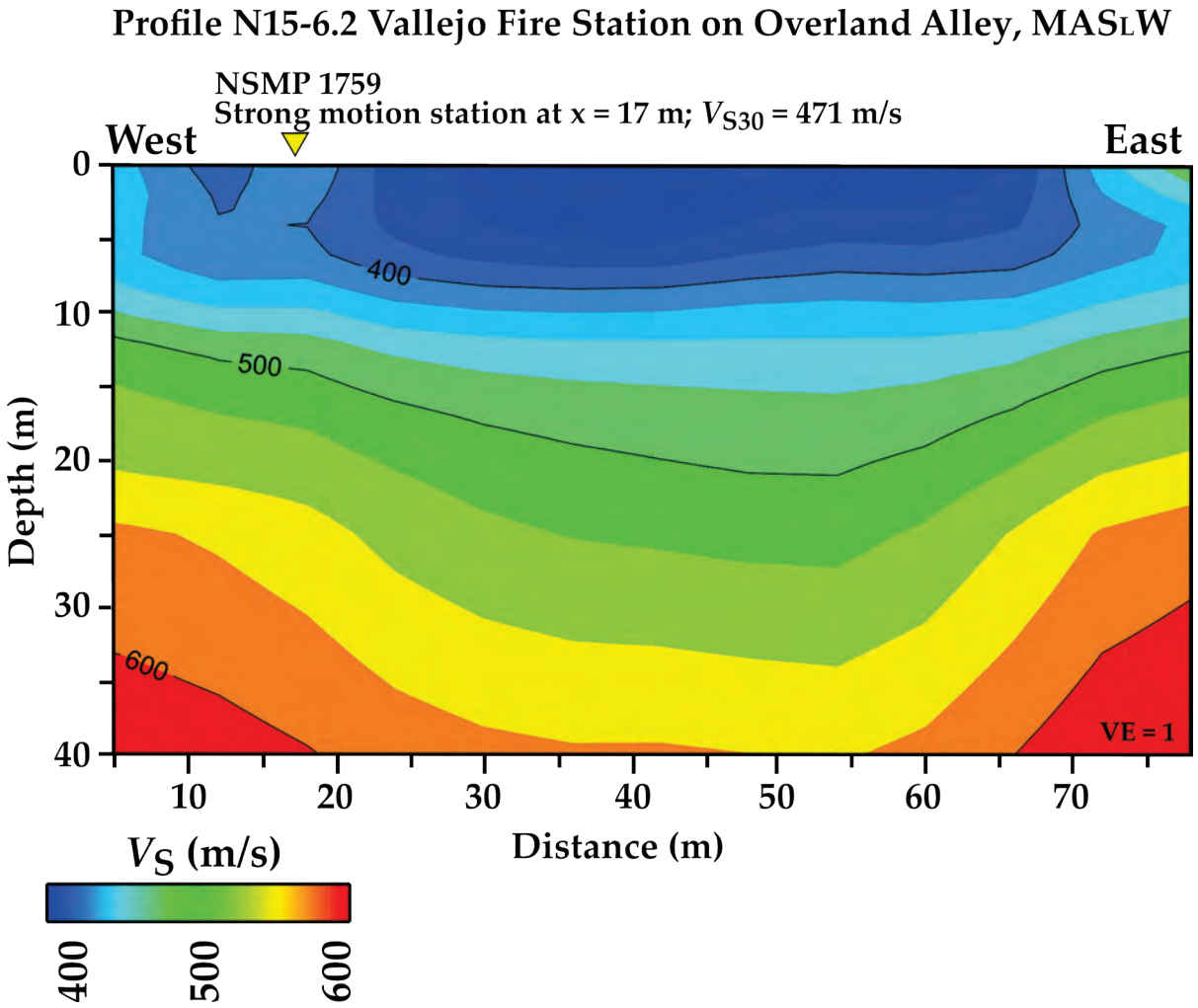

Figure 20. Illustration showing two-dimensional MASLW (multichannel analysis of surface waves for Love waves) shear-wave velocity model for profile N15-6.2 on Overland Alley adjacent to Vallejo Fire Station in Vallejo, California. S-wave velocities range from 350 meters per second (m/s) in the near surface to more than 600 m/s at the bottom of the model. Velocities increase towards both ends of the profile at depths below 10 meters (m). Strong-motion station is nearest to distance meter 17 of our seismic profile, where we calculated time-averaged shear-wave velocity in the upper 30 meters of the subsurface (V_{S30}) to be 490 m/s based on MASLW. NSMP, National Strong Motion Project VE, vertical exaggeration; V_S, shear-wave velocity.

MASRW 2D S-wave Velocity Model

The Rayleigh wave dispersion curves (appendix 1, left column), which represent the location (meter 17) on our seismic profile nearest to the strong-motion recording station, show adjusted picks (red circles) for the fundamental mode at phase velocities between 200 and 600 m/s and at frequencies between 4 and 36 Hz. Fundamental modes are distinct from higher modes, which are observed at higher frequencies and at higher phase velocities. Rayleigh wave dispersion curve picks across the entire length

of the profile (appendix 2, red triangles) vary between the number of shots used during CMPCC construction (all shots along the profile versus two end shots) and at each single shot gather along the profile. Table 3 and figures in appendix 3 show V_{S30} and 1D velocity-depth models near the strong-motion station; the results come from using varying MASRW methods—2D MASRW (all shots; V_{S30}=442 m/s), 2D MASRW (end shots; V_{S30}=467 m/s), and at a shot gather located at distance meter 17 (V_{S30}=372 m/s), the closest location to the strong-motion recorder.

Along the Overland Alley seismic profile, V_S ranges from 350 m/s in the near surface to more than 600 m/s at depths below 20 m (fig. 21). The lowest S-wave velocities (<400 m/s) occur in the upper 15 m, between distance meters 18 and 56. Velocity contours show higher velocities at both ends of the profile that extend from the surface to the bottom of the model, indicating strong lateral variation in velocities across the profile. All three MASRW, MASLW, and S-wave tomography models show a low velocity (<400 m/s) area in the upper 10 to 15 m of the subsurface; however, the MASRW model shows a high velocity structure at distance meters 60 to 75 that is not apparent in either the MASLW or S-wave tomography models. Generally, we observe V_S along the Vallejo Fire Station on Overland Alley profile to be higher below 15 m depth in the MASRW model relative to the MASLW model, and lower in the MASRW model relative to the S-wave tomography model.

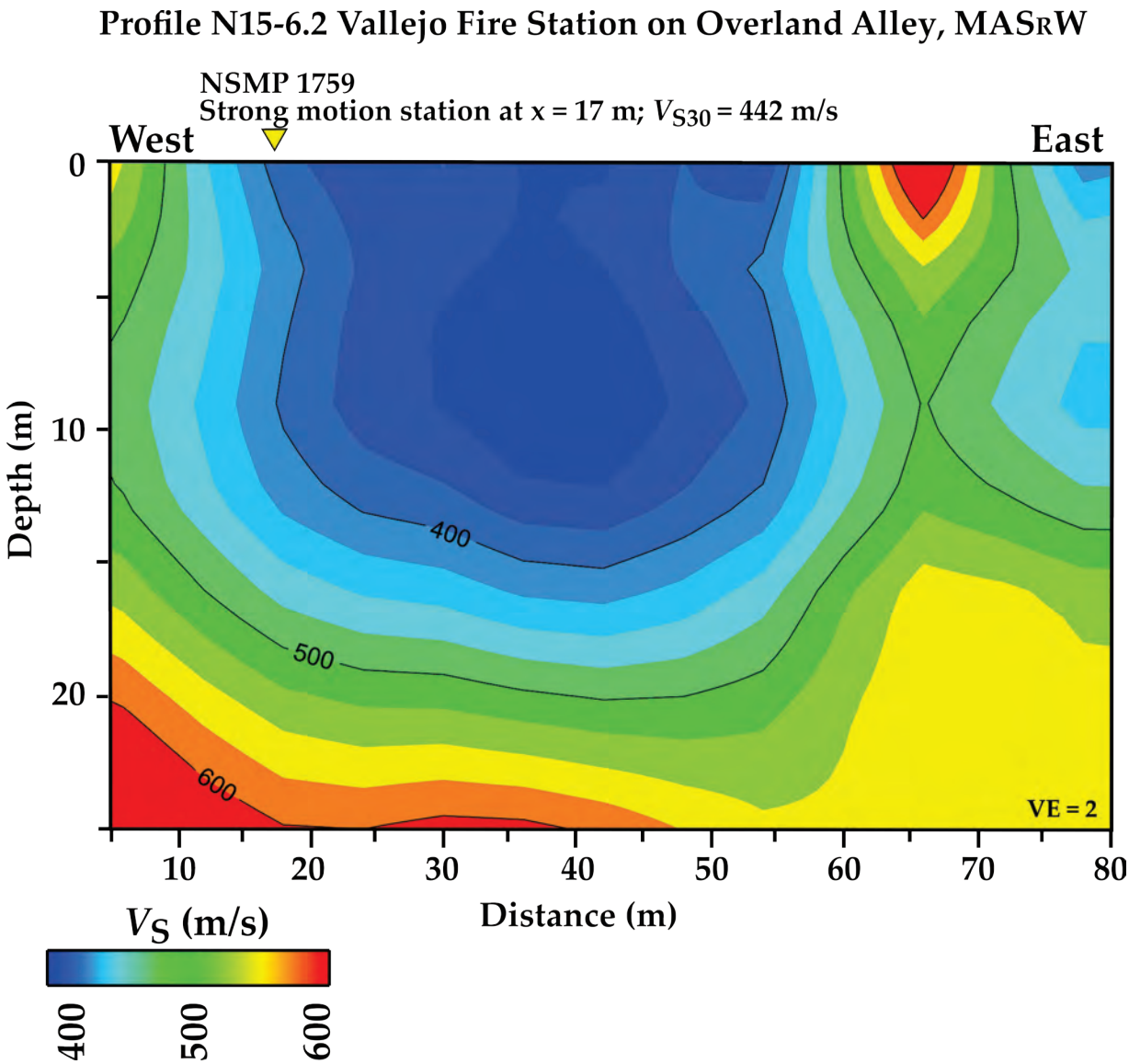

Figure 21. Illustration showing two-dimensional MASRW (multichannel analysis of surface waves for Rayleigh waves) shear-wave velocity model for profile N15-6.2 on Overland Alley adjacent to Vallejo Fire Station in Vallejo, California. S-wave velocities range from 350 meters per second (m/s) in the near surface to more than 600 m/s at depths below 20 meters (m). The model shows significant lateral changes in velocities across the profile. Strong-motion station is nearest to distance meter 17 of our seismic profile, where we calculated time-averaged shear-wave velocity in the upper 30 meters of the subsurface (V_{S30}) to be 442 m/s based on interpolated velocities below 20 m based on MASRW. NSMP, National Strong Motion Project VE, vertical exaggeration; V_S, shear-wave velocity.

V_P/V_S Ratios

The ratio of P-wave velocities to S-wave velocities (V_P/V_S) can provide additional information about the lithology and the physical state of subsurface materials (Castagna and others, 1985; Tatham, 1982). We derived V_P/V_S models for each of the three seismic profiles presented in this report by dividing the modeled P-wave velocity by the modeled S-wave velocity at each grid of the tomography velocity models. V_P/V_S graphical results are in appendix 4.

V_P/V_S values along the seismic profile near Lovall Valley Loop Road range from 1.3 to 1.75. Generally, the highest V_P/V_S ratios occur at the near surface and at depth, where they are separated by a zone of low V_P/V_S ratios between 5 and 40 m depth. Along the seismic profile on Alameda Street near the Broadway and Sereno strong-motion station in Vallejo, V_P/V_S ratios range from about 1.4 to about 4.2. The ratios generally increase to the north, and the highest values occur below 27 m depth between distance meters 95 and 140, which coincide with the decrease in slope of the surface topography. V_P/V_S ratios along Marin Street at Vallejo Fire Station range from 2.1 to 4.4, and the ratios generally decrease toward the north end of the profile. The lowest ratios are in the upper 5 m between distance meters 20 and 92, and the highest ratios are below 21 m depth near distance meter 40. V_P/V_S ratios along Overland Alley at Vallejo Fire Station range from 3 to 8, and the ratios increase toward the upper 3 to 5 m near distance meter 60. High V_P/V_S ratios, such as seen at distance meter 60, often correlate with subsurface faults (Catchings and others, 2014).

Poisson's Ratios

We developed models of Poisson's ratio directly from the tomographic V_P and V_S models using the calculation determined by Thomsen (1990). Poisson's ratio has been shown in other studies to correlate well with known water saturation levels, determined from boreholes, in the subsurface (Gregory, 1977; Castagna and others, 1985; Catchings and others, 2006). Because liquids have a Poisson's ratio of 0.5, saturated subsurface materials generally have relatively high Poisson's ratios, and Poisson's ratios (as determined from tomographic seismic data) above 0.44 have been shown to coincide with the top of groundwater (Catchings and others, 2006, 2014). Poisson's ratio plots are in appendix 5 of this report.

Poisson's ratios for our seismic profile near Lovall Valley Loop Road range from 0.01 to 0.26, which are indicative of unsaturated material along the entire seismic profile from the near surface to the base of the model. The lowest ratios (<0.05) appear as a lateral zone that separates higher ratios at the surface from those at depth. Poisson's ratios for our seismic profile on Alameda Street, near the Broadway and Sereno strong-motion station, range from 0.04 to 0.48. Ratios indicative of the top of groundwater (>0.44) occur approximately 10 to 32 m below the surface and dip to the south. The higher Poisson's ratios (>0.44) also suggest saturation reaching to the surface at distance meters 140 to 160, which coincide with the bottom of a hill. Poisson's ratios on Marin Street, at Vallejo Fire Station, range from 0.26 to 0.47. The top of groundwater (>0.44) occur approximately 2 to 14 m below the surface and nearly coincides with the 1,500 m/s velocity contour of the P-wave refraction tomography image. Poisson's ratios that exceed 0.44 indicate shallow saturation in the southern end of the profile relative to the entire profile. Poisson's ratios on Overland Alley at Vallejo Fire Station range from approximately 0.46 to 0.49, which indicate saturation from the surface to the base of the model at 20 m depth. The highest Poisson's ratio (0.49) coincides well with the location of high V_P/V_S ratios (>7), which in previous studies (Catchings and others, 2013, 2014) have coincided with the presence of a fault.

Summary

V_S Comparison

Profile N15-4—Lovall Valley Loop Road (NCSN N019B)

S-wave refraction tomography indicates S-wave velocities range from about 400 to 1,200 m/s in the upper 55 m, with significant lateral variations in velocities along the profile in the upper 40 m that become less complex from 40 m to bottom of the model. MASLW-determined V_S ranges from 400 to

925 m/s in the upper 50 m, with minor lateral variations in velocities at depths from 15 to 35 m of the profile. MAS_RW-determined V_S ranges from 250 to 700 m/s in the upper 30 m, with minor lateral variations in velocities at discreet locations between 15 to 25 m depth. V_S is similar (400 to 750 m/s) in the upper 15 m for both S-wave refraction tomography and MAS_LW models, whereas V_S determined by MAS_RW is as much as 150 m/s lower in the upper 15 m of the profile. V_S models developed by $MAS_{R,L}$W methods do not show a peak-shaped structure as seen in the S-wave refraction tomography model at distance meters 10 to 130; however, they do show a minor low-velocity structure at distance meters 65 to 120 below approximately 15 m depth.

V_{S30} calculated near the strong-motion station from the varying $MAS_{R,L}$W methods and S-wave refraction tomography show results between Love waves and S-wave refraction tomography differ by 8 to 14 percent (table 3); results between Rayleigh waves and S-wave refraction differ by 37 to 45 percent. V_{S30} calculated from Rayleigh waves are significantly lower (29 to 37 percent) than those calculated from Love waves using 2D $MAS_{R,L}$W methods, and V_{S30} calculated from Love waves are generally closer in value to those from S-wave refraction tomography.

Profile N15-5—Broadway Street and Sereno Drive in Vallejo (CGS 68294)

S-wave refraction tomography indicates S-wave velocities range from 300 m/s to more than 1,000 m/s in the upper 40 m of the profile, and the S-wave velocity contours show a broad, peak-shaped structure from distance meters 15 to 130 that dips toward the south. V_S determined from MAS_LW ranges from 300 to more than 1,000 m/s in the upper 60 m, and velocities generally decrease towards the northern end of the profile. S-wave velocity contours show a peak-shaped structure from distance meters 12 to 80 that does not dip to the south, as seen in the S-wave tomography model. V_S determined from MAS_RW ranges from 300 in the near surface to more than 800 m/s at 30 m depth. Velocity contours show a peak-shaped structure from distance meters 40 to 100 m that also does not dip to the south and is offset by approximately 30 m to the north from the peak-shaped structure seen in the MAS_LW model. V_S in the upper 10 m is similar (<400 m/s) in models determined from S-wave refraction tomography, MAS_LW, and MAS_RW; however, V_S is higher in the S-wave tomography and MAS_RW models below 10 m depth. All three models show a peak-shaped structure at depth but at various distances along the profile.

V_{S30} calculated near the strong-motion station from the varying $MAS_{R,L}$W methods and S-wave refraction tomography show results between Love waves and S-wave refraction tomography differ by 8 to 39 percent (table 3); results between Rayleigh waves and S-wave refraction differ by 1 to 23 percent. V_{S30} calculated from Rayleigh waves are higher (9 to 20 percent) than those calculated from Love waves and closer to those calculated from S-wave refraction tomography near the Broadway Street and Sereno Drive strong-motion station.

Profile N15-6.1—Vallejo Fire Station on Marin Street (NSMP 1759)

S-wave refraction tomography shows S-wave velocities range from 360 m/s to approximately 700 m/s in the upper 25 m, with significant lateral variation in velocities in the upper ~15 m of the profile. V_S determined from MAS_LW ranges from 250 m/s to approximately 900 m/s in the upper 40 m, with significant lateral variation in velocities in the upper ~15 m of the model and V_S increasing toward the north end of the profile. V_S determined from MAS_RW ranges from 300 to 700 m/s in the upper 20 m, with complex velocity structures from the near surface to the bottom of the model. V_S determined from S-wave refraction tomography, MAS_RW, and MAS_LW all show complex lateral variations in velocities across the profile, with discreet low velocities below 400 m/s in the upper 5 to 15 m of the models.

Generally, V_S is higher in the MAS_RW model relative to the MAS_LW model along the profile, and V_S is similar (<100 m/s) between the MAS_RW and S-wave refraction tomography models.

V_{S30} calculated near the strong-motion station from the varying $MAS_{R,L}W$ methods and S-wave refraction tomography show results between Love waves and S-wave refraction tomography differ by ~3 percent to 13 percent (table 3); results between Rayleigh waves and S-wave refraction differ by 5 to 14 percent. Despite overall higher V_S in the 2D MAS_RW model relative to the 2D MAS_LW model, V_{S30} calculated from Love waves are generally higher than those calculated from Rayleigh waves on Marin Street adjacent to Vallejo Fire Station.

Profile N15-6.2—Vallejo Fire Station on Overland Alley (NSMP 1759)

S-wave refraction tomography shows S-wave velocities range from 325 m/s in the near surface to more than 650 m/s at the bottom of the model, with higher velocities towards both ends of the profile. V_S determined from MAS_LW ranges from 350 m/s in the near surface to more than 600 m/s at depth, with velocities increasing towards both ends of the profile at depths below 10 m. V_S determined from MAS_RW ranges from 350 m/s to more than 600 m/s at depths below 20 m, with velocity contours showing strong lateral variations in velocities in the upper 10 m of the profile. All three S-wave models (refraction tomography, MAS_LW, and MAS_RW) show a low velocity (<400 m/s) structure in the upper 10 to 15 m of the subsurface; however, the MAS_RW model shows a high-velocity structure that extends from the surface to the bottom of the model that is not apparent in neither the MAS_LW nor the S-wave refraction tomography models.

V_{S30} calculated near the strong-motion station from the varying $MAS_{R,L}W$ methods and S-wave refraction tomography show results between Love waves and S-wave refraction tomography differ by 14 to 25 percent (table 3); results between Rayleigh waves and S-wave refraction differ by 18 to 41 percent. V_{S30} calculated from Love waves are generally higher (2 to 16 percent) than those calculated from Rayleigh waves on Overland Alley adjacent to Vallejo Fire Station.

Vallejo Fire Station—Marin Street and Overland Alley Intersection

The two profiles were perpendicular to each other and nearly intersected at distance meter 46 on Marin Street where they were approximately 5 m apart (fig. 5). P-wave refraction tomography models show consistent velocities near the line of intersection in the upper 10 m of the profile (fig. 22*A*). S-wave refraction tomography models show good correlation in shear wave velocities near the line of intersection of the two profiles from the surface to the bottom of both models (fig. 22*B*), whereas MAS_LW and MAS_RW models show consistent shear wave velocities near the line of intersection in the upper 35 m and 20 m of the models, respectively (fig. 22*C*, *D*).

A. **P-wave Refraction Tomography**

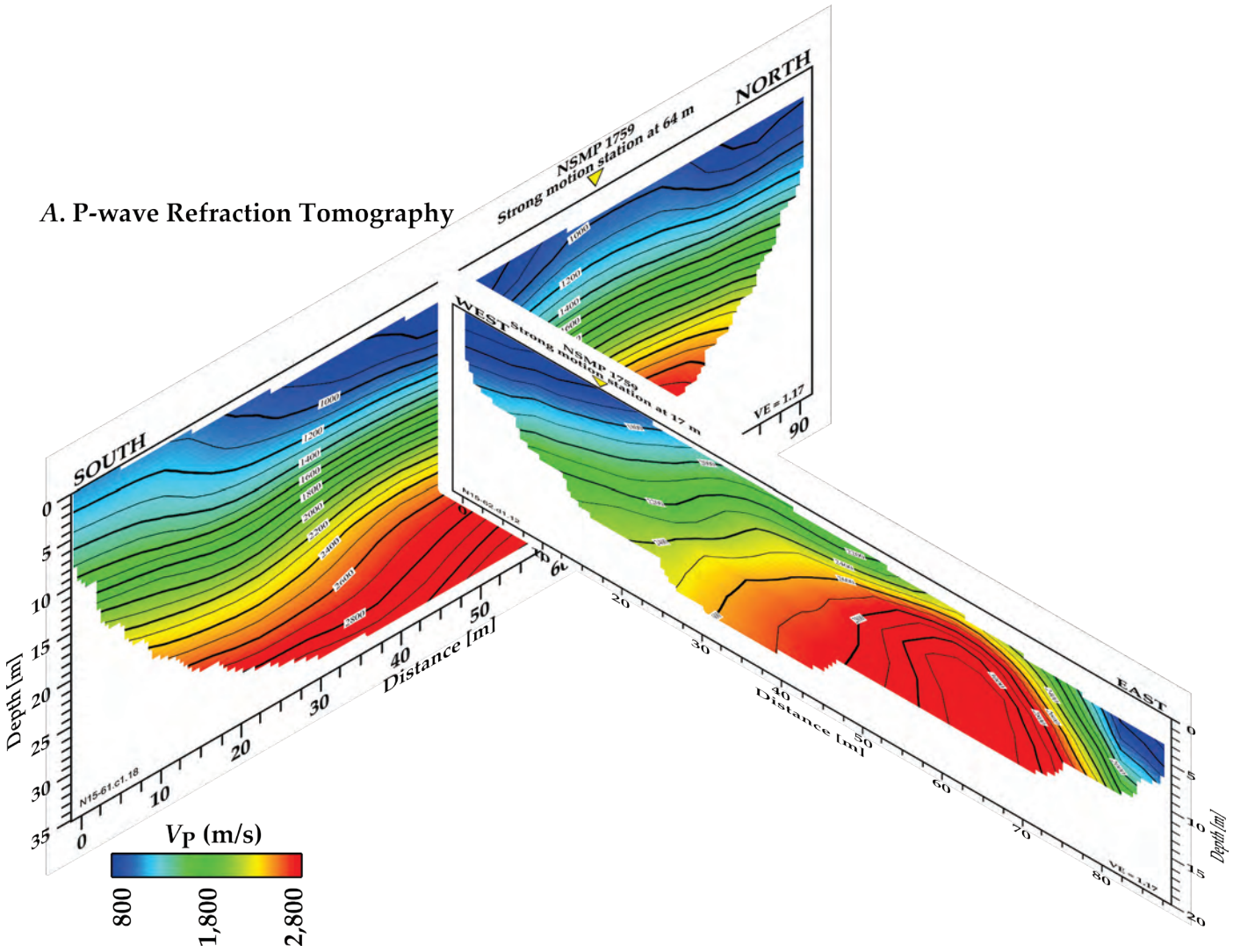

B. **S-wave Refraction Tomography**

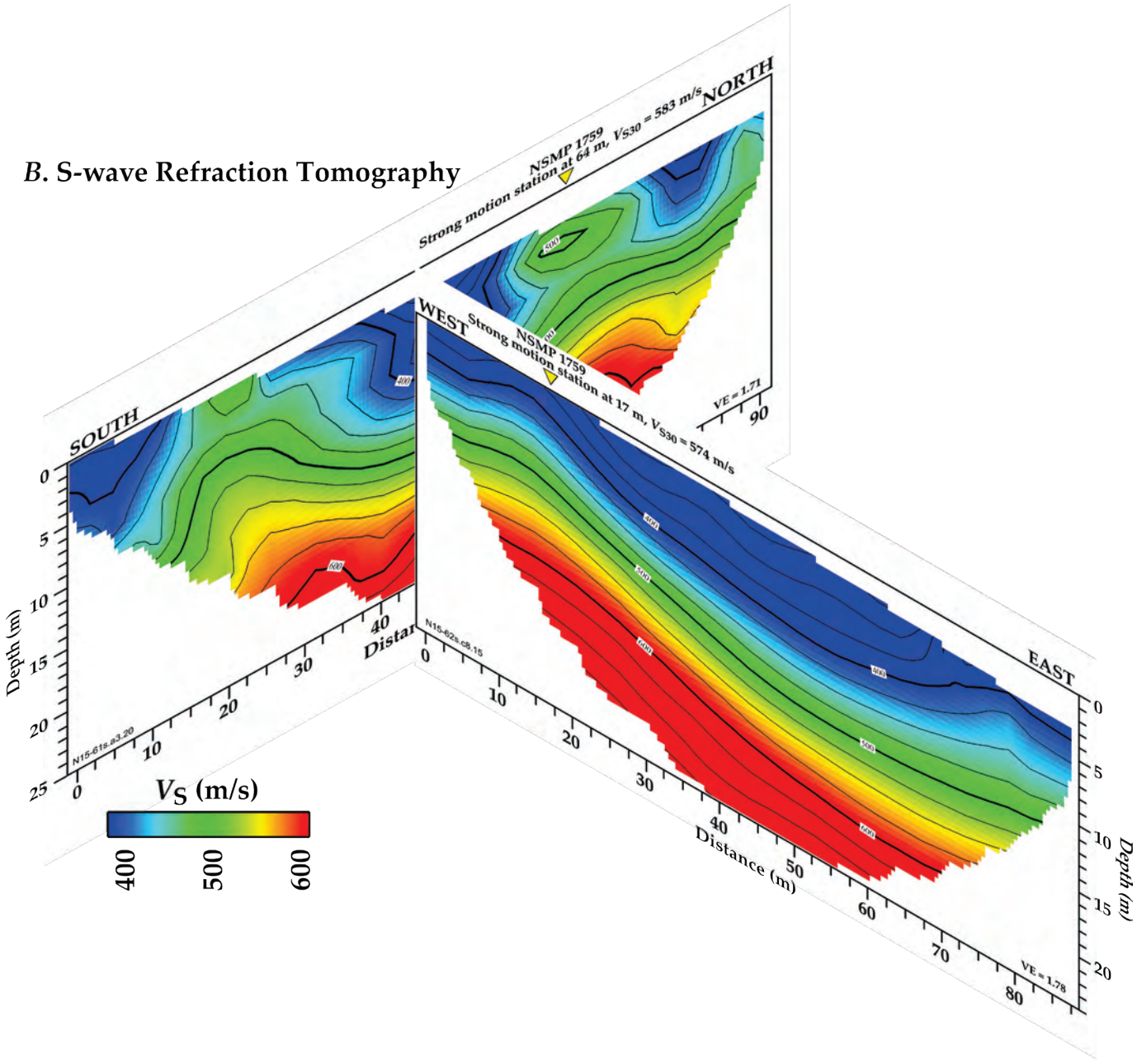

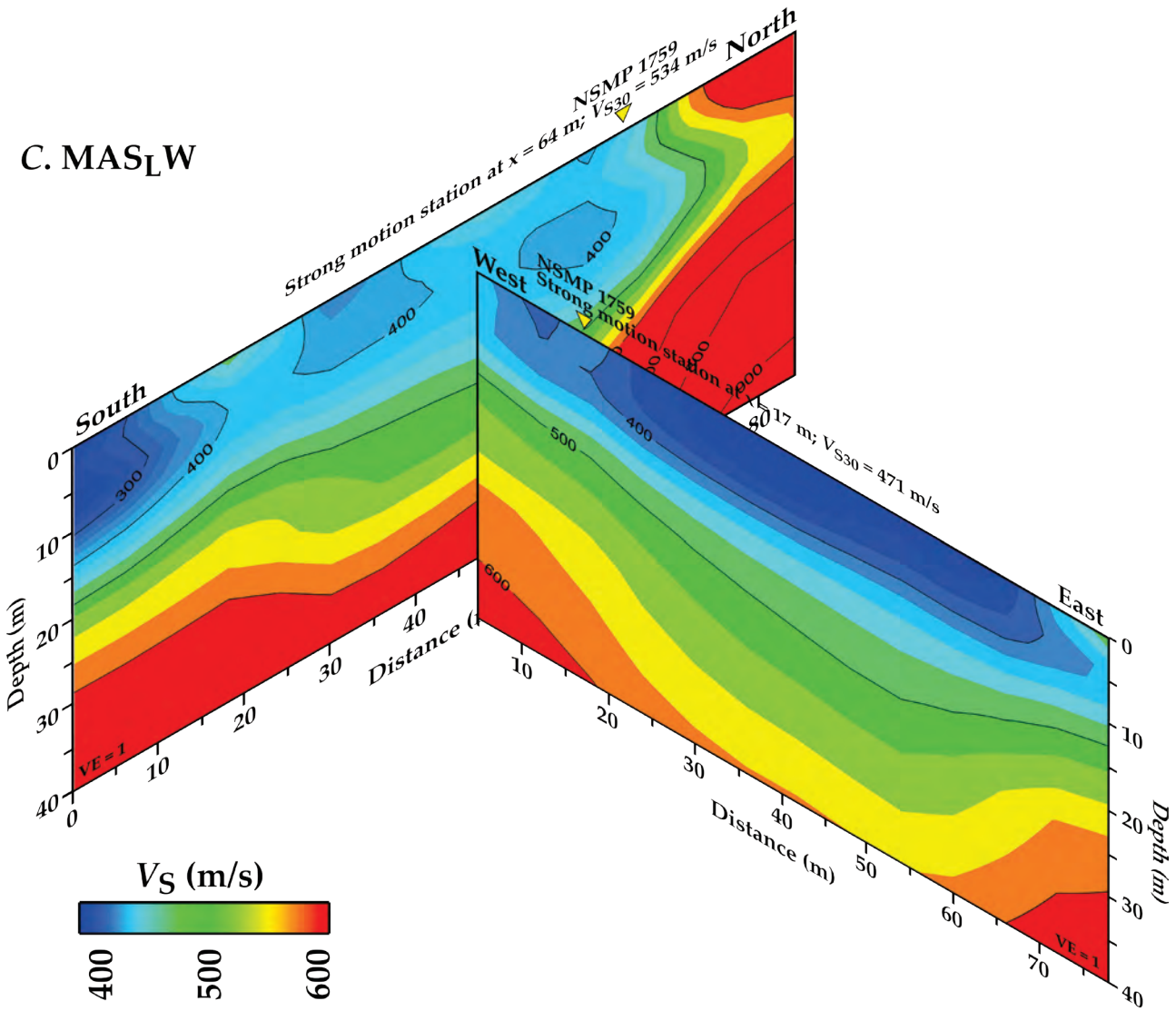
C. MASLW
North
South
West
East
NSMP 1759
Strong motion station at x = 64 m; VS30 = 534 m/s
NSMP 1759
Strong motion station
17 m; VS30 = 471 m/s
Depth (m)
Distance (m)
VE = 1
VS (m/s)
400
500
600

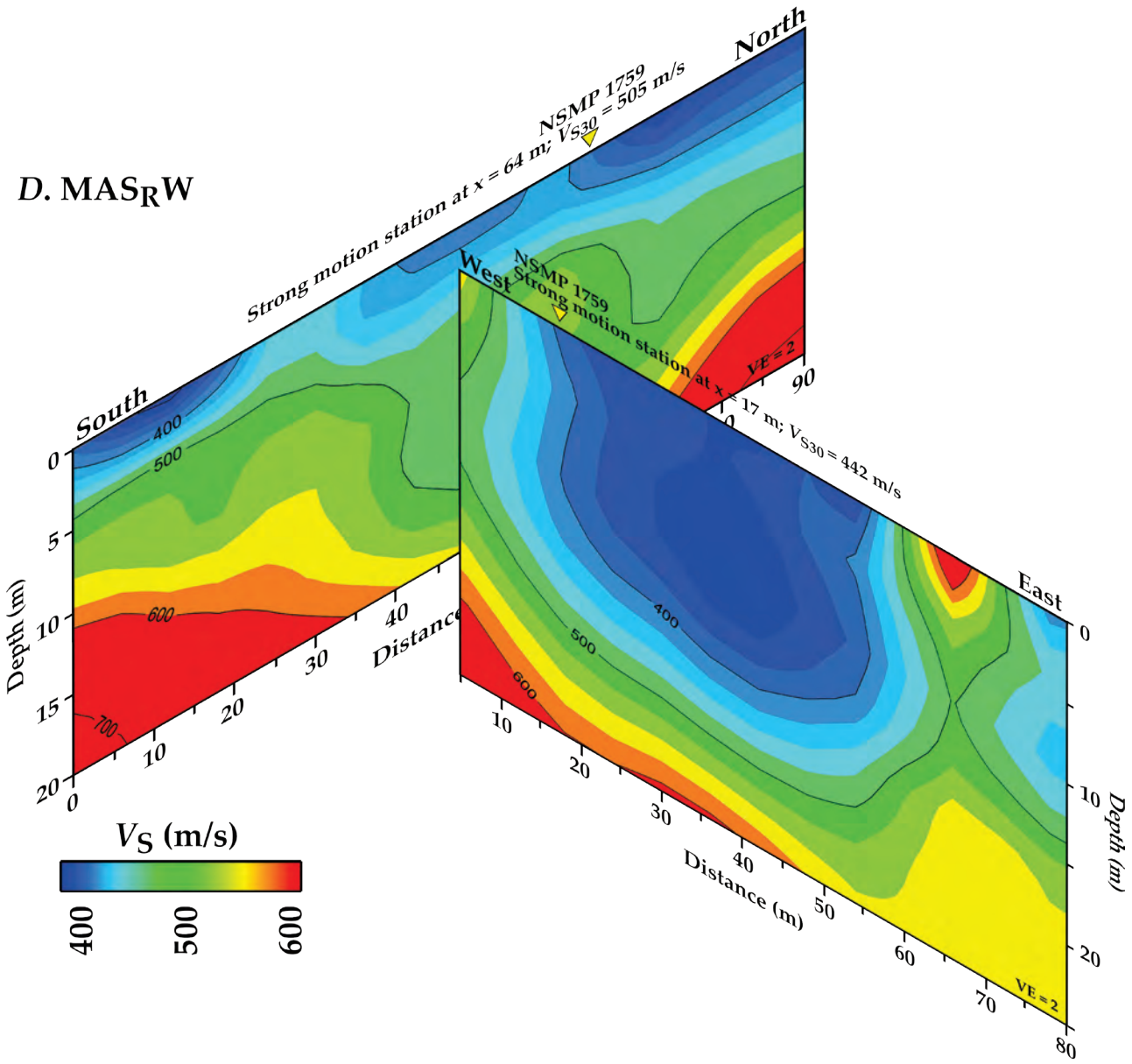

Figure 22. Velocity models showing Vallejo Fire Station, Vallejo, California, profiles N15-6.1 on Marin Street and N15-6.2 on Overland Alley, which were perpendicular to each other (fig. 5) and nearly intersected at distance meter 46 on Marin Street and separated by approximately 5 meters (m). *A*, P-wave refraction tomography models show similar velocities near the intersection of the two profiles in the upper 10 m. *B*, S-wave refraction tomography models show a good correlation in shear wave velocities near the intersection of the two profiles. *C*, MAS_LW (multichannel analysis of surface waves for Love waves) shear-wave velocity models show close correlation in shear wave velocities near the intersection of the two profiles in the upper 35 m. *D*, MAS_RW (multichannel analysis of surface waves for Rayleigh waves) shear-wave velocity models show close correlation in shear wave velocities near the intersection of the two profiles in the upper 20 m. NSMP, National Strong Motion Project VE, vertical exaggeration; V_P, P-wave velocity; V_S, shear-wave velocity; V_{S30}, time-averaged shear-wave velocity in the upper 30 meters of the subsurface.

Conclusion

Our results show that V_S determined from all models tended to have similar V_S in the upper 5 to10 m of the subsurface; however, in general, V_S determined from S-wave refraction tomography is higher than those determined from MAS_RW and MAS_LW at depths below ~10 m. V_S determined from MAS_LW is generally lower than MAS_RW at depth, with the exception of Lovall Valley Loop Road, where V_S determined from MAS_LW is higher than MAS_RW. Our $MAS_{R,L}W$ results show Love wave models have deeper depth of resolution than Rayleigh wave models, with the depth of resolution less than 30 m for Rayleigh wave models at Vallejo Fire Station. In general, we found V_S determined from MAS_RW is closer to those determined from S-wave refraction tomography at sites with significant changes in topography (Broadway Street and Sereno Drive in Vallejo and Vallejo Fire Station); whereas, V_S determined from MAS_LW is closer to those determined from S-wave refraction tomography at sites with minor changes in topography (Lovall Valley Loop Road).

V_{S30} calculated from $MAS_{R,L}W$ methods tended to be lower than those calculated from S-wave refraction tomography. Comparison between the varying $MAS_{R,L}W$ methods suggest 2D MAS_LW models using all shot gathers along a profile generally have closer V_{S30} values to those calculated from S-wave refraction tomography.

References Cited

Atwater, T., and Stock, J.M., 2010, Pacific-North America plate tectonics of the Neogene southwestern United States—An update: International Geology Review, v. 40, p. 375–402.

Baltay, A.S., and Boatwright, J., 2015, Ground-motion observations of the 2014 south Napa earthquake: Seismological Research Letters, v. 86, no. 2A, p. 355–360.

Boatwright, J., Blair, J.L., Aagaard, B.T., Wallis, K., 2015, The distribution of red and yellow tags in the city of Napa: Seismological Research Letters, v. 86, no. 2A, p. 361–368.

Boore, D.M., Thompson, E.M., and Cadet, H., 2011, Regional correlations of V_{S30} and velocities averaged over depths less than and greater than 30 meters: Bulletin of the Seismological Society of America, v. 101, no. 6, p 3046–3059.

Brocher, T.M., Baltay, A.S., Hardebeck, J.L., Pollitz, F.F., Murray, J.R., Llenos, A.L., Schwartz, D.P., Blair, J.L., Ponti, D.J., Lienkaemper, J.J., Langenheim, V.E., Dawson, T.E., Hudnut, K.W., Shelly, D.R., Dreger, D.S., Boatwright, J., Aagaard, B.T., Wald, D.J., Allen, R.M., Barnhart, W.D., Knudsen, K.L., Brooks, B.A., and Scharer, K.M., 2015, The M_w 6.0 24 August 2014 south Napa earthquake: Seismological Research Letters, v. 86, no. 2A, p. 309–326.

Building Seismic Safety Council, 2003, Recommended provisions for seismic regulations for new buildings and other structures, part 1—Provisions: Washington, D.C., Federal Emergency Management Agency, Report No. FEMA-450, 303 p.

Castagna, J.P., Batzle, M.L., and Eastwood, R.L., 1985, Relationships between compressional-wave and shear-wave velocities in clastic silicate rocks: Geophysics, v. 50, no. 4, 571–581.

Catchings, R.D., Gandhok, G., Goldman, M. R., Okaya, D., 2001, Seismic images and fault relations of the Santa Monica Thrust Fault, West Los Angeles, California: U.S. Geological Survey Open-File Report 01–111, 34 p., https://pubs.usgs.gov/of/2001/0111/.

Catchings, R.D., Borchers, J.W., Goldman, M.R., Gandhok, G., Ponce, D.A., and Steedman, C.E., 2006, Subsurface structure of the East Bay plain ground-water basin: San Francisco Bay to the Hayward Fault, Alameda County, California: U.S. Geological Survey Open-File Report 2006–1084, 61 p., https://pubs.usgs.gov/of/2006/1084/.

Catchings, R.D., Rymer, M.J., Goldman, M.R., Prentice, C.S., and Sickler, R.R., 2013, Fine-scale delineation of the location of and relative ground shaking within the San Andreas Fault zone at San Andreas Lake, San Mateo County, California: U.S. Geological Survey Open-File Report 2013–1041, 53 p., http://pubs.usgs.gov/of/2013/1041/.

Catchings, R.R., Rymer, M.J., Goldman, M.R., Sickler, R.R., and Criley, C.J., 2014, A method and example of seismically imaging near-surface fault zones in geologically complex areas using V_P, V_S, and their ratios: Bulletin of the Seismological Society of America, v. 104, p. 1989–2006.

Catchings, R.D., Goldman, M.R., Li, Y.-G., and Chan, J.H., 2016, Continuity of the West Napa-Franklin Fault Zone inferred from guided waves generated by earthquake following the 24 August 2014 M_w 6.0 South Napa earthquake: Bulletin of the Seismological Society of America, v. 106, 2721–2746, https://doi.org/10.1785/0120160154.

Catchings, R.D., Goldman, M.R., Trench, David, Buga, Michael, Chan, J.H., Criley, C.J., and Strayer, L.M., 2017a, Shallow-depth location and geometry of the Piedmont Reverse splay of the Hayward Fault, Oakland, California: U.S. Geological Survey Open-File Report 2016–1123, 22 p., https://pubs.usgs.gov/of/2016/1123/.

Catchings, R.D., Goldman, M.R., Chan, J.H., Sickler, R.R., Strayer, L.M., Boatwright, J., and Criley, C.J., 2017b, Basin-wide V_P, V_S, V_P/V_S, and Poisson's ratios of the Napa Valley, California: Seismological Society of America 2017 Annual Meeting Announcement and Program, Seismological Research Letters, v. 88, no. 2B, p. 463–723, https://doi.org/10.1785/0220170035.

Center for Engineering Strong Motion Data, 2017, Peak ground motion data: Center for Engineering Strong Motion Data web page, accessed April 2017 at http://strongmotioncenter.org/cgi-bin/CESMD/apktable.pl?iqrid=SouthNapa_24Aug2014_72282711.

Chan, J.H., Catchings, R.D., Goldman, M.R., and Criley, C.J., 2018, V_{S30} for the August 24, 2014, M_w 6.0 South Napa earthquake at three strong-motion recording stations in Napa and Napa County, California—Main Street in downtown Napa, Napa fire station number 3, and Kreuzer Lane: U.S. Geological Survey Open-File Report 2018–1161, 47 p., https://doi.org/10.3133/ofr20181161.

City of Vallejo, 2014, 2014/2015-2016/2017 Goals and accomplishments: City of Vallejo, accessed June 2018 at http://www.ci.vallejo.ca.us/common/pages/DisplayFile.aspx?itemId=1663201.

DeLong, S.B., Lienkaemper, J.J., Pickering, A.J., and Avdievitch, N.N., 2015, Rates and patterns of surface deformation from laser scanning following the South Napa earthquake, California: Geosphere, v. 11, no. 6, p. 2015–2030., https://doi.org/10.1130/GES01189.1.

Fimrite, P., 2014, Northern California earthquake—Blue-collar Vallejo hit hard: San Francisco Chronicle, August 26, 2014, accessed June 2018 at https://www.sfgate.com/bayarea/article/Northern-California-earthquake-Blue-collar-5711775.php.

Fox, K.F. Jr., Sims, J.D., Bartow, J.A., and Helley, E.J., 1973, Preliminary geologic map of eastern Sonoma County and western Napa County, California: U.S. Geological Survey Miscellaneous Field Studies Map MF–483, scale 1:62,500. [Also available at https://pubs.er.usgs.gov/publication/mf483.]

Fox, K.F., Jr., Fleck, R.J., Curtis, G.H., and Meyer, C.E., 1985a, Implications of the northwesterly younger age of the volcanic rocks of west-central California: Geological Society of America Bulletin, v. 96, p. 647–654.

Fox, K.F., Jr., Fleck, R.J., Curtis, G.H., and Meyer, C.E., 1985b, Potassium-argon and fission-track ages of the Sonoma Volcanics in an area north of San Pablo Bay, California: U.S. Geological Survey Miscellaneous Field Studies Map MF 1753, scale: 1:250,000. [Also available at https://pubs.er.usgs.gov/publication/mf1753.]

Geometrics, Inc., 2016, SeisImager/SW-Pro™ manual—windows software for analysis of surface waves, ver. 1.2: Geometrics, Inc., 74 p.

Goldman, M.R., Catchings, R.D., Chan, J.H., and Criley, C.J., 2018, 2015 high resolution seismic data recorded at six strong motion seismograph sites in Napa and Solano counties, California: U.S. Geological Survey data release, https://doi.org/10.5066/P9F4IAAL.
Graymer, R.W., Sarna-Wojcicki, A.M., Walker, J.P., McLaughlin, R.J., and Fleck, R.J., 2002, Controls on timing and amount of right-lateral displacement on the East Bay fault system, San Francisco Bay region, California: Geological Society of American Bulletin, v. 114, p. 1471–1479.
Graymer, R.W., Bryant, W., McCabe, C.A., Hecker, S., and Prentice, C.S., 2006, Map of Quaternary-active faults in the San Francisco Bay region: U.S. Geological Survey Scientific Investigations Map 2919, https://pubs.usgs.gov/sim/2006/2919.
Graymer, R.W., Brabb, E.E., Jones, D.L., Barnes, J., Nicholson, R.S., and Stamski, R.E., 2007, Geologic map and map database of eastern Sonoma and western Napa Counties, California: U.S. Geological Survey Scientific Investigations Map 2956, http://pubs.usgs.gov/sim/2007/2956/.
Gregory, A.R., 1977, Fluid saturation effects on dynamic elastic properties of sedimentary rocks: Geophysics, v. 41, 895–921.
Hayashi, K., 2003, CMP analysis of multi-channel surface wave data and its application to near-surface S-wave velocity delineation: Symposium on the Application of Geophysics to Engineering and Environmental Problems 2003—Proceedings of the Symposium on the Application of Geophysics to Engineering and Environmental Problems, p. 1348–1355.
Hayashi, K., Cakir, R., and Walsh, T.J., 2016, Comparison of dispersion curves and velocity models obtained by active and passive surface wave methods: Society of Exploration Geophysicist Technical Program Expanded Abstracts 2016, p. 4983–4988, https://doi.org/10.1190/segam2016-13846390.1.
Hayashi, K., and Suzuki, H., 2004, CMP cross-correlation analysis of multi-channel surface-wave data: Exploration Geophysics, v. 35, p. 7–13.
Helley, E.J., and Herd, D.G., 1977, Map showing faults with Quaternary displacement, northeastern San Francisco Bay area region, California: U.S. Geological Survey Miscellaneous Field Studies Map MF–881, scale 1:125,000.
Hole, J.A., 1992, Nonlinear high-resolution three-dimensional seismic travel time tomography: Journal of Geophysical Research, v. 97, no. B5, p. 6553–6562.
Howell, D.G., and Swinchatt, J.P., 2000, A discussion of geology, soils, wines, and history of the Napa Valley region, *in* Lageson, D.R., Peters, S.G., and Lahren, M.M., eds., Great Basin and Sierra Nevada: Boulder, Colorado, Geological Society of America Field Guide 2, p. 415–422.
International Code Council, Inc., 2009, International building code: International Code Council, Inc., 752 p.
Ivanov, J., Miller, R.D., Park, C.P., and Ryden, N., 2003, Seismic search for underground anomalies: Society of Exploration Geophysicists Technical Program Expanded Abstract 2003, p. 1223–1226.
Ivanov, J., Leitner, B., Shefchik, W., Shwenk, J.T., and Peterie, S.L., 2013, Evaluating hazards at salt cavern sites using multichannel analysis of surface waves: The Leading Edge, v. 32, no. 3, p. 298–305.
Ivanov, J., Miller, R.D., and Tsoflias, G., 2008, Some practical aspects of MASW analysis and processing: Symposium on the Application of Geophysics to Engineering and Environmental Problems, 21, 1186–1198.
Knudsen, K.L., Sowers, J.M., Witter, R.C., Wentworth, C.M., and Helley, E.J., 2000, Preliminary maps of Quaternary deposits and liquefaction susceptibility, nine-county San Francisco Bay region, California; a digital database: U.S. Geological Survey Open-File Report 00–444, 2 sheets, scale 1:275,000, https://pubs.usgs.gov/of/2000/of00-444.

Kunkel, F., and Upson, J.E., 1960, Geology and ground water in Napa and Sonoma valleys, Napa and Sonoma Counties, California: U.S. Geological Survey Water-Supply Paper 1495, 252 p., https://pubs.usgs.gov/wsp/1495.

Langenheim, V.E., Graymer, R.W., and Jachens, R.C., 2006, Geophysical settings of the 2000 ML 5.2 Yountville, California, earthquake: implications for seismic hazard in Napa Valley, California: Bulletin of the Seismological Society of America, v. 96, no. 3, p. 1192–1198.

Langenheim, V.E., Graymer, R.W., Jachens, R.C., McLaughlin, R.J., Wagner, D.L., and Sweetkind, D.S., 2010, Geophysical framework of the northern San Francisco Bay region, California: Geosphere, v. 6, no. 5, p. 594–620.

Lienkaemper, J.J., Delong, S.B., Domrose, C.J., and Rosa, C.M., 2016, Afterslip behavior following the 2016 M 6.0 South Napa earthquake with implications for afterslip forecasting on other seismogenic faults: Seismological Research Letters, v. 87, no. 3, p. 609-619, doi:10.1785/0220150262.

Li, Y.G., Catchings, R.D., and Goldman, M.R., 2016, Subsurface fault damage zone of the 2014 M_W 6.0 South Napa, California, earthquake viewed form fault-zone trapped waves: Bulletin of the Seismological Society of America, v. 106, no. 6, p. 2747-2763, doi:10.1785/0120160039.

Miller, R.D., Xia, J., Park, C.B., and Ivanov, J., 1999, Using MASW to map bedrock in Olathe, Kansas: Kansas Geological Survey Open-File Report No. 99–9, 9 p.

Morelan, A.E., Trexler, C.C., and Oskin, M.E., 2015, Surface-rupture and slip observations on the day of the 24 August 2014 south Napa earthquake: Seismological Research Letters, v. 86, no. 4, p. 1119–1127.

Odum, J.K., Stephenson, W.J., Williams, R.A., and Hillebrandt-Andrade, C., 2013, V_{S30} and spectral response from collocated shallow, active-, and passive-source V_S data at 27 sites in Puerto Rico: Bulletin of the Seismological Society of America, v. 103, no. 5, p. 2709–2728.

Park, C., 2013, MASW for geotechnical site investigation: The Leading Edge, v. 32, no. 6, p.656–662.

Park, C., Miller, R., and Xia, J., 1999, Multichannel analysis of surface waves: Geophysics, v. 64, no. 3, p. 800–808.

Park, C., Miller, R., Xia, J., and Ivanov, J., 2000, Multichannel analysis of surface waves (MASW)—active and passive methods: The Leading Edge, v. 26, p. 60–64, https://doi.org/10.1190/1.2431832.

Pujol, J., 2003, Elastic wave propagation and generation in seismology: Cambridge University Press, United Kingdom, 462 p.

Reynolds, J.M., 2011, An introduction to applied and environmental geophysics: Wiley, 710 p.

Stonebridge Research Group LLC, 2012, The economic impact of Napa County's wine and grapes: Stonebridge Research Group LLC, accessed March 2017 at https://napavintners.com/community/docs/napa_economic_impact_2012.pdf.

Sweetkind, D.S., Rytuba, J.J., Langenheim, V.E., and Sarna-Wojcicki, A.M., 2005, Contrasting styles of volcanism along the east side of Napa Valley, CA: Geological Society of America Abstracts with Program, v. 37, no. 4, p. 84.

Tatham, R.H., 1982, V_P/V_S and lithology: Geophysics, v. 47, no. 3, p. 336–344.

Thomsen, L., 1990, Poisson was not a geophysicist!: The Leading Edge, v. 9, p. 27–29.

U.S. Census Bureau, 2010, QuickFacts: U.S. Census Bureau web page accessed March 2017 at https://www.census.gov/quickfacts/fact/table/napacitycalifornia,napacountycalifornia/PST045216.

U.S. Geological Survey, 2015, South Napa Earthquake – One Year Later: U.S. Geological Survey page accessed June 2018 at https://www.usgs.gov/news/south-napa-earthquake-%E2%80%93-one-year-later.

Wagner, D.L., Saucedo, G.J., Clahan, K.B., Fleck, R.J., Langenheim, V.E., McLaughlin, R.J., Sarna-Wojcicki, A.M., Allen, J.R., and Deino, A.L., 2011, Geology, geochronology, and paleogeography of

the southern Sonoma volcanic field and adjacent areas, northern San Francisco Bay region, California: Geosphere, v. 7, no. 3, p. 658–683.
Weaver, C.E., 1949, Geology of the Coast Ranges immediately north of the San Francisco Bay region, California: Geological Survey of America Memoir 35, 242 p.
Xia, J., Miller, R., Park, C., and Ivanov, J., 2000, Construction of 2 D Vertical Shear Wave Velocity Field by the Multichannel Analysis of Surface Wave Technique, *in* Symposium on the Application of Geophysics to Engineering and Environmental Problems 2000: Society of Exploration Geophysicists, Environment and Engineering Geophysical Society, p. 1197–1206, https://doi.org/10.4133/1.2922726.
Yong, A., Martin, A., Stokoe, K., and Diehl, J., 2013, ARRA-funded V_{S30} measurements using multi-technique approach at strong motion stations in California and Central-Eastern United States: U.S. Geological Survey Open-File Report 2013–1102, 60 p. and data files, https://pubs.usgs.gov/of/2013/1102/.

Appendix 1—Rayleigh and Love Wave Dispersion Curves

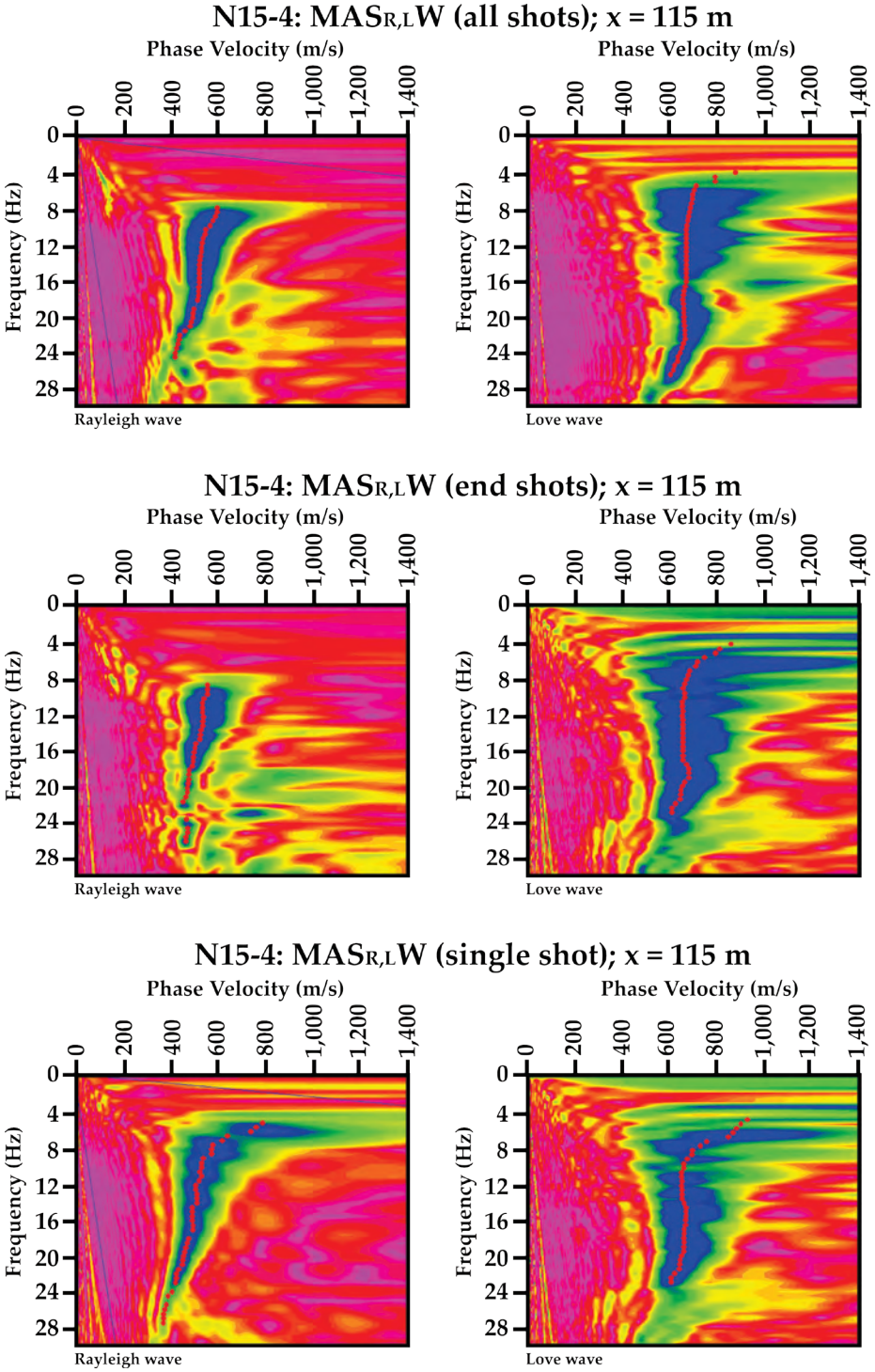

Figure 23. Graphs showing Rayleigh and Love wave dispersion curves representing the point on our seismic profile N15-4: Lovall Valley Loop Road in Napa, California, that is nearest to the strong-motion station. Adjusted picks (red dots) for the fundamental mode are at phase velocities between 400 and 900 meters per second (m/s) and at frequencies between 3 and 28 hertz (Hz). MASR,LW, multichannel analysis of surface waves for both Rayleigh and Love waves.

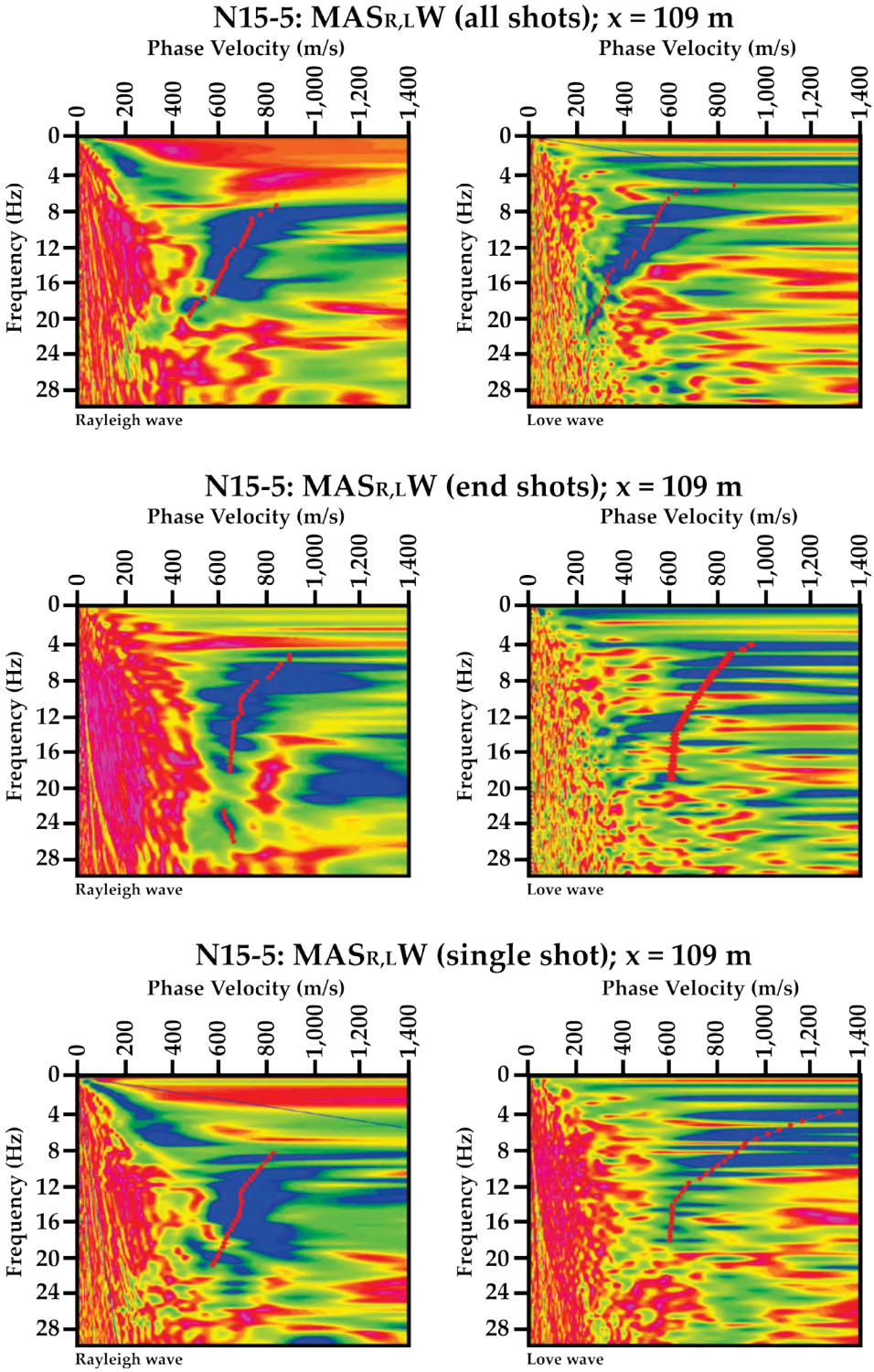

Figure 24. Graphs showing Rayleigh and Love wave dispersion curves representing the point on our seismic profile N15-5: Broadway Street and Sereno Drive in Vallejo, California, that is nearest to the strong-motion station. Adjusted picks (red dots) for the fundamental mode are at phase velocities between 200 and 1,400 meters per second (m/s) and at frequencies between 4 and 28 hertz (Hz). MASR,LW, multichannel analysis of surface waves for both Rayleigh and Love waves.

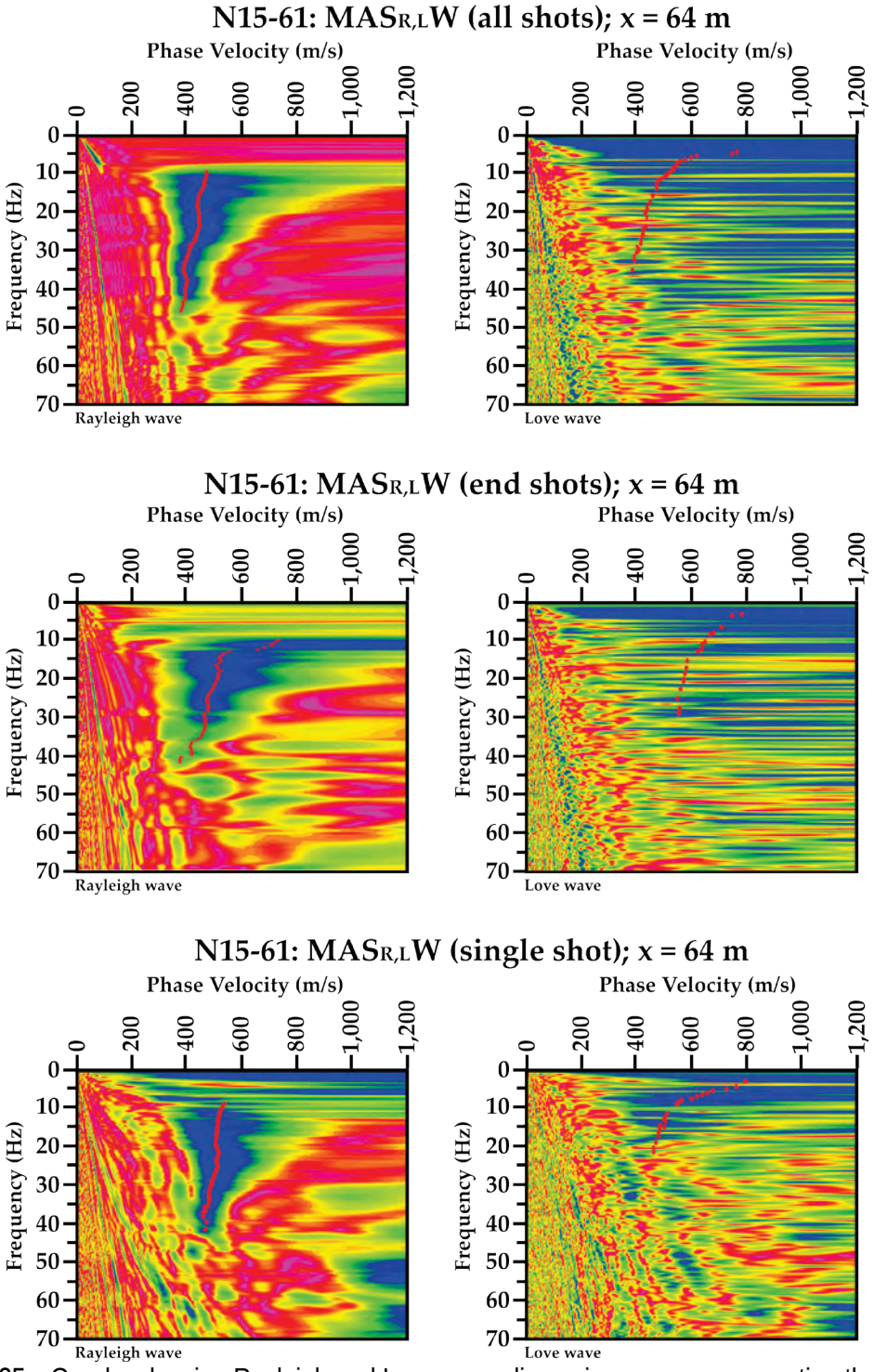

Figure 25. Graphs showing Rayleigh and Love wave dispersion curves representing the point on our seismic profile N15-6.1: Vallejo Fire Station on Marin Street in Vallejo, California, that is nearest to the strong-motion station. Adjusted picks (red dots) for the fundamental mode are at phase velocities between 300 and 800 m/s and at frequencies between 3 and 48 hertz (Hz). Dispersion curves for the various methods of multichannel analysis of surface waves (MASW) analysis using Love waves are less clear than those from using Rayleigh waves. MAS$_{R,L}$W, multichannel analysis of surface waves for both Rayleigh and Love waves.

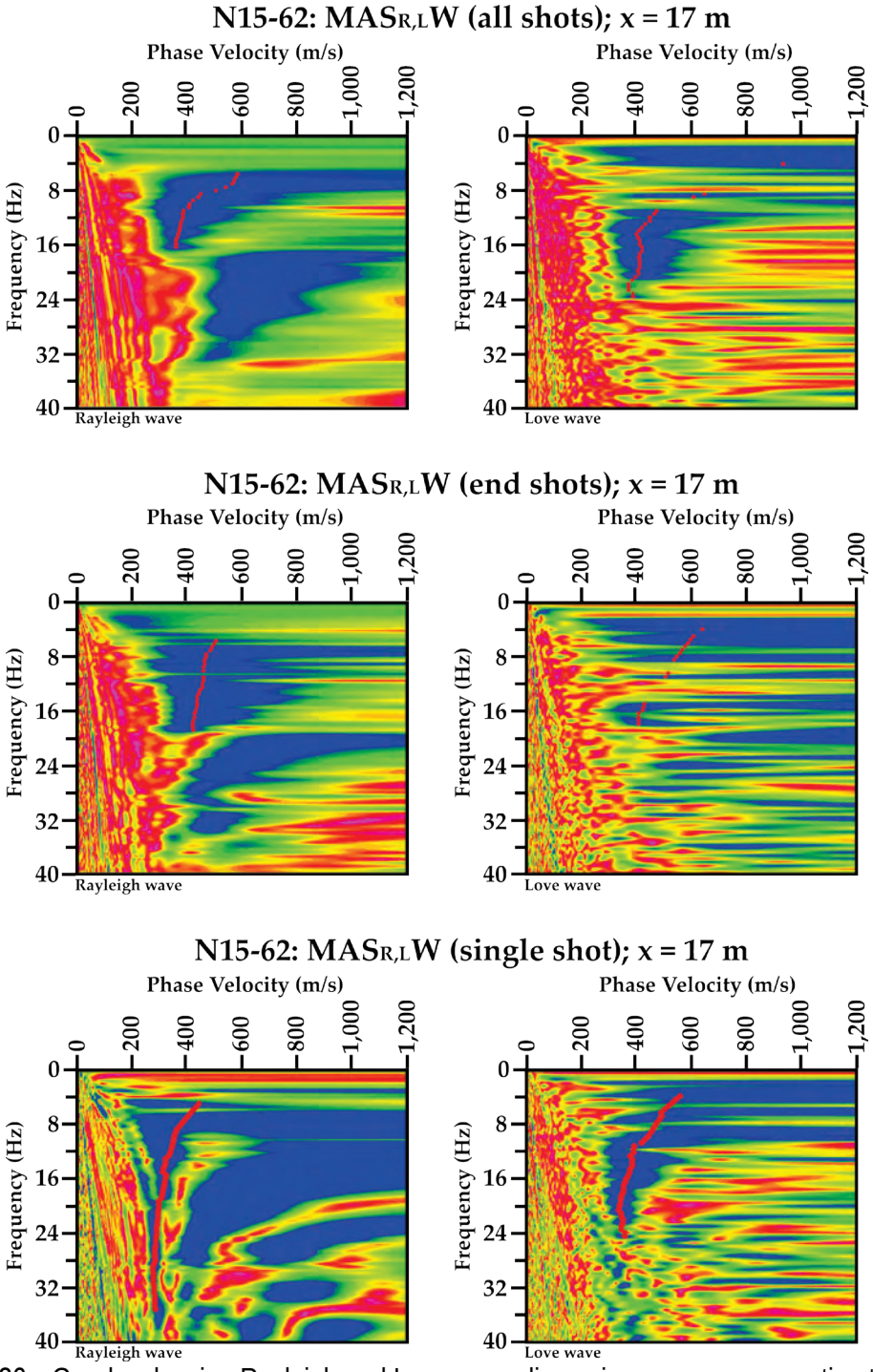

Figure 26. Graphs showing Rayleigh and Love wave dispersion curves representing the point on our seismic profile N15-6.2: Vallejo Fire Station on Overland Alley in Vallejo, California, that is nearest to the strong-motion station. Adjusted picks (red dots) for the fundamental mode are at phase velocities between 200 and 800 meters per second (m/s) and at frequencies between 3 and 36 hertz (Hz). Rayleigh wave dispersion curves show distinct higher modes from 500 and 900 m/s. Generally, dispersion curves for the various methods of multichannel analysis of surface waves (MASW) analysis using Love waves are less clear than those from using Rayleigh waves. MASR,LW, multichannel analysis of surface waves for both Rayleigh and Love waves.

Appendix 2—Rayleigh and Love Wave Fundamental Mode Dispersion Curve Picks

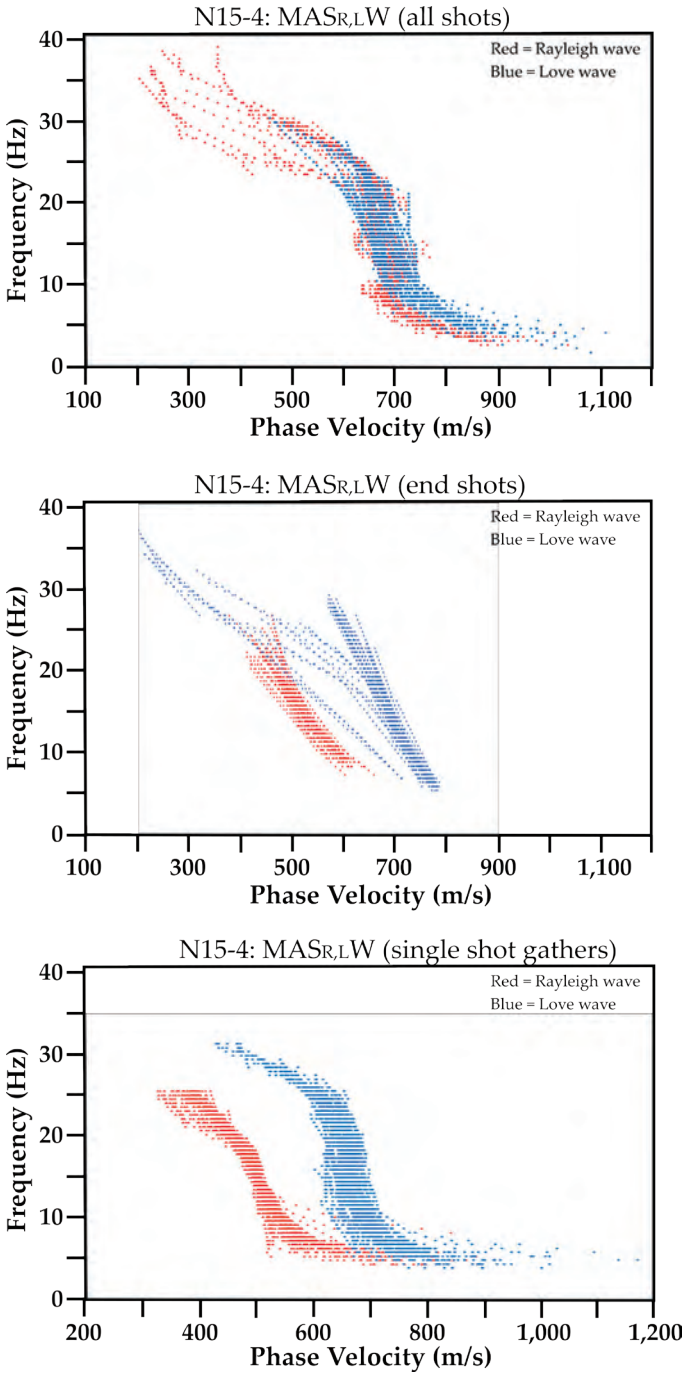

Figure 27. Graphs showing Rayleigh (red dots) and Love (blue dots) wave fundamental mode dispersion curve picks for our seismic profile N15-4: Lovall Valley Loop Road in Napa, California. Love wave dispersion curves have higher phase velocities then Rayleigh waves in the end shots and single shot gathers models, whereas both Love and Rayleigh wave dispersion curve picks cover similar range in phase velocities for the $MAS_{R,L}W$ (multichannel analysis of surface waves for both Rayleigh and Love waves) model using all shots. Hz, hertz; m/s, meters per second.

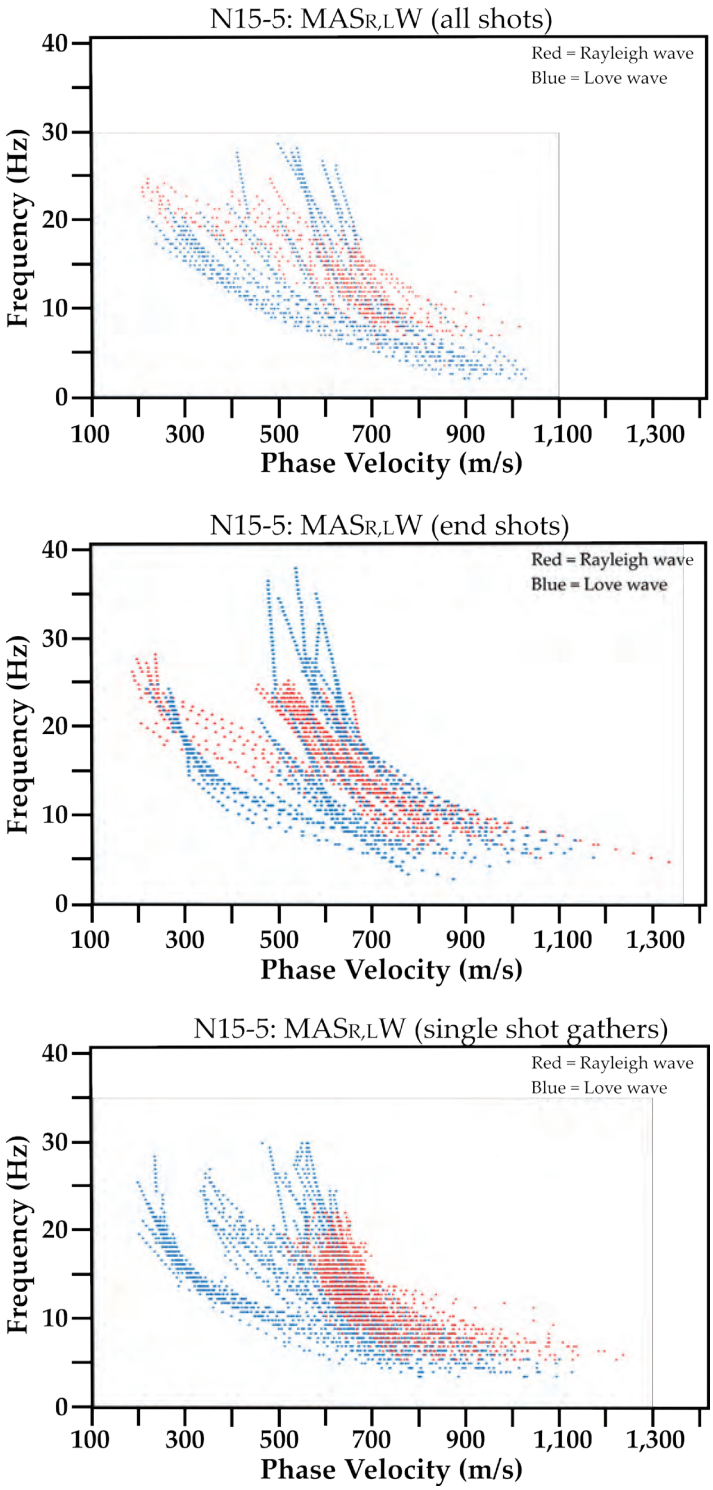

Figure 28. Graphs showing Rayleigh (red dots) and Love (blue dots) wave fundamental mode dispersion curve picks on our seismic profile N15-5: Broadway Street and Sereno Drive in Vallejo, California. Love wave dispersion curve picks generally cover a wider range of phase velocities and frequencies than Rayleigh wave in the various multichannel analysis of surface waves (MASW) methods. MASR,LW, multichannel analysis of surface waves for both Rayleigh and Love waves. Hz, hertz; m/s, meters per second.

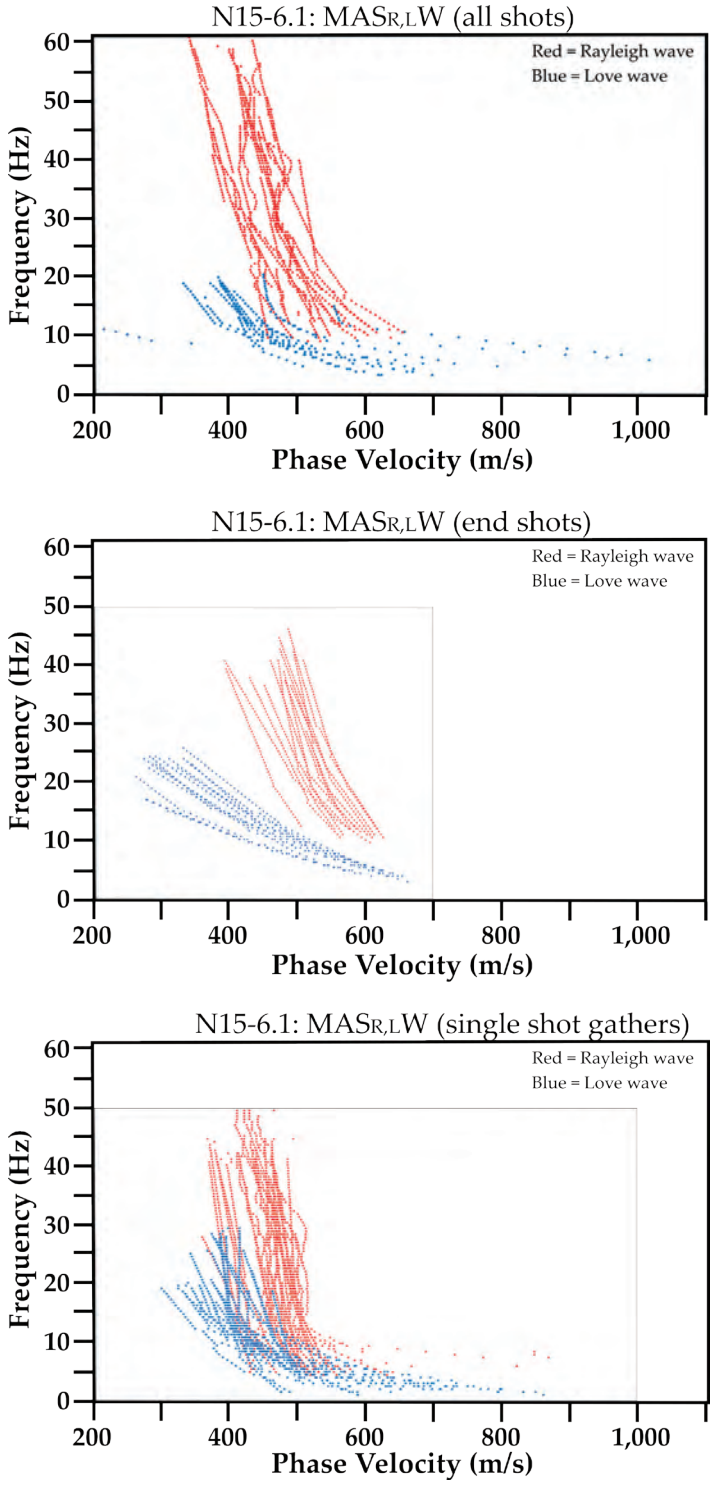

Figure 29. Graphs showing Rayleigh (red dots) and Love (blue dots) wave fundamental mode dispersion curve picks on our seismic profile N15-6.1: Vallejo Fire Station on Marin Street in Vallejo, California. Love wave dispersion curve picks generally cover a wider range of phase velocities but smaller range of frequencies than Rayleigh wave in the various (MASW) methods. MASR,LW, multichannel analysis of surface waves for both Rayleigh and Love waves. Hz, hertz; m/s, meters per second.

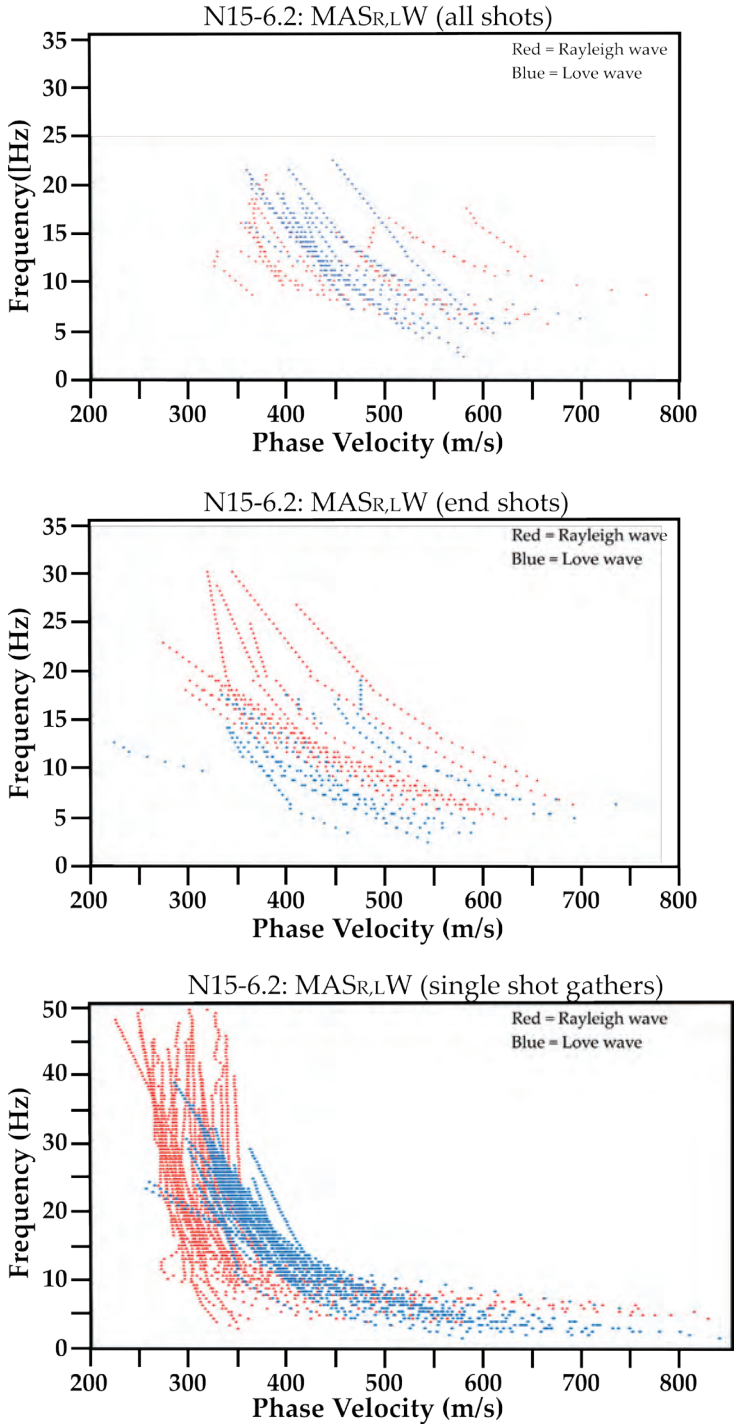

Figure 30. Graphs showing Rayleigh (red dots) and Love (blue dots) wave fundamental mode dispersion curve picks on our seismic profile N15-6.2: Vallejo Fire Station on Overland Alley in Vallejo, California. Love wave dispersion curve picks generally cover a wider range of phase velocities but smaller range of frequencies than Rayleigh wave in the models using end shots and single shot gathers. Love wave dispersion curve picks cover a smaller range of phase velocities but at a larger range of frequencies than Rayleigh waves in the model using all shots. MASR,LW, multichannel analysis of surface waves for both Rayleigh and Love waves. Hz, hertz; m/s, meters per second.

Appendix 3—Rayleigh Wave, Love Wave, and S-Wave Refraction Tomography 1D Velocity-Depth Profiles

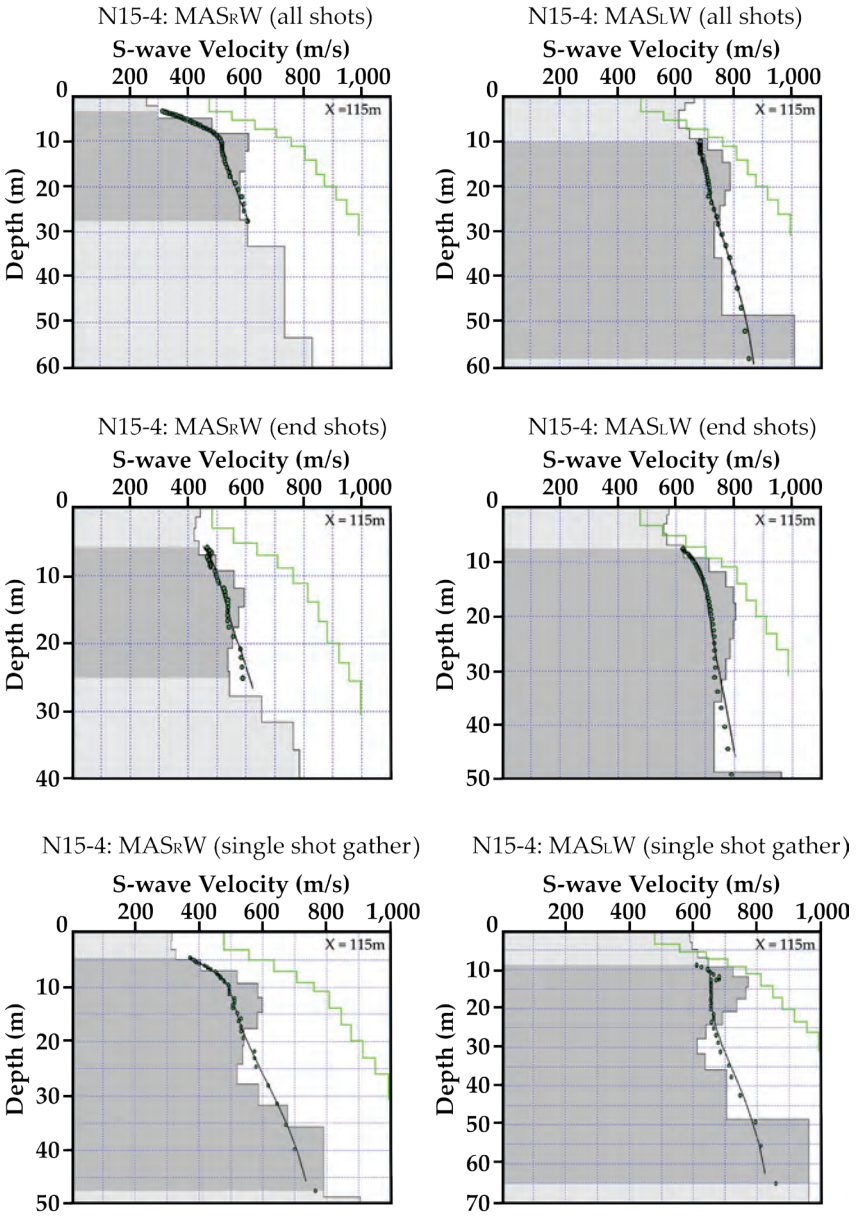

Figure 31. Graphs showing Rayleigh wave (left column), Love wave (right column), and S-wave refraction tomography (green line) one-dimensional (1D) depth-velocity profiles representing the point on our seismic profile N15-4: Lovall Valley Loop Road in Napa, California, that is nearest to the strong-motion station. One-dimensional depth-velocity profiles from multichannel analysis of surface waves for Rayleigh waves (MAS_RW) generally are lower than S-wave refraction tomography, whereas 1D depth-velocity profiles from multichannel analysis of surface waves for Love waves (MAS_LW) are higher than S-wave refraction tomography in the upper 5 meters (m). Green dots on the 1D depth-velocity profiles are dispersion curve picks, and black lines are the model fit to the picks. m/s; meters per second.

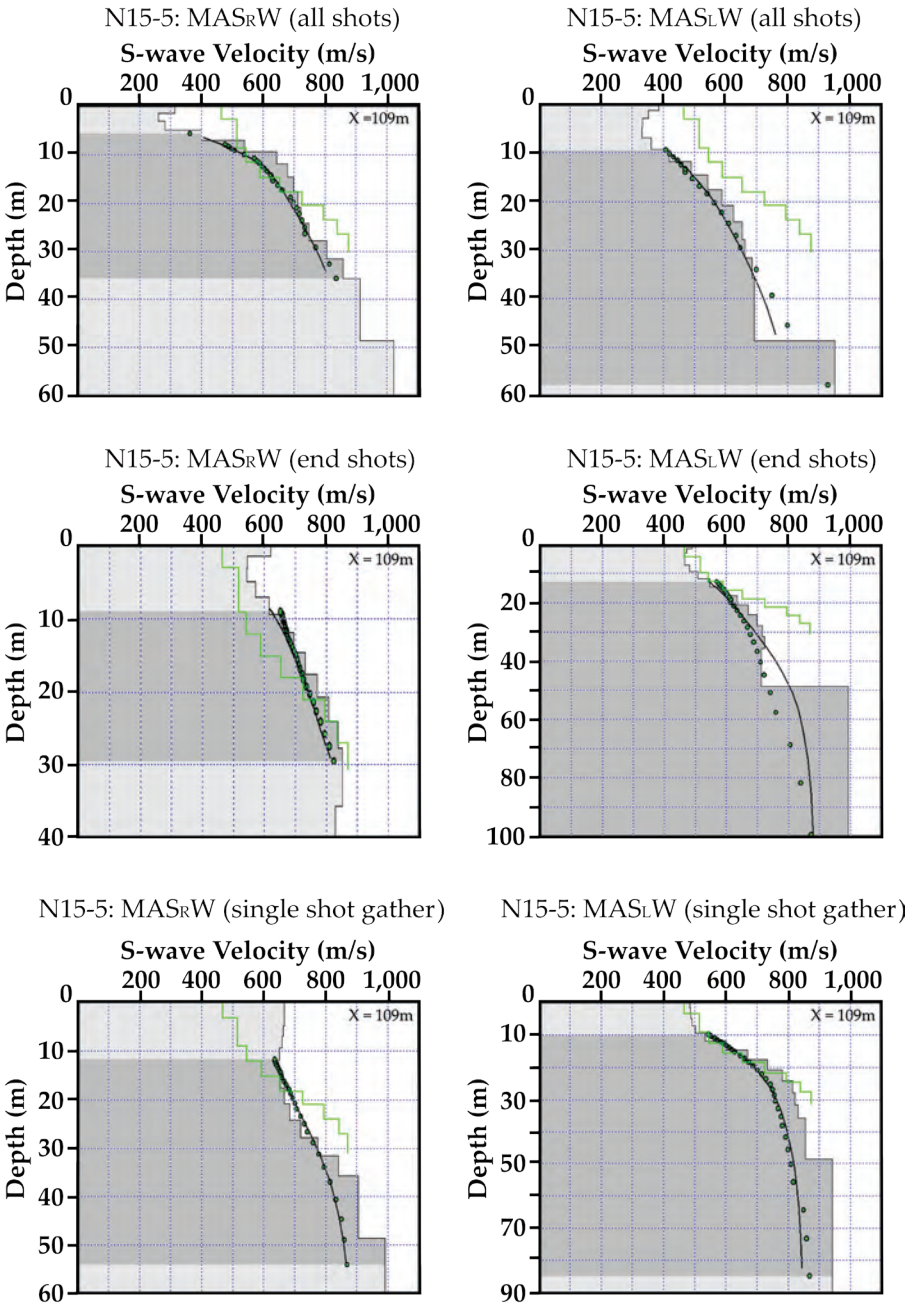

Figure 32. Graphs showing Rayleigh wave (left column), Love wave (right column), and S-wave refraction tomography (green line) one-dimensional (1D) depth-velocity profiles representing the point on our seismic profile N15-5: Broadway Street and Sereno Drive in Vallejo, California, that is nearest to the strong-motion station. One-dimensional depth-velocity profiles from multichannel analysis of surface waves analysis using both Rayleigh and Love waves (MASRW and MASLW, respectively) generally are slower than S-wave refraction tomography, except for the MASRW model using end shots. Green dots on the 1D depth-velocity profiles are dispersion curve picks, and black lines are the model fit to the picks. m, meters; m/s; meters per second.

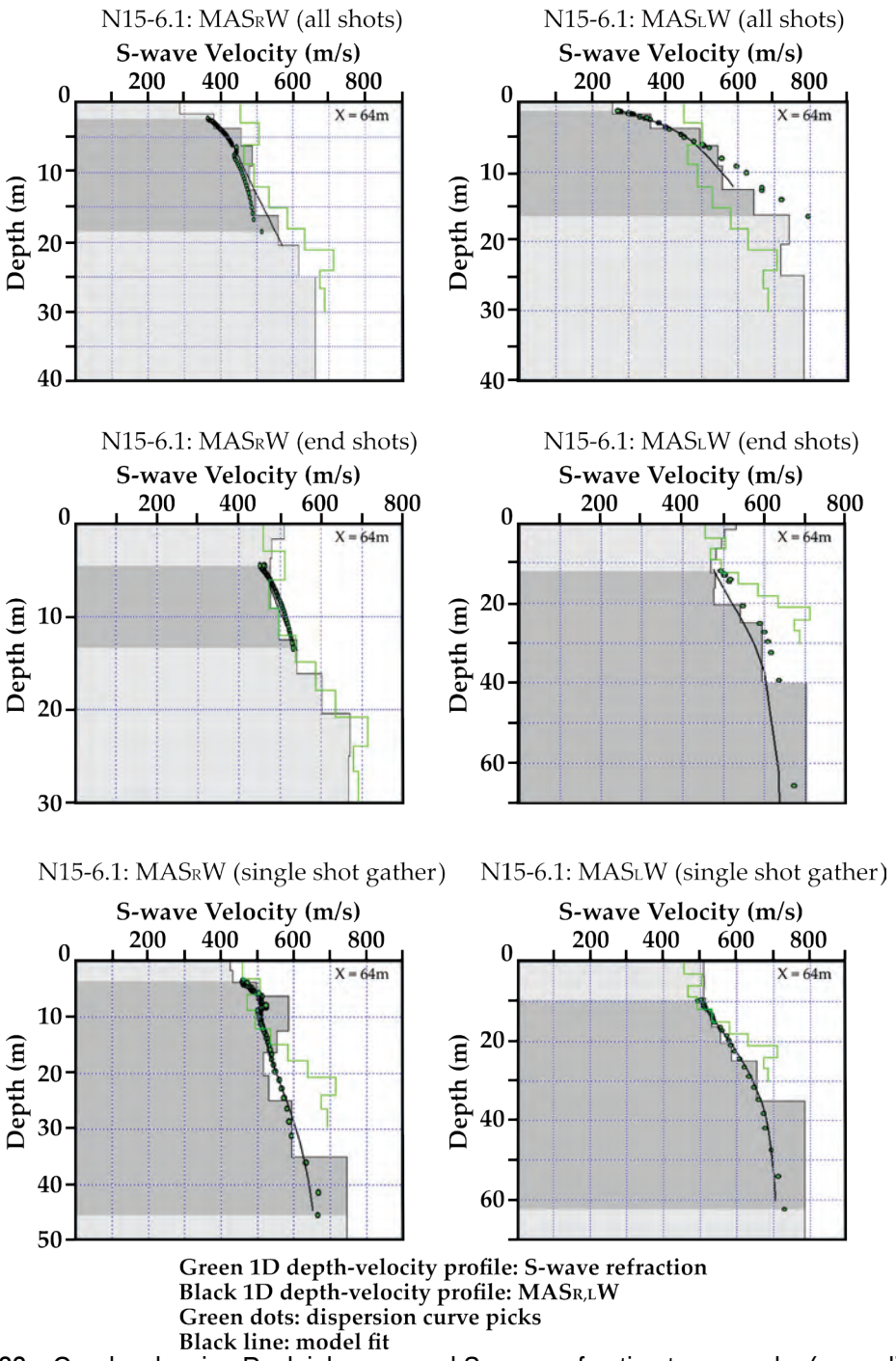

Figure 33. Graphs showing Rayleigh wave and S-wave refraction tomography (green line) one-dimensional (1D) depth-velocity profiles representing the point on our seismic profile N15-6.1: Vallejo Fire Station on Marin Street in Vallejo, California, that is nearest to the strong-motion station. One-dimensional depth-velocity profiles from multichannel analysis of surface waves analysis using both Rayleigh and Love waves (MAS_RW and MAS_LW, respectively) analysis using all shots generally are lower than S-wave refraction tomography in the upper 5 to 8 meters (m), whereas 1D depth-velocity profiles from $MAS_{R,L}W$ analysis using only end shots are higher than S-wave refraction tomography in the upper 5 to 10 m. Green dots on the 1D depth-velocity profiles are dispersion curve picks, and black lines are the model fit to the picks. m, meters; m/s; meters per second.

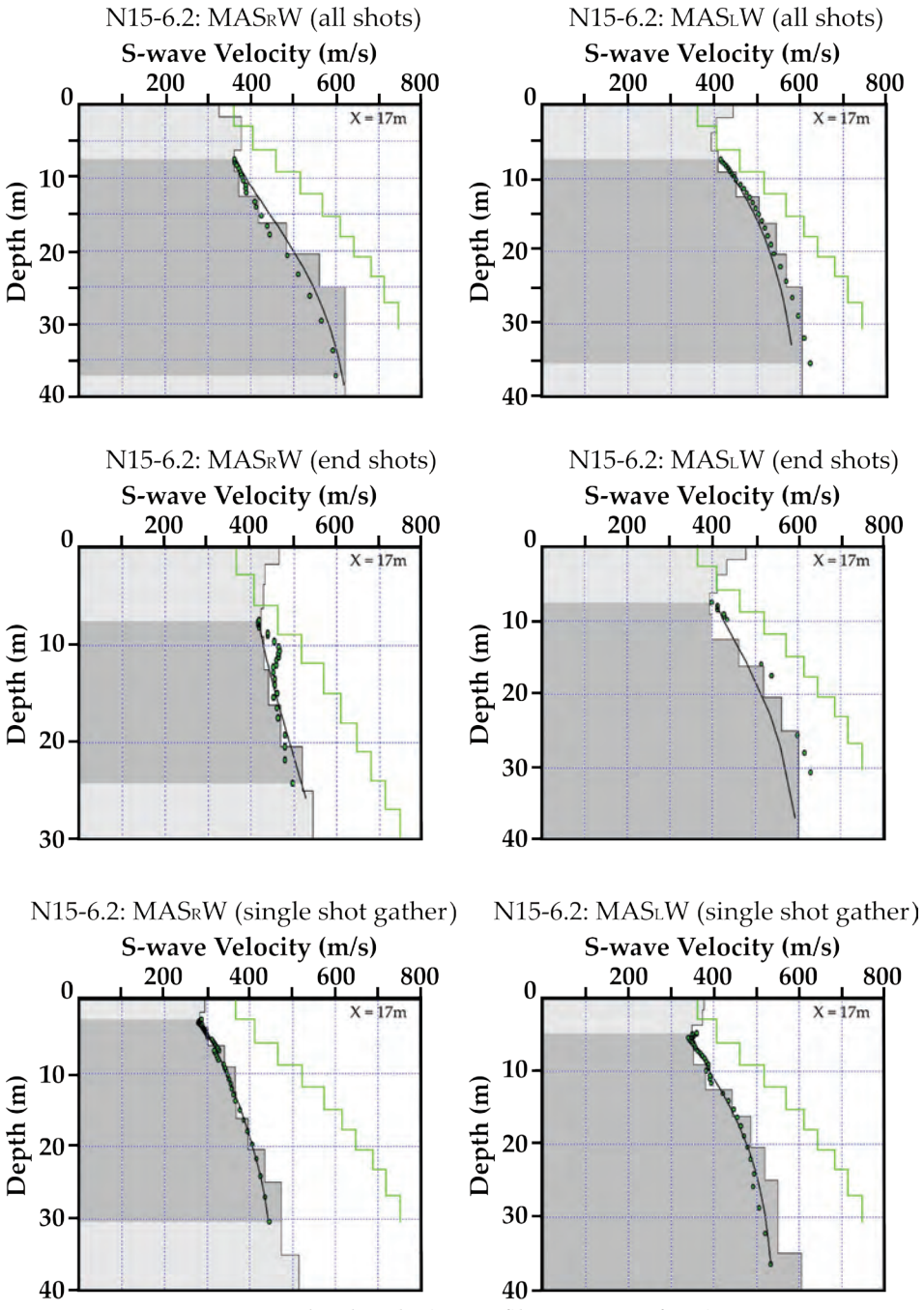

Figure 34. Graphs showing Love wave and S-wave refraction tomography (green line) one-dimensional (1D) depth-velocity profiles representing the point on our seismic profile N15-6.2: Vallejo Fire Station on Overland Alley in Vallejo, California, that is nearest to the strong-motion station. One-dimensional depth-velocity profiles from multichannel analysis of surface waves analysis using both Rayleigh and Love waves ($MAS_{R,L}W$) using the various methods are generally lower than S-wave refraction tomography. Green dots on the 1D depth-velocity profiles are dispersion curve picks, and black lines are the model fit to the picks. m, meters; m/s; meters per second.

Appendix 4—V_P/V_S Ratio Determined from P- and S-Wave Refraction Tomography

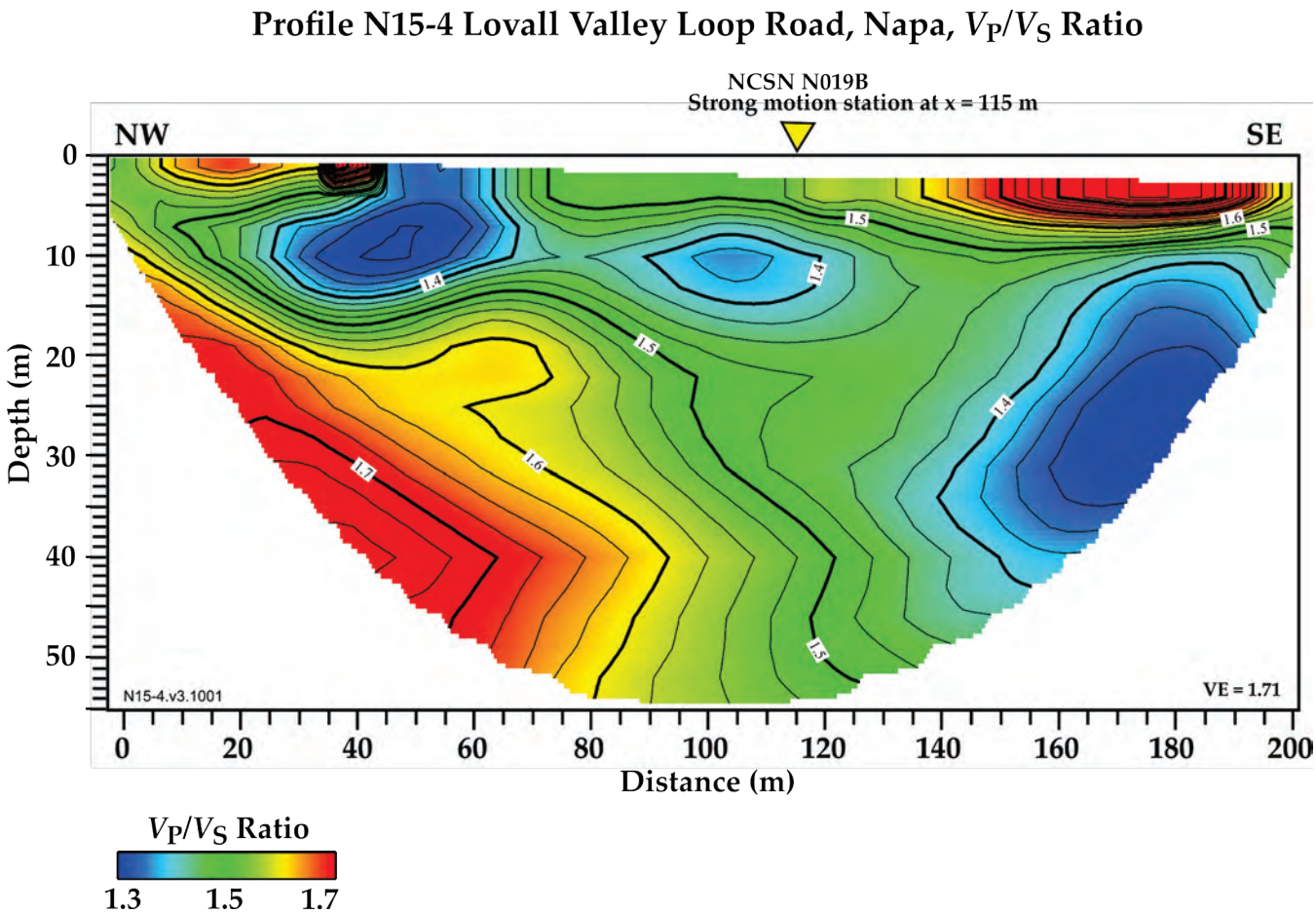

Figure 35. Illustration showing the ratio of P-wave velocity to S-wave velocity (V_P/V_S) determined from P- and S-wave refraction tomography along Lovall Valley Loop Road, Napa, California, seismic profile range from 1.3 to 1.75, with the highest values in the near surface and at depth, where they are separated by a zone of low V_P/V_S ratios. NCSN, Northern California Seismic Network; NW, northwest; SE, southeast; VE, vertical exaggeration; m, meters.

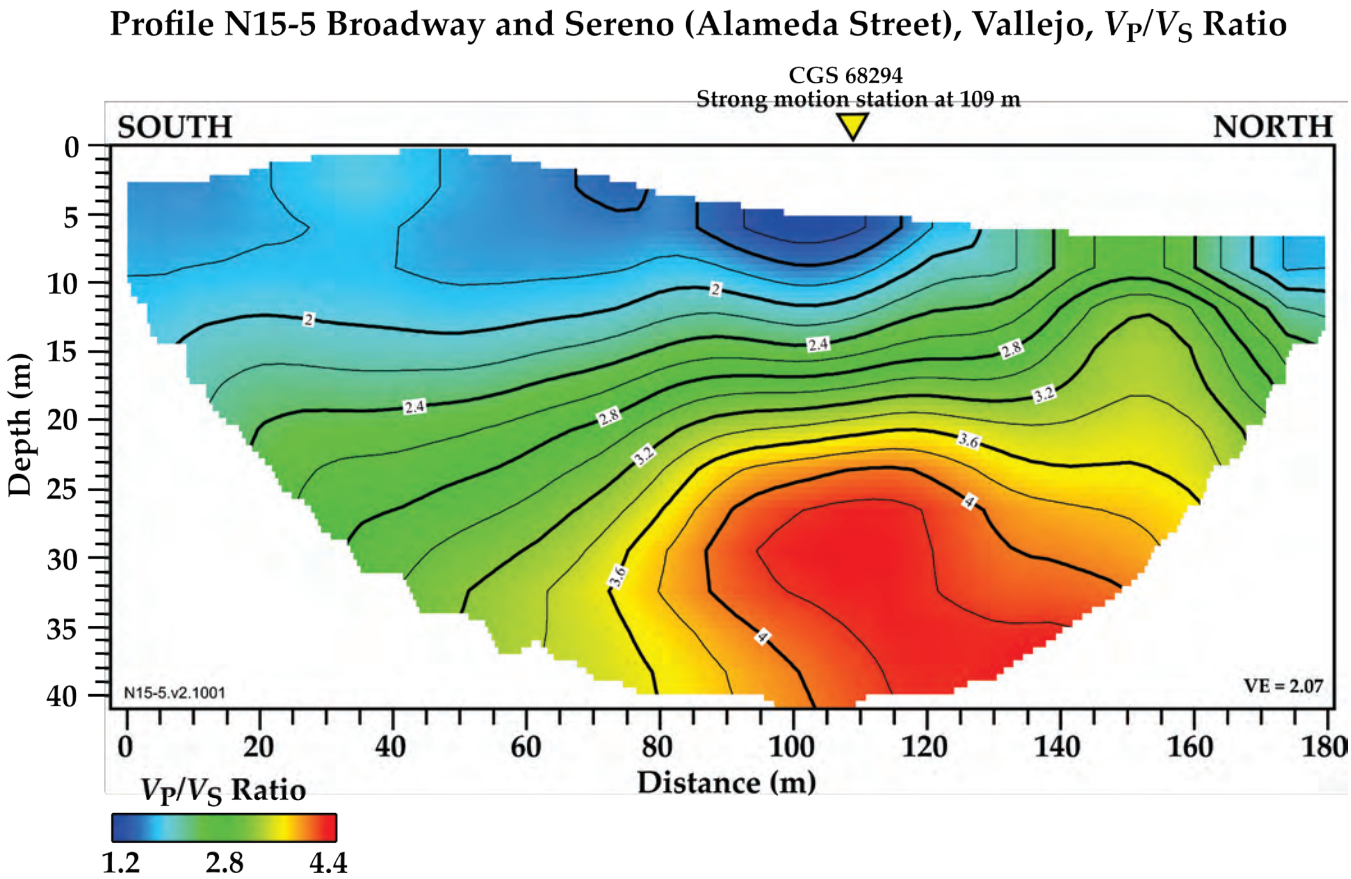

Figure 36. Illustration showing the ratio of P-wave velocity to S-wave velocity (V_P/V_S) determined from P- and S-wave refraction tomography along the seismic profile near Broadway Street and Sereno Drive, Vallejo, California, strong-motion station range from 1.4 to 4.2, with the highest values at depth below the strong-motion station. CGS, California Geological Survey; VE, vertical exaggeration; m, meters.

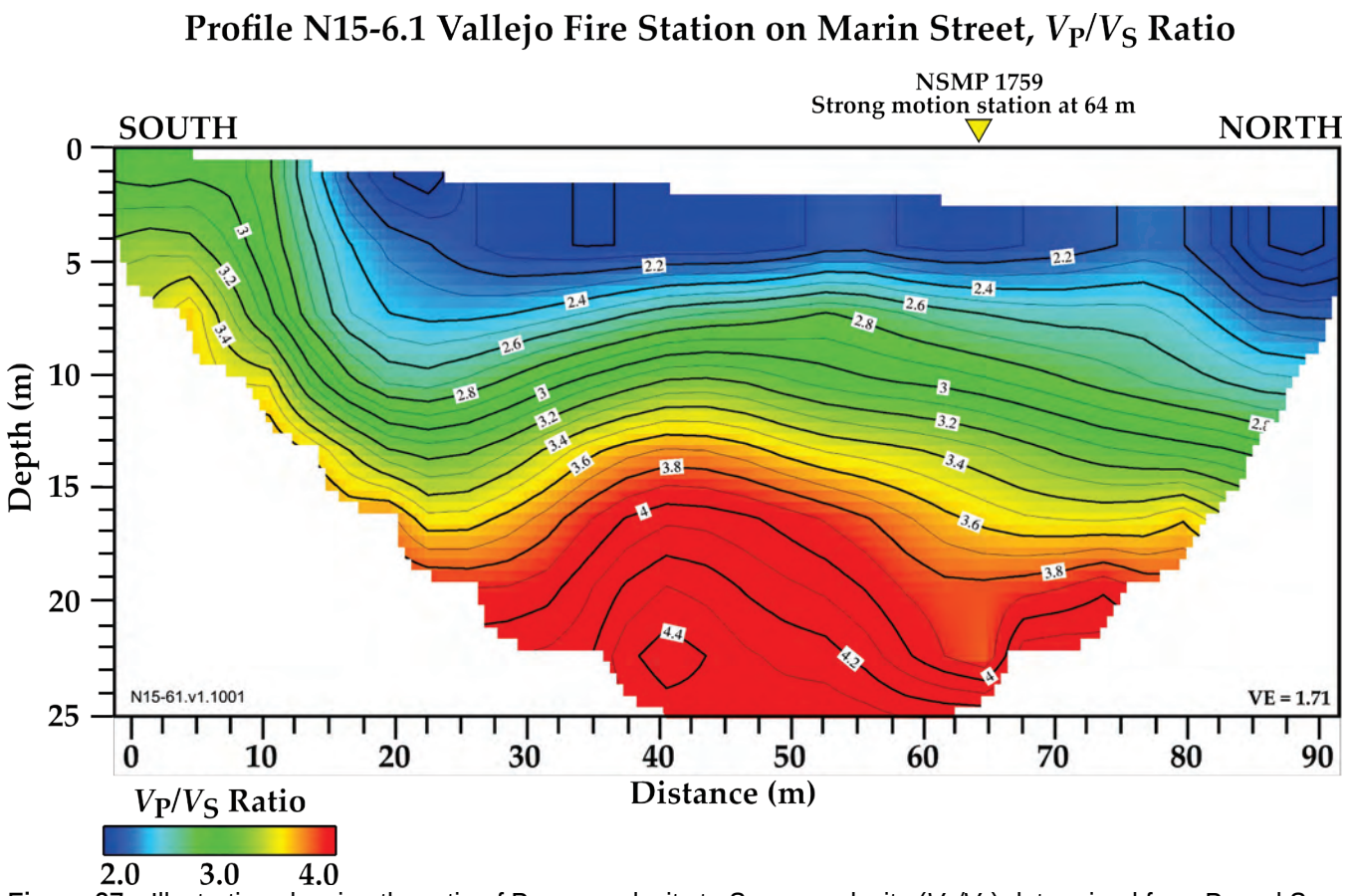

Figure 37. Illustration showing the ratio of P-wave velocity to S-wave velocity (V_P/V_S) determined from P- and S-wave refraction tomography along Marin Street seismic profile adjacent to Vallejo Fire Station in Vallejo, California, range from 2.1 to 4.4. The highest V_P/V_S ratios occur at depth and increasing slightly to the south. NSMP, National Strong Motion Project; VE, vertical exaggeration; m, meters.

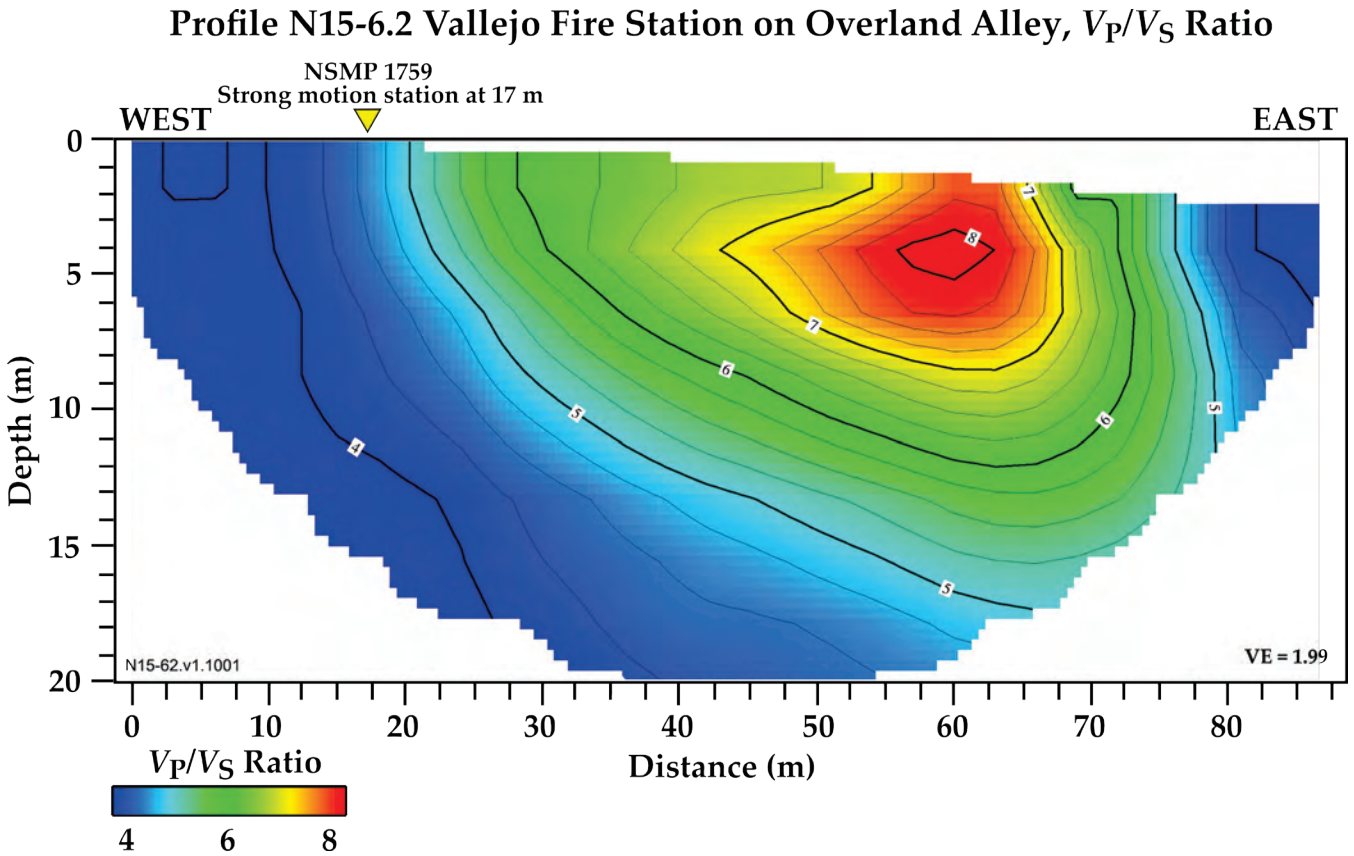

Figure 38. Illustration showing showing the ratio of P-wave velocity to S-wave velocity (V_P/V_S) determined from P- and S-wave refraction tomography along Overland Alley seismic profile adjacent to Vallejo Fire Station in Vallejo, California, range from 3 to 8. The highest V_P/V_S ratios occur at distance meter 60 in the upper 5 meters (m) of the profile. Previous studies (Catchings and others, 2013, 2014) have shown that V_P/V_S ratio higher than 7 suggests the presence of a fault. NSMP, National Strong Motion Project; VE, vertical exaggeration.

Appendix 5—Poisson's Ratio Determined From P- and S-Wave Refraction Tomography

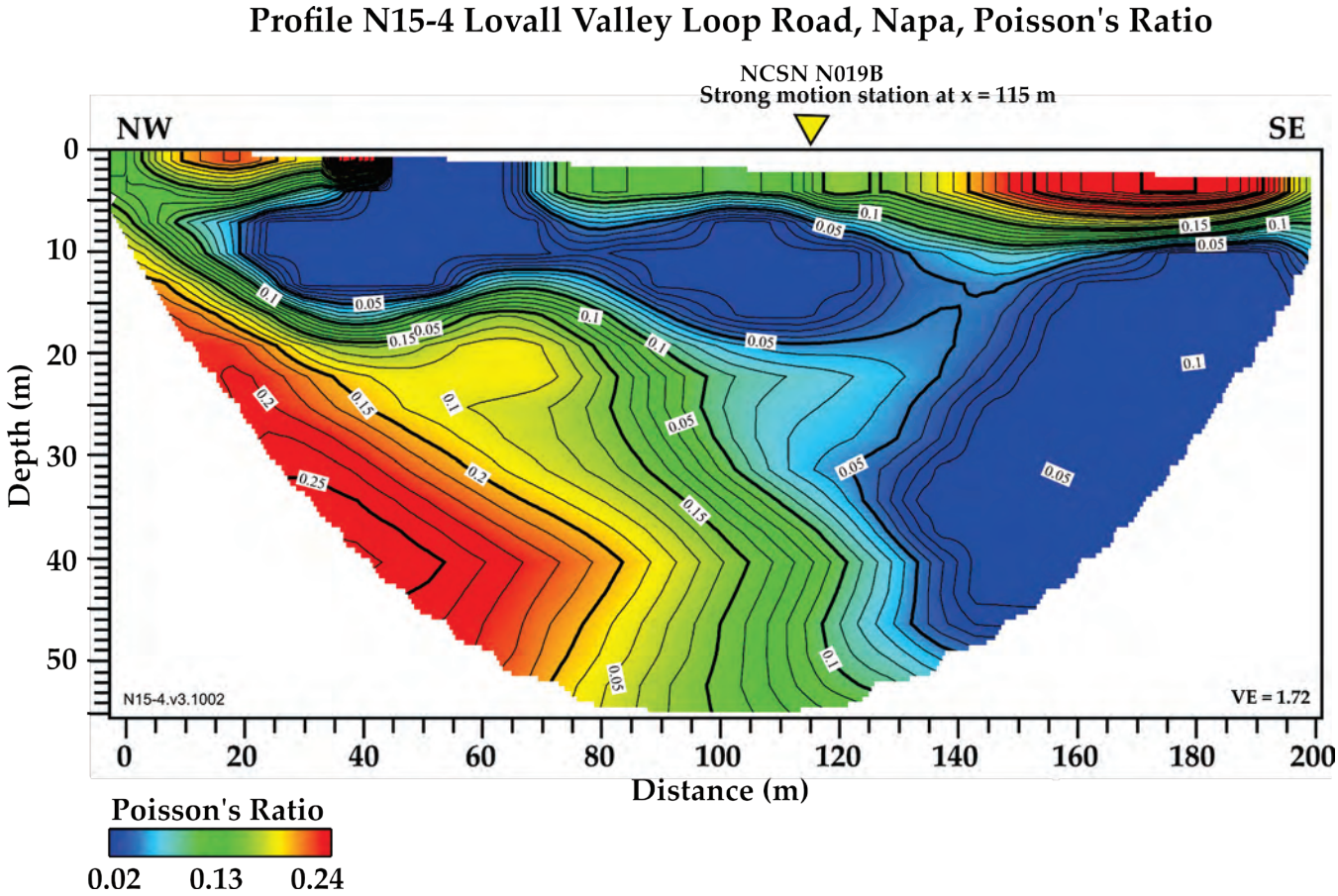

Figure 39. Illustration showing Poisson's ratios determined from P- and S-wave refraction tomography along Lovall Valley Loop Road, Napa, California, seismic profile range from 0.01 to 0.26, which are indicative of an unsaturated subsurface along the entire seismic profile. NCSN, Northern California Seismic Network; NW, northwest; SE, southeast; VE, vertical exaggeration; m, meters.

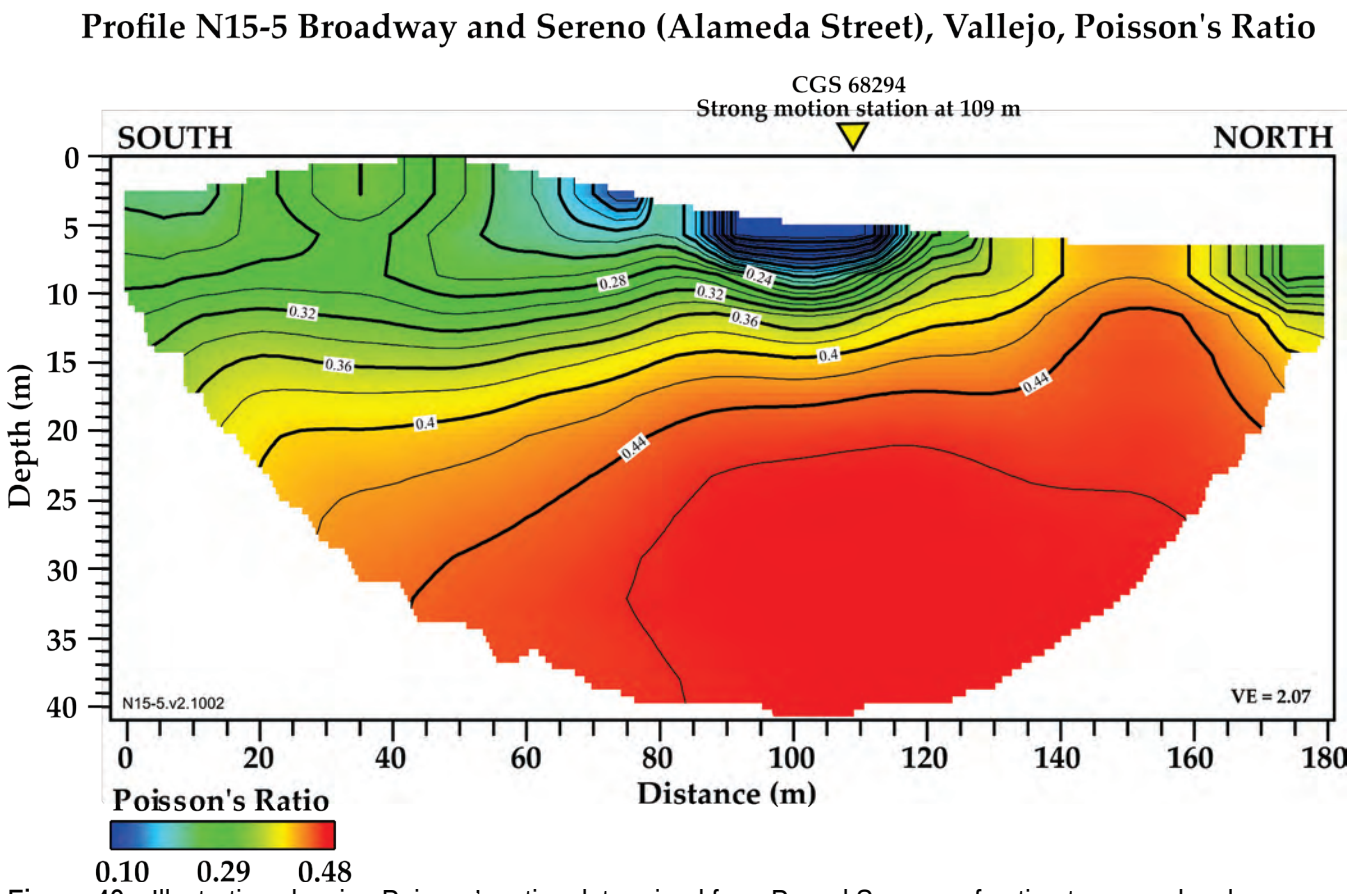

Figure 40. Illustration showing Poisson's ratios determined from P- and S-wave refraction tomography along Alameda Street seismic profile near Broadway Street and Sereno Drive, Vallejo, California, strong-motion station range from 0.04 to 0.48. Ratios indicative of the top of groundwater (>0.43) occur approximately 10 to 32 m below the surface and dip to the south. CGS, California Geological Survey; VE, vertical exaggeration; m, meters.

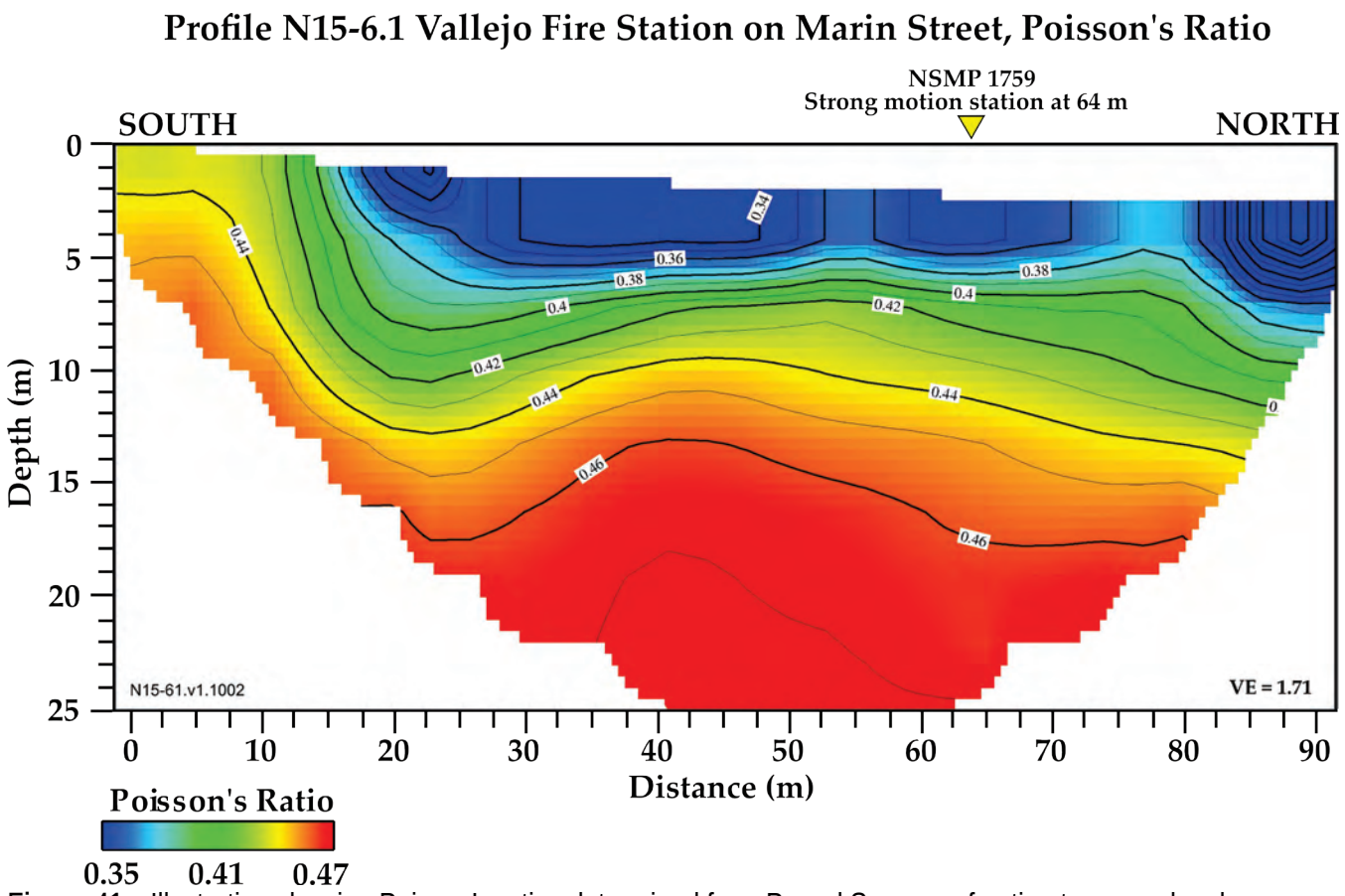

Figure 41. Illustration showing Poisson's ratios determined from P- and S-wave refraction tomography along Marin Street seismic profile adjacent to Vallejo Fire Station in Vallejo, California, range from 0.26 to 0.47. The top of groundwater (>0.43) occur approximately 2 to 14 meters (m) below the surface and nearly coincides with the 1,500 meters per second velocity contour of the P-wave refraction tomography image. NSMP, National Strong Motion Project; VE, vertical exaggeration.

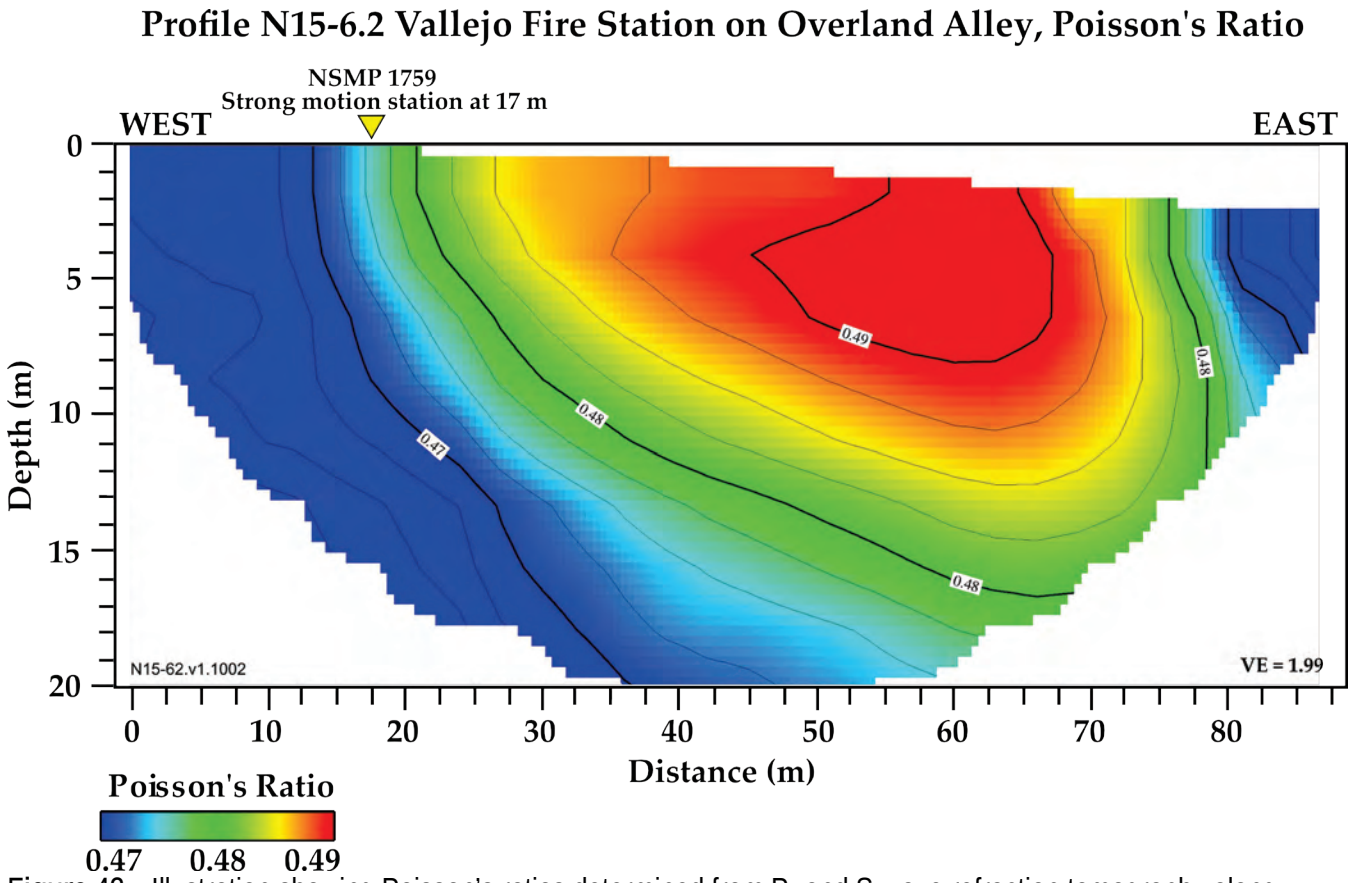

Figure 42. Illustration showing Poisson's ratios determined from P- and S-wave refraction tomography along Overland Alley seismic profile adjacent to Vallejo Fire Station in Vallejo, California, range from 0.463 to 0.49, which indicate saturation from the surface to the base of the model. The highest Poisson's ratio (0.49) coincides well with the location of high ratios of P-wave velocity to S-wave (V_P/V_S), greater than 7, which in previous studies (Catchings and others, 2013, 2014) suggested the presence of a fault. NSMP, National Strong Motion Project; VE, vertical exaggeration; m, meters.

ISSN 2331-1258 (online)
https://doi.org/10.3133/ofr20181162